NTIA Technical Memorandum TM-11-477

Examining the Validity of Rayleigh Distribution Assumptions in Characterizing the Fading Channel at 162 and 793 MHz

Chris Redding
Chris Behm
Tim Riley
Rob Stafford

technical memorandum

U.S. DEPARTMENT OF COMMERCE • National Telecommunications and Information Administration

NTIA Technical Memorandum TM-11-477

Examining the Validity of Rayleigh Distribution Assumptions in Characterizing the Fading Channel at 162 and 793 MHz

Chris Redding
Chris Behm
Tim Riley
Rob Stafford

U.S. DEPARTMENT OF COMMERCE

June 2011

DISCLAIMER

Certain commercial equipment and materials are identified in this report to specify adequately the experimental procedure. In no case does such identification imply recommendations or endorsement by the National Telecommunications and Information Administration, nor does it imply that the material or equipment identified is the best available for this purpose.

ACKNOWLEDGEMENTS

The authors would like to thank the Department of Homeland Security's Office for Interoperability and Compatibility (DHS/OIC), Mr. Dereck Orr, Program Manager, and Mr. Jeff Bratcher, Technical Manager of the Public Safety Communications Research (PSCR) program for support of this work. The PSCR program is a joint effort of the National Institute of Standards and Technology Office of Law Enforcement Standards (NIST/OLES) and the National Telecommunications and Information Administration's Institute for Telecommunication Sciences (NTIA/ITS).

CONTENTS

Page

FIGURES

Page

TABLES

EXAMINING THE VALIDITY OF RAYLEIGH DISTRIBUTION ASSUMPTIONS IN CHARACTERIZING THE FADING CHANNEL AT 162 AND 793 MHZ

Chris Redding, Chris Behm, Tim Riley, Rob Stafford

Wireless communications experience temporal variations in received signal level that are characteristic of the propagation channel. Propagation channel fading at VHF and above is predominantly caused by the complex scattering environment through which the radio waves travel. The techniques used in receiver design to mitigate the effects of fading are well established, but the constraints of limited spectral resources and the insidious characteristics of the propagation environment demand increasingly complex modulation techniques to accomplish this mitigation. To maintain system reliability and usability, receivers must be built to increasingly higher tolerances to cope with propagation-induced errors.

This report describes a re-examination of the fading channel. Specifically, it presents a reassessment of the assumptions implicit in the understanding of fading channels. This effort involves the measurement, analysis, and assessment of propagation fading and describes the limitations of classical fading theories when applied to ever more sophisticated modulation techniques. The ultimate purpose of this report is to investigate the statistical fading behavior of the radio channel within time frames significant to the reception of digitally-modulated signals. Measurements of the mobile radio channel were conducted to analyze the fast fading characteristics of the public safety frequency band. The measurement system is described, as are improvements made to increase its capability to measure the channel characteristics. Data analysis was conducted without bias toward conventional fading assumptions to provide an independent theoretical understanding of RF fading propagation. Finally, an assessment of the efficacy of classical fading theory in the testing of existing public safety VHF transceivers is discussed with conjectures about future transceiver testing and design.

Key words: propagation characteristics; fading channel; Rayleigh distribution; short-term measurements; quadrature channel measurements; public safety; 700 MHz

1 INTRODUCTION

Wireless communications experience temporal variations in received signal level that are characteristic of the propagation channel. The voltage envelope variations of the received radio signal are referred to as fading. Propagation channel fading at VHF and above is predominantly caused by the complex scattering environment through which the radio waves travel. Large and small scale scattering from either stationary or mobile objects creates a multitude of propagation paths between the transmitter and the receiver. The resultant signal at the receiver is an aggregate of all these scattered paths. Each scatterer reflects the transmitted signal at an attenuated level and with a unique phase. The received signal from these scattered paths then experiences multipath fading.

Due to the insidious characteristics of the propagation environment, receivers need to be highly sophisticated to maintain reliable communications. The techniques used in receiver design to mitigate the effects of fading are well established, but—due to the constraints of limited spectral resources—increased technical knowledge of propagation effects and more complex modulation techniques are needed to minimize fading. Since scattering can be described statistically, most theoretical models are the result of matching statistical models to measured data. In an effort to increase spectral efficiency, the typical digital modulation constellation relies on high levels of symbol discrimination in amplitude, phase, and frequency. The ability of a receiver to detect slight variations in the modulated signal requires that error inducing channel effects be well understood and accommodated. Receivers must be built to increasingly higher tolerances to cope with these propagation-induced errors otherwise the communication system's reliability and usability is reduced.

This report describes a re-examination of the fading channel. Specifically, it presents an effort to determine if assumptions implicit in the understanding of fading channels are appropriate in light of the persistent desire to increase bit density in limited spectral bandwidths. This effort involves the measurement, analysis, and assessment of propagation fading and describes the limitations of classical fading theories when applied to increasingly sophisticated modulation techniques. The ultimate purpose of this report is to investigate the statistical fading behavior of the radio channel within time frames significant to the reception of digitally-modulated signals.

Fading is typically modeled as a statistical distribution, either Rayleigh or Rician, depending on whether a line-of-sight (LOS) component is present. The Rayleigh fading model has been the most widely-used distribution model and is considered to represent the worst case condition because it does not contain a LOS component. The worst case assumption has been under examination since there are known conditions where Rayleigh predictions are too ideal [1]. The assumptions that must be met for true Rayleigh behavior are described in [2]. These assumptions are defined as:

1) the interfering waves must be randomly varying in phase and be of nearly equal power,
2) the phases of the component waves must be randomly distributed between 0 and 2π, and
3) there must be a minimum of five interfering waves.

While assumptions 2 and 3 are borne out in most urban/suburban environments in the 800/900 MHz band, it is more difficult to satisfy assumption 1. It is improbable that the condition of nearly equal power interfering waves would be met in an actual environment and the randomness criteria can be easily violated by the presence of a direct (or predominant) wave component. This supports the contention [1] that measurement results rarely compare well with the Rayleigh distribution across the entire fading signal range.

The phase variation of the channel has not been well studied, probably because empirical data about channel phase is hard to obtain. Although some analytical results about channel phase correlation based on Rayleigh assumptions are available [4], [5], [7], questions as simple as the typical rate of channel phase variation in real environments are not addressed in the research literature. This is troubling, since most digital modulations in use today depend heavily in whole or in part on phase modulation. If the channel is causing rapid phase variations in time regimes on the order of a symbol period, bit errors will result in the decoded signal.

This project involved measurements to verify if the Rayleigh fading model is an appropriate model for land mobile radio (LMR) channels at public safety frequencies. This was accomplished by analyzing the statistical characteristics of measured fading data. In addition, measurements were conducted on a Rayleigh channel simulator and an analysis of the significance of channel fading on the Project 25[1] protocol was performed.

2 THE MEASUREMENT SYSTEM

The measurement system was initially designed as a lab-based system using off-the-shelf test instruments. Over the course of this project, improvements were made to the initial system that increased the dynamic range and accuracy of the measured data. Some of the improvements made with each version were implemented as a result of preliminary data analysis. The increase in measured signal dynamic range was necessary to achieve the desired resolution of the statistical measure of the channel. Without these improvements, analysis of low probability events, relative to the eventual 400 msec measurement window (as described in the next section), would not have been readily discernible.

2.1 Lab System

The lab system consisted of transmitter and receiver sub-systems as shown in Figure 1. Integration of the test instrumentation and configuration of the front panel settings were the goals of this phase. Lab measurements were conducted and data was processed to confirm initial design considerations. Three initial test frequencies of 183, 430, and 915 MHz were chosen, based on equipment currently on hand.

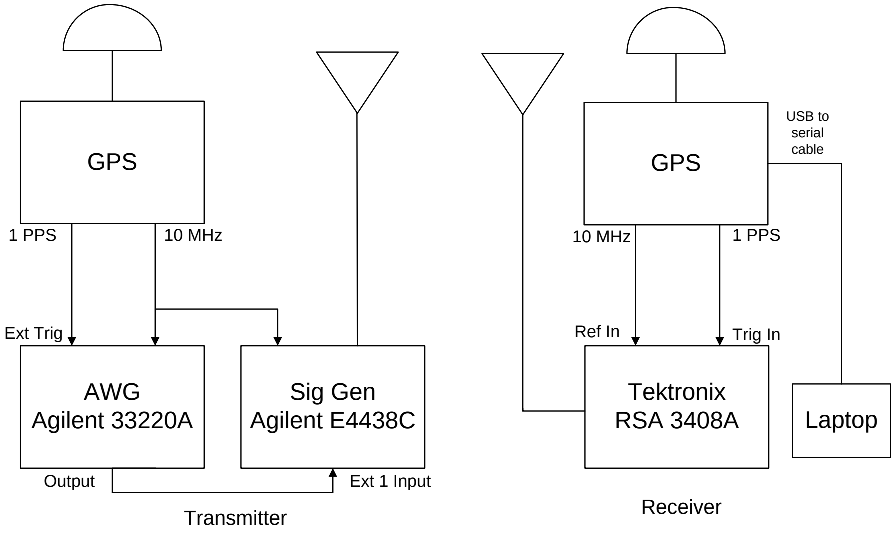

Figure 1. Lab version of the measurement system.

---

[1] Project 25 (P25) is the voluntary consensus process led by governmental entities and the Association of Public-Safety Communications Officials – International (APCO) to enable and promote the development of American

The transmitter system consisted of an Agilent E4438C Vector Signal Generator, an Agilent 33220A Arbitrary Waveform Generator (AWG), a Trimble Accutime GPS receiver and associated antennas. The transmitter was configured to transmit a continuous wave (CW) pulse once per second. The AWG was used to convert the GPS 1 pulse per second (PPS) output to the 400 msec long trigger input required by the signal generator. In this way, the signal generator transmitted its CW pulse on each one-second boundary. In addition, the GPS unit provided a 10 MHz reference to each test instrument.

The receiver system consisted of a Tektronix RSA 3408A real-time spectrum analyzer (RTSA), a Trimble Accutime GPS receiver, associated antennas, and a laptop computer. The receiver was synchronized with the transmitter by connecting the GPS 1 PPS output to the RTSA trigger input. In addition, the GPS unit provided a 10 MHz reference to the RTSA. The RTSA automatically saved in-phase and quadrature (I and Q) data acquisitions internally at each one-second trigger via the instrument's "save-on-trigger" function. Latitude and longitude data was logged separately via the laptop computer from the GPS receiver.

The initial GPS units proved to be inadequate due to timing and synchronization difficulties so they were replaced by two Trimble Thunderbolt-E units. Also, GPS data logging difficulties were encountered when the GPS logging software was operating on the RTSA, resulting in timing inaccuracies in the logged data, so a dedicated laptop computer was added to log GPS data separately. The transmit GPS unit was set to the "over determined clock" mode. At the receiver, the GPS unit was set to the "land dynamics" mode to provide more accurate latitude and longitude data; the land dynamics mode is used if the antenna is moving while the device is operating.

As a result of detected problems, several design improvements were incorporated and were verified by preliminary data processing. It was determined that the received signal level was insufficient as it was frequently below the noise floor as observed on the RTSA. Post processing of the data confirmed this as well. To improve the dynamic range of system, a power amplifier and associated high current power supply were added to the transmitter system. The transmitter output power was set to provide 20 W and the dynamic range of the system was subsequently improved.

Due to the poor quality of the receiver's broadband whip antenna, tuned antennas were employed for the three test frequencies of 183, 430, and 915 MHz. A variable band pass filter was also added to the front end of the RTSA to reduce RF interference at the test frequencies, but proved to be inadequate. Ultimately, due to the excessive interference at these frequencies, it was decided to switch to 162 and 793 MHz with tuned antennas. The new frequencies had acceptable low levels of interference and were used for the remainder of the testing. Interference mitigation was also improved with the addition of a tuned-cavity band pass filter (BPF) placed at the input to the RTSA. Another benefit in switching to the new frequencies is that they are closer to existing public safety analog frequencies and planned, next-generation, digital frequencies.

Multiple RTSA span settings were investigated in order to reduce the noise in the acquired data and simplify the post processing stage. The RTSA employs a constant analog-to-digital converter sampling rate (the span) to digitize the received signal. When an acquisition is triggered and stored, the length of the time record produced varies in relationship to the span. As the span is decreased, the record length increases. Measurements were conducted using spans of 1 kHz, 10 kHz, and 100 kHz. A span of 1 kHz produces an acquisition length of 800 msec, which the RTSA could not store internally and still maintain acquisitions on one-second boundaries. At a span of 10 kHz, the RTSA could not maintain the acquisitions on one-second boundaries reliably. The 100 kHz span, with an acquisition length of 400 msec, made possible reliable acquisition of data on one-second measurement boundaries while enabling storage of the data; therefore this setting was applied to the remainder of the measurements. The 100 kHz span has a sample rate of 128k samples/sec; over a 400 msec acquisition length it would collect and store 51,200 samples for each one-second's data file.

Multiple RTSA measurement settings were explored with the final configuration being: 100 kHz span, 400 msec acquisition length, 0 dB RF attenuation level, and the 10 MHz reference oscillator set to external.

2.2 Mobile Measurement System

After the improvements to increase dynamic range and minimize timing and accuracy issues were made to the laboratory system, the mobile measurement system was deployed in the configuration diagrammed in Figure 2. It was installed in a vehicle as shown in Figure 3. To ensure measurements taken over several days were repeatable, the test equipment set-up and configuration was documented in the procedure reproduced in Appendix A and used consistently throughout the course of the measurements.

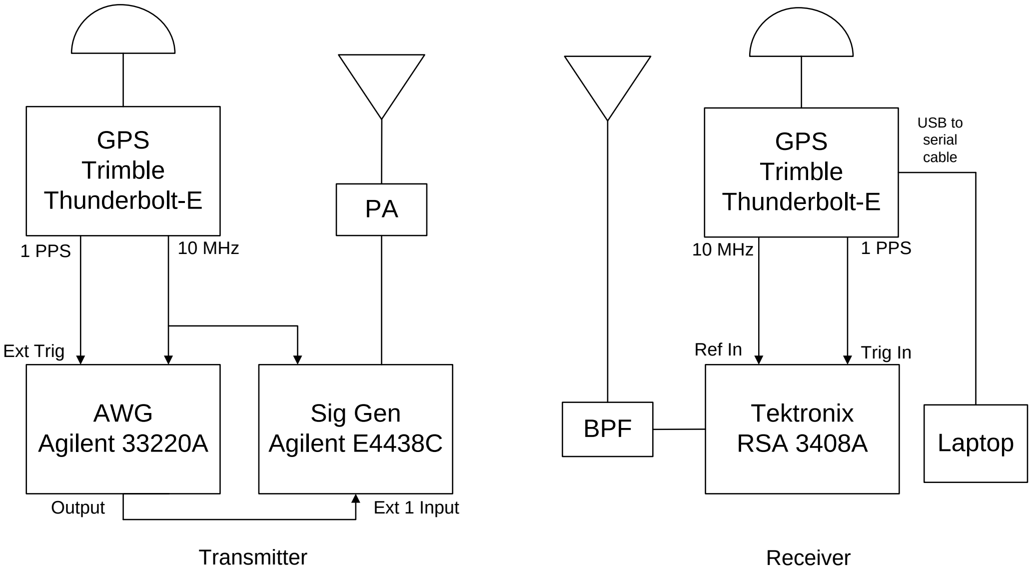

Figure 2. Final version of the measurement system.

Figure 3. Mobile receiver vehicle.

3 MEASUREMENT ENVIRONMENTS

To examine different fading conditions, measurements were conducted over the course of several days in rural, residential, and low-rise urban environments at both 162 and 793 MHz frequencies. The rural environment was at the Table Mountain field site several miles north of Boulder, the residential environment was located in south Boulder, and the low-rise urban environment was located in downtown Boulder. Each test route was repeated three times at each frequency in an attempt to provide statistically significant results. In each environment, the transmitter system was set up at a fixed location, while the receiver system was driven along a fixed path. The intent was to simulate a fixed base station and mobile subscriber environment.

In addition, a fading channel simulator was used to gather simulated data for comparison purposes. Since the simulator implemented the theoretical fading channel, it served as a reference environment. This reference environment was used to further validate the measurement technique and was intended to be used to show the differences between real channels and theoretical fading channels.

3.1 Rural Measurement Environment: Table Mountain

The rural environment measurements were taken along a route at the Table Mountain field site located north of Boulder. The transmitter was placed at the intersection of the two main roads (shown in Figure 4 as a yellow icon) and the receiver vehicle drove the route shown by the red line. Because of the minimal scattering characteristics of the environment, the measurement data proved to be inadequate in demonstrating Rayleigh conditions. Measurements were taken at 183, 430, and 915 MHz frequencies.

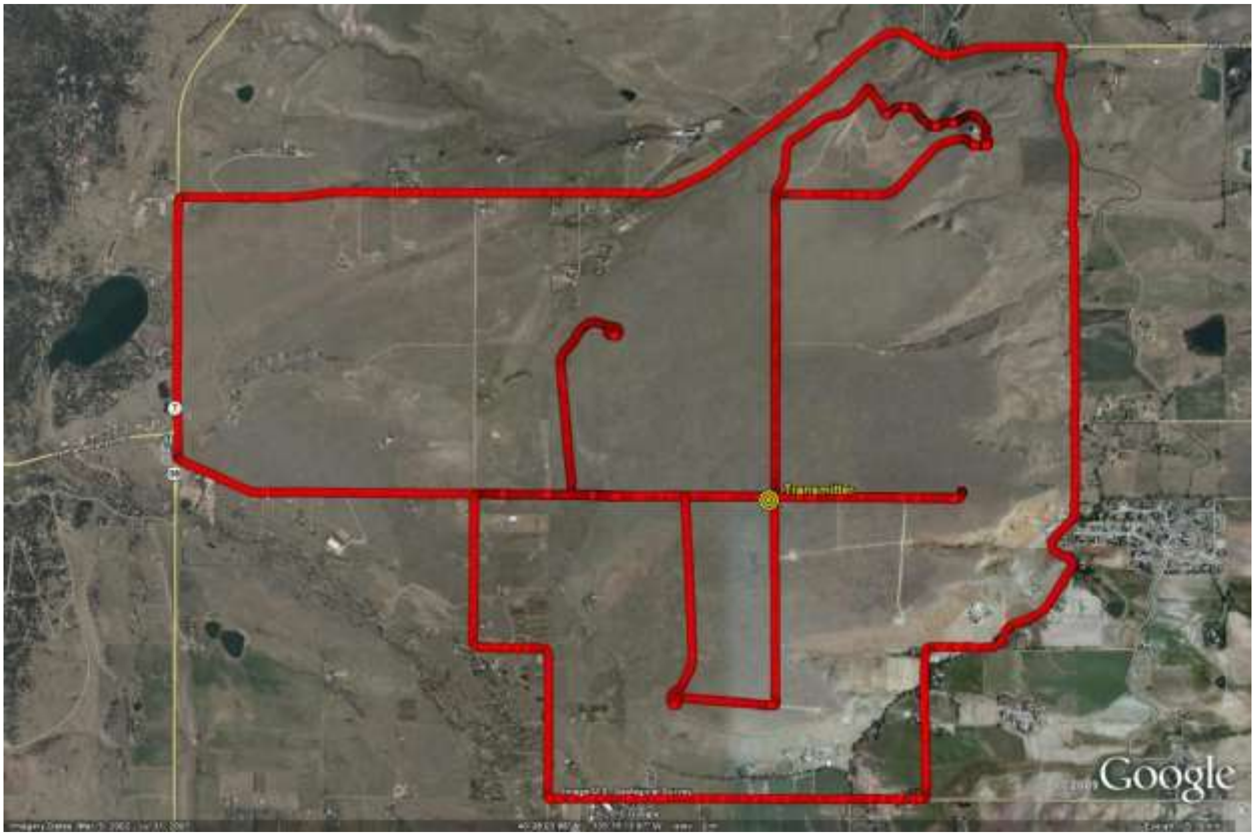

Figure 4. Rural measurement route at Table Mountain field site.[2]

3.2 Residential Measurement Environment: South Boulder

The residential environment measurements were taken along a route in south Boulder. The receiver vehicle drove from a starting point near Moorhead Ave and 27th Way, down to Table Mesa Drive and up to the NCAR facilities as shown by the red line in Figure 5 and the transmitter was placed at the end of Wing 2 of the ITS facilities at 325 Broadway as shown by a yellow icon. Three identical routes were driven successively for both the 162 and 793 MHz frequencies.

---

[2] Map data © 2010 Google, Imagery ©2010DigitalGlobe, USFA Farm Service Agency, GeoEye, U.S. Geological Survey TerraMetrics.

Figure 5. Residential measurement route in south Boulder.[3]

3.3 Mid-level High Rise Measurement Environment: Downtown Boulder

The low rise urban environment measurements were taken along a route in downtown Boulder. The receiver vehicle drove around downtown as shown by the red line in Figure 6 and the transmitter was placed on the uppermost level of a parking garage at 14th St and Walnut as shown by a yellow icon. Three identical routes were driven successively for both the 162 and 793 MHz frequencies.

---

[3] Map data © 2010 Google, Imagery ©2010DigitalGlobe, USFA Farm Service Agency, GeoEye, U.S. Geological Survey TerraMetrics.

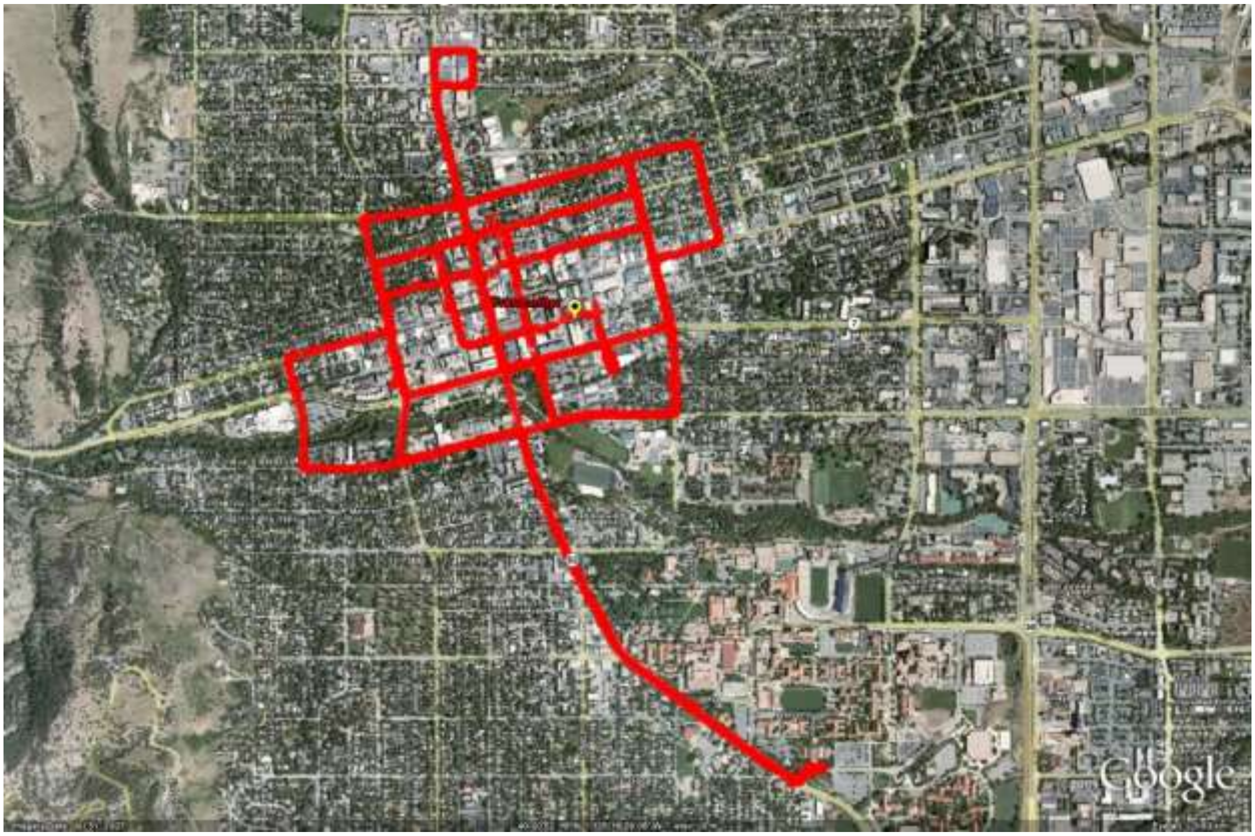

Figure 6. Low rise urban route in downtown Boulder.[4]

3.4 Faded Channel Simulator

Simulated Rayleigh channel data was collected using a fading channel simulator based on the Rohde and Schwarz SMIQ vector signal generator as shown in Figure 7. The simulator's channel conditions were set to the Rayleigh model, 30 MPH, one path and power output of -70 dBm (in an attempt to match the measured signal levels).

---

[4] Map data © 2010 Google, Imagery ©2010DigitalGlobe, USFA Farm Service Agency, GeoEye, U.S. Geological Survey TerraMetrics.

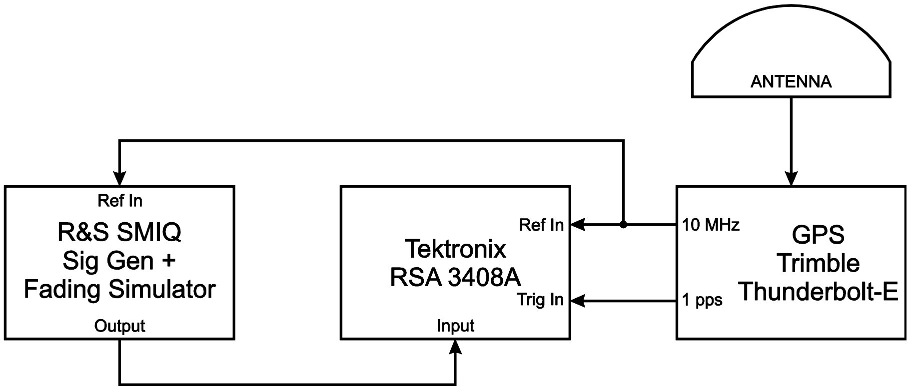

Figure 7. Faded channel simulator test configuration.

3.5 The Collected Data

Since each revision to the mobile measurement system required demonstration of the modification's effectiveness, many measurement runs were made as shown in Table 1. In total, 60 measurement runs were conducted over the course of 15 days, producing almost 100,000 files amounting to 22 GB of data. Each test route was repeated three times at each frequency for each equipment configuration. Over the course of the project, much of the data was deemed not useful due to stability, interference, or signal level issues. The final version of the measurement system produced four days of suitable data that was used for analysis purposes.

Table 1. Measurement Data

Date		Route Location	No. of runs	Frequency (MHz)	RTSA Parameters	No. of files	Size (GB)
Version 1	9/11/09	South Boulder	3	183		11,612	2.33
	9/25/09	Table Mountain	5	183,430,915		12,148	1.93
	10/22/09	Downtown	3	183,430,915		11,125	2.26
	11/23/09	South Boulder	2	183		1412	0.29
	11/24/09	South Boulder	6	162		6983	1.30
	11/30/09	SMIQ Fader	3	162	1,2,6 paths	7337	1.66
Version 2	1/20/10	Downtown	3	162		10,625	2.17
	4/9/10	South Boulder	6	162	Acq. Length: 10 sec	4813	2.50
	4/16/10	South Boulder	5	793	Span: 1k,10k,100k	2621	0.16
	4/23/10	South Boulder	4	793	Span: 1k,10k,100k	524	1.13
	4/29/10	Screen Room	2	793	Internal noise test	4067	0.92
Version 3	4/16/10	South Boulder	3	793	Span: 100 kHz Acq. Length: 400 msec RF Attn: 10 dB Ext. 10 MHz Ref. Osc.	4546	0.92
	5/10/10	Downtown	6	793		9015	1.83
	5/17/10	South Boulder	3	162		4466	0.91
	5/19/10	Downtown	3	162		7857	1.60
	5/28/10	SMIQ Fader	3	162	1 path	120	0.25
Total			60			99,271	22.16

4 PROCESSING OF MEASUREMENT DATA

The intent of this measurement project was to determine how well the faded propagation channel can be characterized by the Rayleigh distribution commonly used to describe the statistics of the fading envelope. There are many assumptions regarding the behavior of the propagation channel that have led to the use of a Rayleigh fading distribution. The earliest explanation of the observed fading envelope statistics was carried out by Ossana [3]. Ossana based his explanation on the scattering of reflected waves off randomly aligned flat-sided buildings. Under this assumption, the scattering field can be described by a number of horizontally traveling plane waves with random phase. Clarke [4] suggested a fading model, based on these assumptions, that has been used quite extensively by the scientific community. In Clarke's model, the scattering field experienced at the receiver is comprised of a number of randomly phased horizontally traveling plane waves. Although the introduction of the Clarke model made practical implementations possible given the computing capabilities at the time, in actual practice, Clarke's model has often proved unsatisfactory since the urban environments which generate the scattering field at the receiver can have preferred scattering directions.

Fading models are based on the assumptions that scatterers are uniformly distributed in bearing, have a random phase, and can be represented by horizontally traveling plane waves. However, the models are unable to account for the random orientation of the reflected plane wave or the lack of scattering along a particular arc of bearing. Consequently, most current fading models are considered essentially two-dimensional [5]. There have been a number of modifications to the Clarke model to reduce the discrepancies between measured data and simulations [6]. Real difficulties in validating simulations and measurements arise because the underlying assumptions about real fading propagation channels are too simple.

The modeling assumptions associated with real fading environment can cloud the understanding of the actual physical phenomena that govern fading channels. It is important that the modeling bias (which is necessary to make fading simulators practical) not be taken into account when examining the measured data. In the past, measurements of the faded channel were predominately based on envelope detection techniques. Contemporary measurement equipment can shed new light on the propagation environment since it can easily collect high speed complex samples of the channel. Compared to analog, the discrimination of more complex, digitally modulated signals requires that the radio channel fading mechanisms be better understood. It is important that any conclusions made regarding the faded channel be based solely on the collected data. The processing of the data for this effort was done under the philosophy that only minimal and unavoidably necessary modifications should be made to the data.

4.1 Initial Data File Processing

A list of all routines ultimately used in the analysis of the data is included in Appendix D, along with a brief description of each.

The data from the spectrum analyzer is stored in a proprietary format with the file extension **.iqt*. Once the files were collected and stored on a local data server, the MATLAB® routine *iqt2mat.m* was used to convert the**. iqt* files to a complex array that could be stored in native

MATLAB® format as **.mat* files. The output of the GPS receiver is an ASCII formatted file containing, among other things, absolute position (in latitude and longitude) and speed at a given time. A Python script (*gps_csv_tbe_xx.py*) was written to extract the necessary data, calculate additional values, and create a **.csv* (comma-separated-values) file. The values stored in the **.csv* file include:

- Longitude
- Latitude
- Altitude
- TOW (time-of-week)
- Local time
- Calculated velocity along the path (relative to bearing)
- Calculated velocity relative to the transmitter (radial)
- Velocity measured by the GPS
- Calculated Doppler frequency based on the path velocity
- Calculated Doppler frequency based on the radial velocity
- Bearing

Data from the spectrum analyzer and GPS unit were processed so that each received signal measurement could be synchronized with its associated GPS values.

A number of programs and processing scripts were developed to analyze the data files. Although the data processing techniques evolved over the course of the project, the methods were kept as simple as possible. Preliminary examination of the data was performed in the time domain and later in the frequency domain.

4.1.1 Data File Format

Each 400 msec data file consists of 50 688 quadrature samples collected at a 128 kHz sample rate. To accommodate the synchronization of GPS signals at the transmitter and the receiver, and using the measurement device’s ability to buffer and pre-trigger the measurement, the spectrum analyzer was set to trigger approximately 4 msec before the GPS trigger; therefore, during the first 1% of each data file the transmitter is not on. This initial 1% interval allows the background noise level to be examined.

4.1.2 Data Filtering

Following initial analysis of the data, it became apparent that the noise in the collected data was causing false results. Initial attempts to remove, or minimize, the noise involved characterizing the background noise in the “quiet period” (the first 1% of the data file) and then filtering it from the signal contained in the remaining 99%. Examination of these results suggested that the noise was a combination of environmental noise (which varied as the collection system moved along its path) and noise internal to (generated by) the spectrum analyzer. It was also discovered that the noise level varied according to the sample rate.

Additional study, including measurements taken in a shielded “screen” room, was performed to try to identify the source of this internal noise and explain its dependence on the sampling rate. Although there is no way to definitively prove it (short of disassembling the analyzer and its on-board software), the results of these efforts suggest that, regardless of the set sample rate, the analyzer always samples at its maximum rate of 51.2 Msamples/second and then decimates the data (i.e. throws away periodic samples) to reduce the data to the desired sample rate. Simulations of this decimation technique show that it introduces “processing noise” to the data; the lower the desired sampling rate (the more original samples discarded), the more noise is introduced [14 – Section 10.2].

Since this processing noise is combined with (and cannot be separated from) actual environmental noise, a couple of changes had to be made to the collection process as well as the analysis process. First, all data had to be collected at the same desired sampling rate to eliminate the variation in processing noise level (i.e. to make it constant across all measurements). This meant discarding a number of measurement sets and re-running them.

Secondly, a decision was made to filter the data for those statistical analyses that depend on the degree of time-variance of the signal (level crossing rate and average fade duration). Two value judgments were made in the design of the filter: the type of filter and the cut-off point. After consideration of the data and the environment in which it was collected, a 6-pole Butterworth low-pass filter with a 500 Hz cut-off frequency was used (Figure 8) and was implemented in the program *mat2filt.m*. It is a simple filter that introduces little amplitude distortion, and the cut-off frequency is 3 to 4 times higher than the largest measured Doppler frequency. Examples of the effect of the chosen filter parameters on signal noise are shown in Figure 9.The top two plots ((a) and (b)) show the effect on a relatively strong received signal, where the overall shape of the actual signal can be discerned before filtering. The bottom two plots ((c) and (d)) show the effect on a weak received signal which is on the verge of being overwhelmed by the noise.

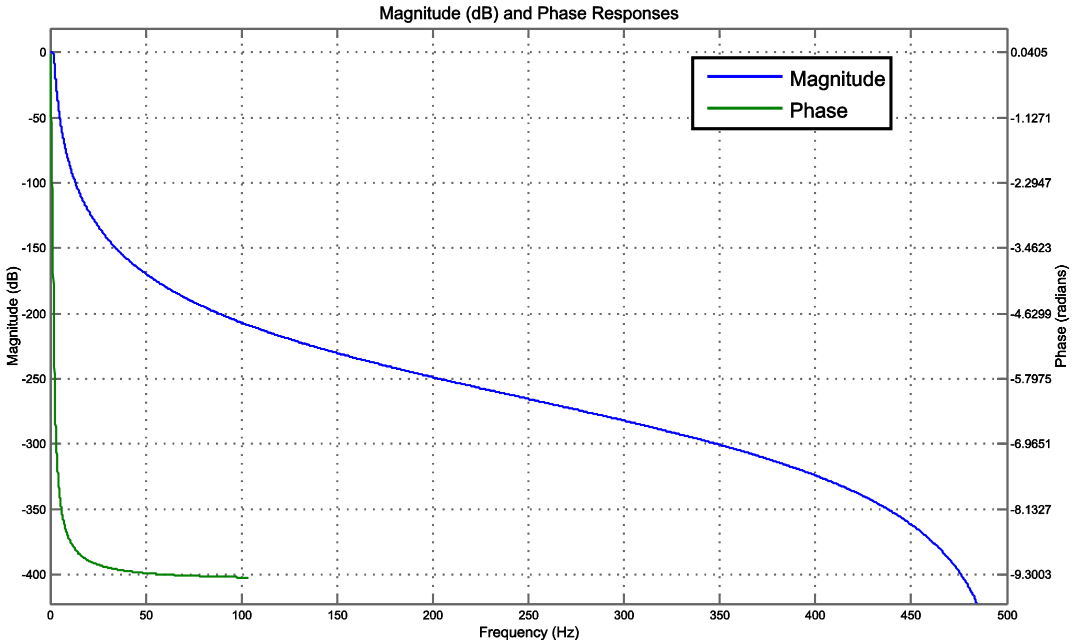

Figure 8. Filter characteristics.

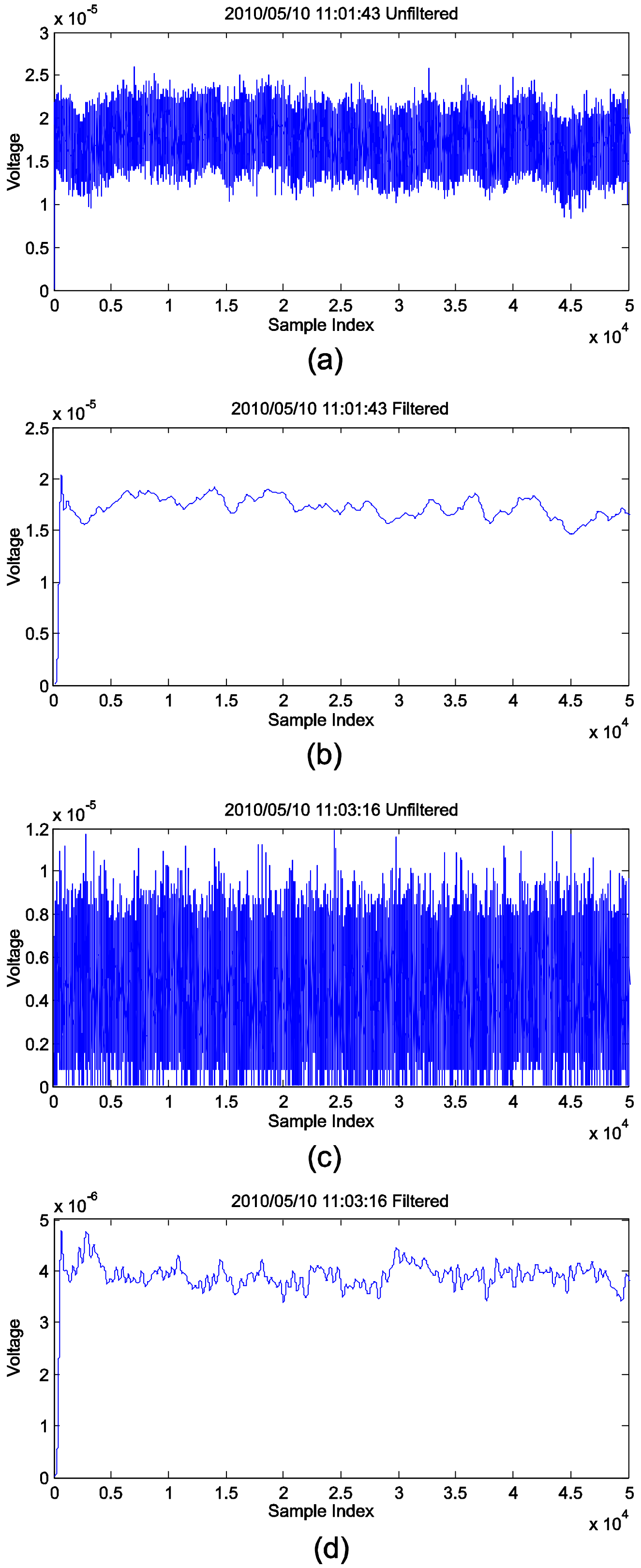
2010/05/10 11:01:43 Unfiltered

2010/05/10 11:01:43 Filtered

2010/05/10 11:03:16 Unfiltered

2010/05/10 11:03:16 Filtered

Figure 9. Examples of filter effect on signal amplitudes (high-amplitude: unfiltered (a) and filtered (b); low-amplitude: unfiltered (c) and filtered (d)).

One drawback to this filter is its undesired effect on the phase of the signal. This becomes an issue when trying to calculate the phase correlation coefficient necessary in one of the TIA tests (see Section 5.4). As can be seen in Figure 10**Error! Reference source not found.**, the noise (both environmental and processing) causes strange results when trying to "unwrap" the phase (more extreme results can be seen in Figure 19). Unwrapping is a process that eliminates the 0→2π transition (wrap-around) in the phase measurement; its use is necessary when performing the correlation function on the phase signal. Figure 10 shows the effects of filtering and unwrapping on the phase of both strong and weak received signals. The left column shows a strong signal, the right column a weak signal. Plots (a1) and (b1) show the phase of the original, unfiltered, signals; (a2) and (b2) show the filtered, wrapped, phases; (a3) and (b3) show the unfiltered, unwrapped phases; and (a4) and (b4) show the filtered, unwrapped phases. Unwrapping has no effect on the weak signal's phase since it never exceeds ±π, but it is worth noting that filtering reverses the slope of the phase's trend compared to (b3). Because the phase signal after filtering is suspect, further study is needed to determine the best way to minimize the effect of noise on phase-related analysis methods.

Once the files were filtered, the quiet time at the beginning of each file remained. As is shown in the next section, the location of the transition point varied from file to file. To assure that the quiet time and the transition point were not included in the data analysis, the first 2000 samples of each measurement were ignored by all analysis routines.

4.1.3 Selecting Data Files for Analysis

The range of signal amplitudes varied greatly (in orders of magnitude) as the data collection system travelled along its route. Physically, the path conditions between the transmitter and the receiver ranged anywhere from conditions where a single, predominant reflected ray existed to strong shadowing conditions where all the scattered rays were below the level of the environmental noise. Where the latter conditions prevailed, not all of the data collected could be analyzed since the signals in strong shadowing environments could not confidently be separated from the noise, so that any analysis performed on such measurements would give suspect results. On the other hand, measurements showing very high signal levels (indicative of a Rician condition of line-of-sight or where a strong reflected ray predominated) were outside the scope of this study; radios are expected to function properly in these conditions. What this study is interested in are those situations where the signal detected at the receive antenna is a combination of multiple reflections, refractions, diffractions and diffusions of the transmitted signal, and whether the signal detected in those situations exhibits Rayleigh characteristics.

Since noise determines the lower limit of signal detection, the calculated signal-to-noise ratio (SNR) was used to select those data sets that displayed mid-range signal strengths, which were presumed to have no LOS component, and whose strength was presumed to be sufficiently greater than the combination of environmental noise and the noise floor of the instrument. The first attempt to calculate SNR was performed in the time domain. The intent was to measure the noise level in the first 1% (the quiet period) of the data file versus the signal level in the remaining 99%. This calculation was performed on unfiltered data since the filtering removed the noise. However, since the signal in the last 99% of the file was a combination of the received signal and noise (environmental and processing), the calculated value actually was a signal-plus-noise-to-noise ratio ((S+N)/N).

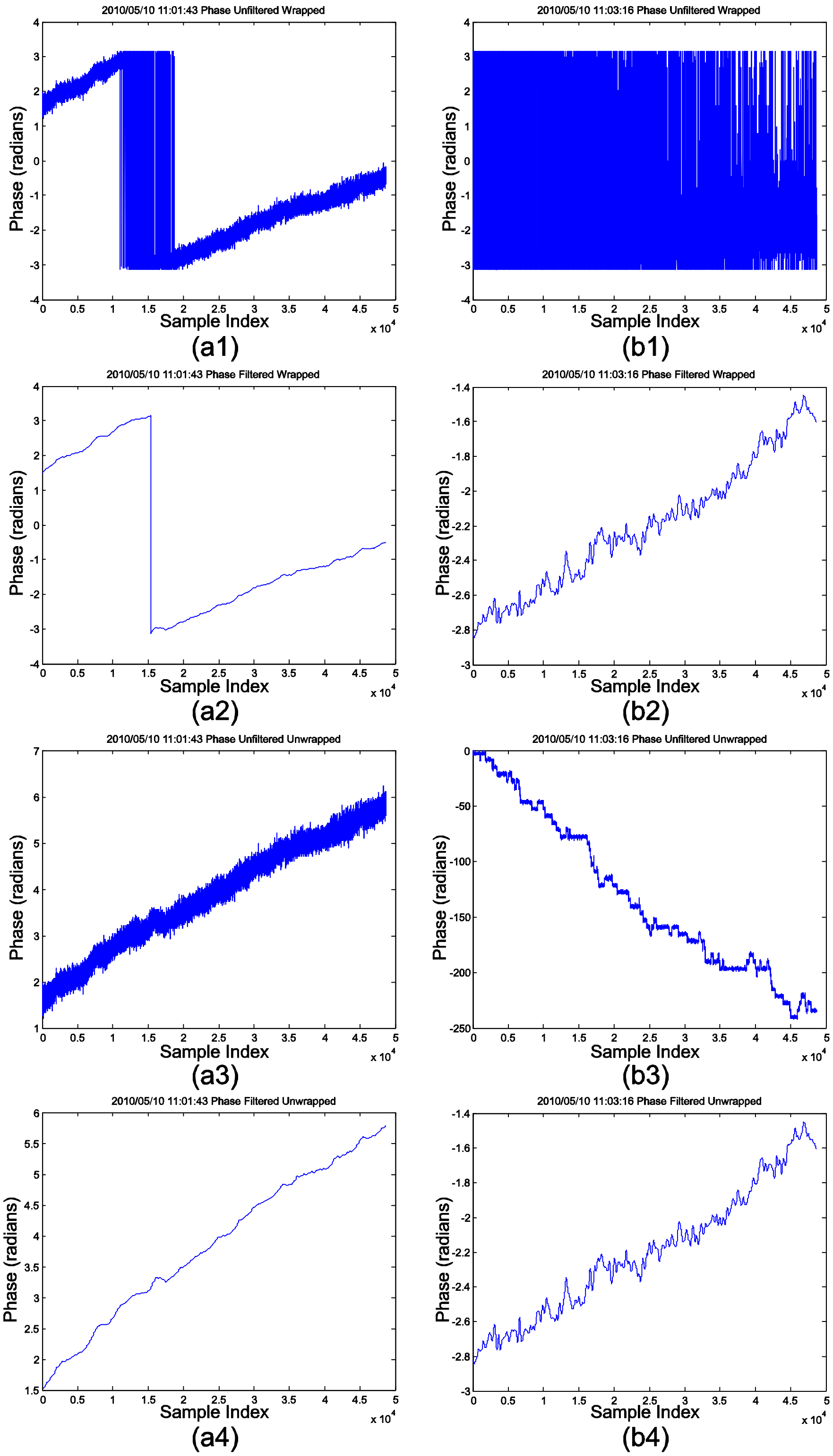

Figure 10. Examples of filter effect on signal phase. Left column is a strong signal; right column is a weak signal. Figures (top to bottom) show wrapped phases of unfiltered signals, wrapped phases of filtered signals, unwrapped phases of unfiltered signals, and unwrapped phases of filtered signals.

This method proved to be unsatisfactory. It became apparent that the transition point between the noise and the signal (the point at which the transmitter turned on) was not reliably constant (Figure 11). Since this was discovered after the measurements were performed, it cannot be determined why this occurred. Perhaps there was enough discrepancy between the GPS signals at the transmitter and receiver ends to cause the transmitter's turn-on time to drift within the measurement window. Whatever the case, a consistent transition point in the data file could not be assumed.

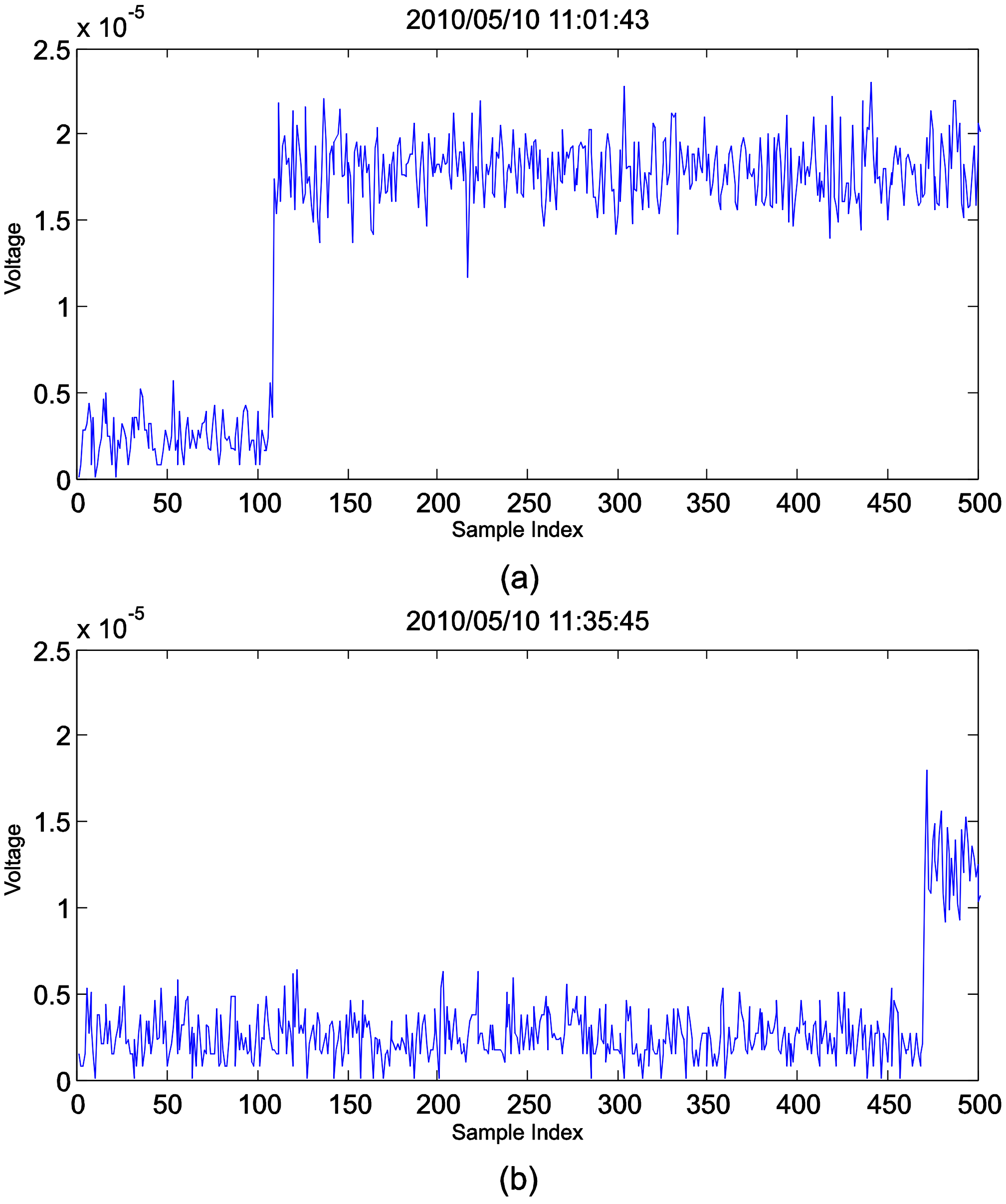

Figure 11. Example of the variation of transition time occurrence.

Since it was necessary to detect the transition point in each data file, the signal's amplitude was differentiated and the highest value was located (**Error! Reference source not found.**Figure 12). This worked when the received signal's amplitude was significantly higher that the noise level, but in those cases where the signal’s time-domain characteristics were obscured by the noise (but not to the extent of rendering the data unusable), the transition point could not be reliably detected. As seen in plot (a2), the peak level clearly corresponds to the turn-on transition point around sample 100, but in (b2), the peak level corresponds to a period in the signal around sample 590; the actual transition point is around sample 100. After examining a number of other weak signal cases, it was apparent that another method to calculate SNR had to be used.

Calculating the SNR in the frequency domain eliminates the need to determine where the transition point occurs and separates the noise from the signal, resulting in a true SNR calculation. The method that was eventually used is shown in Figure 13a and 13b and was implemented in the program *dir_scan.m*. First a fast Fourier transform is performed on the data file (minus the first 2000 samples to eliminate the quiet period) and is converted to power. Then the peak value is detected (plots (a3) and (b3)). The mean noise level is calculated by discarding the upper and lower 5000 values and 20 values either side of the peak and taking the mean of the remainder (plots (a2) and (b2)). The ratio of the detected peak value to the calculated mean noise level was used as the SNR value and was saved, along with the data file’s name, in an array in a **.mat* file.

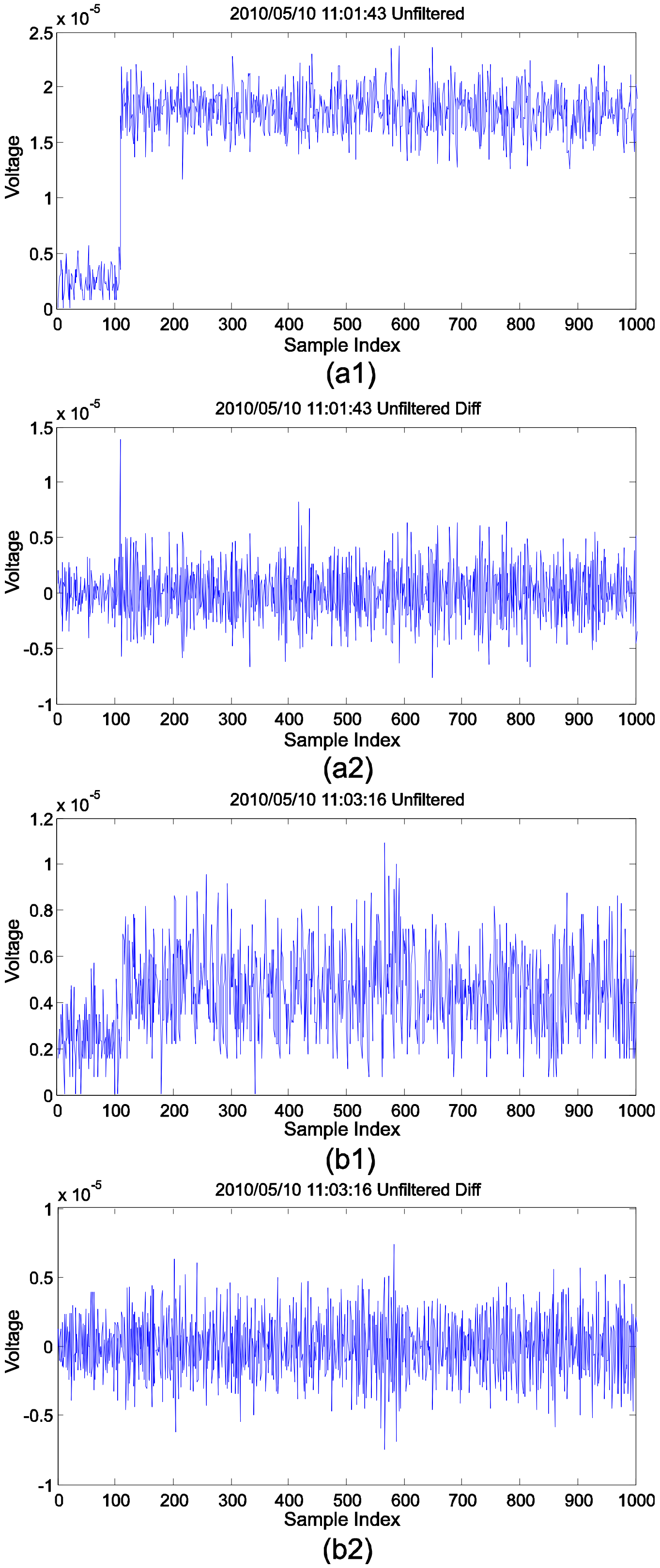

Figure 12. Examples of the transition point in strong (a1) and weak (b1) signal data files. Plots (a2) and (b2) are the respective differentiated signals.

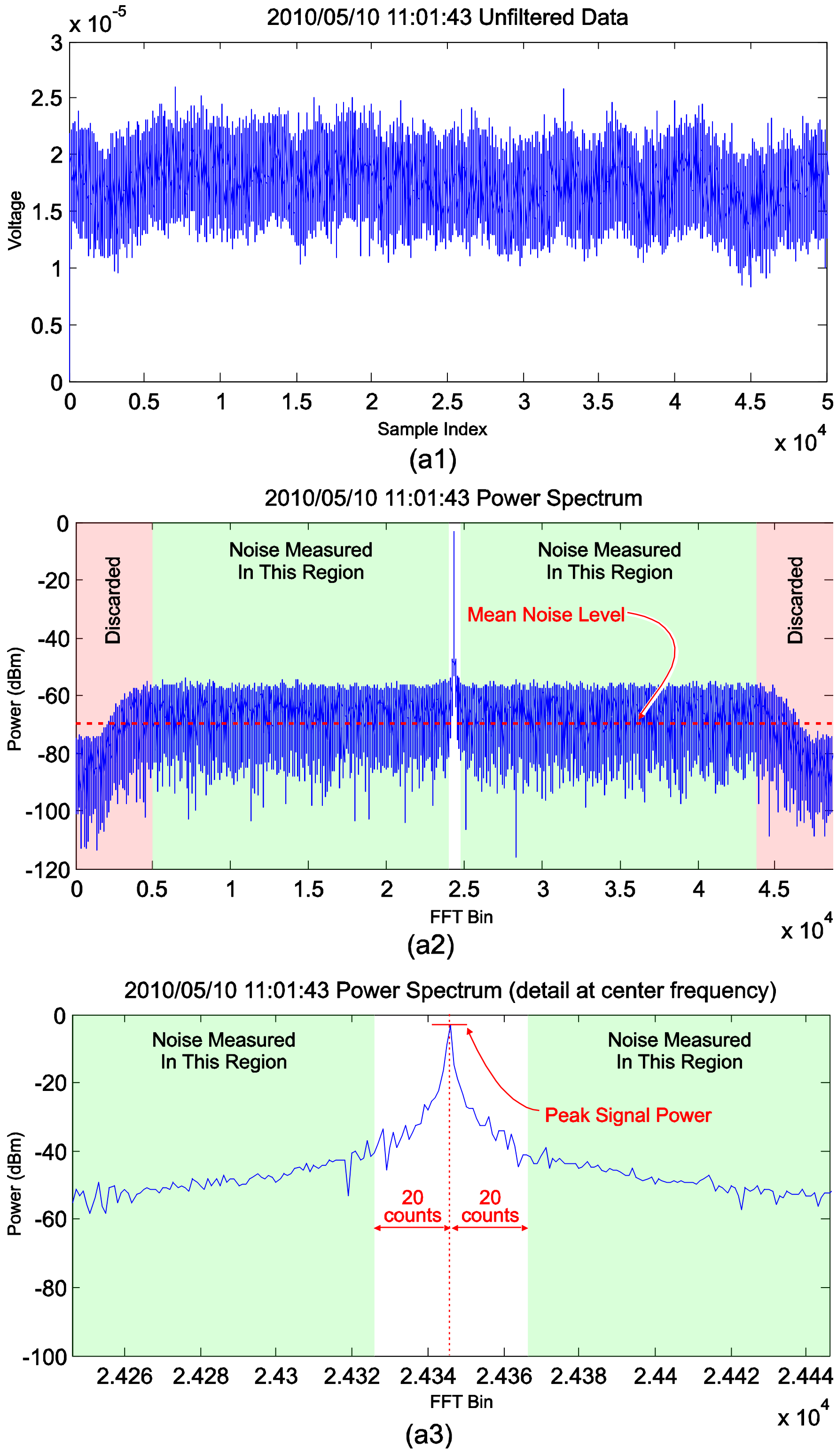

Figure 13. Example of calculating the SNR of a strong signal (a1) in the frequency domain. Plot (a2) shows the regions where the noise is measured and (a3) shows enlarged detail in the vicinity of the peak.

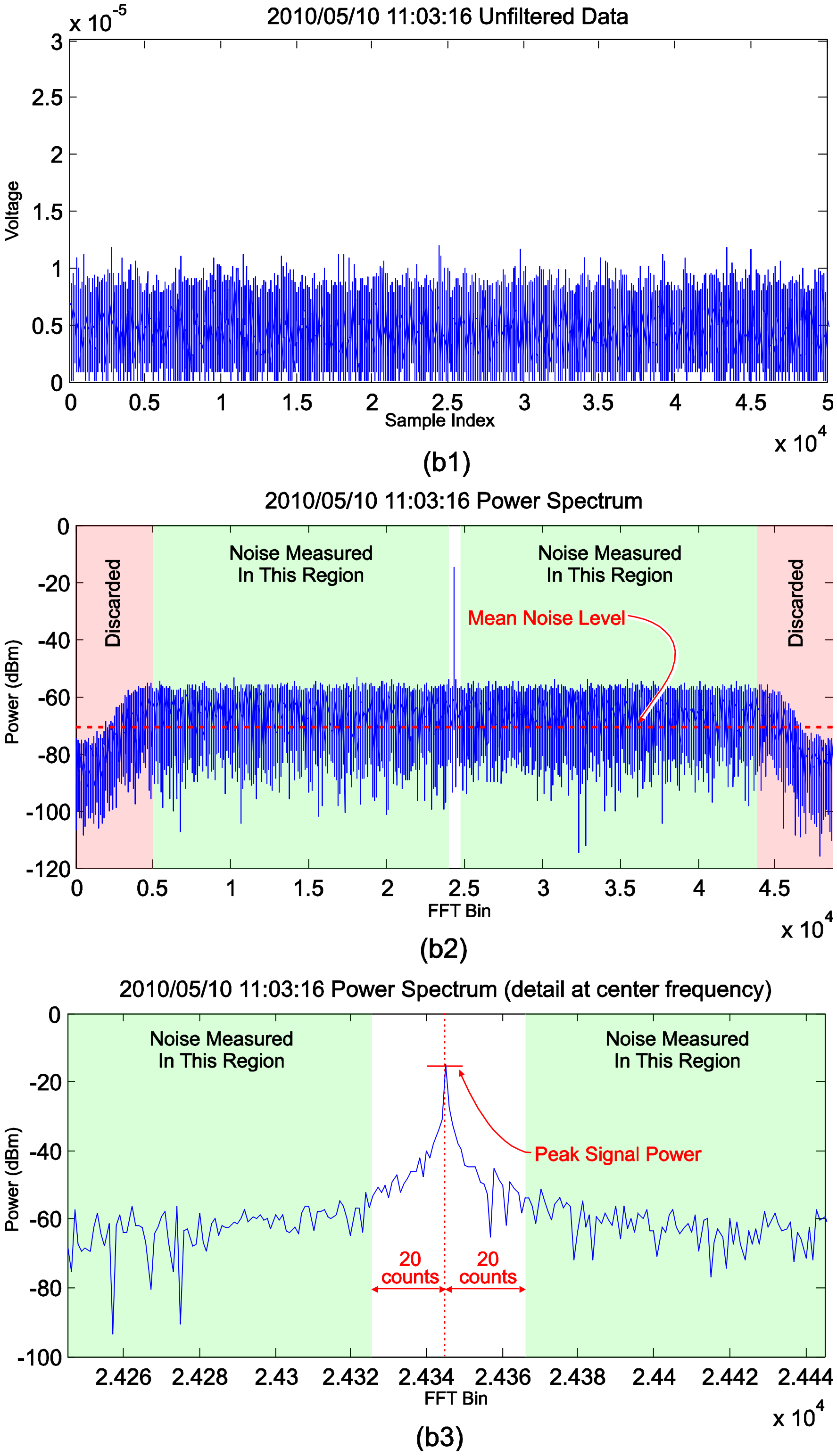

Figure 14. Example of calculating the SNR of a weak signal (b1) in the frequency domain. Plot (b2) shows the regions where the noise is measured and (b3) shows enlarged detail in the vicinity of the peak.

A second program (*snr_freq_cull.m*) then took this array and created a second array of those files that fell within a middle range of SNR values. This range was based on the need to exclude the outer limits of SNR values and reduce the number of data files that needed to be analyzed to a manageable amount but still be statistically significant. A range about the mean SNR of ± (0.5 × standard deviation) appeared to result in a reasonable statistical population (Table 2), but further analysis should be done on the optimum sorting range or method. A final program (*SNR_sort.m*) then took the sorted array and used it to separate the "accepted" data and analysis files from those "rejected." All files were retained, but further analysis was only performed on the "accepted" data files.

Table 2. Count of data files that were "accepted" and "rejected" for each measurement run based on calculated SNR values.

Date	Run #	Total Data Files	# Accepted Files	# Rejected Files
04/16	1	1500	436	1064
04/16	2	1500	489	1011
04/16	3	1526	446	1079
05/10	1	3020	1193	1827
05/10	2	2775	1021	1754
05/10	3	3220	1228	1992
05/17	1	1525	629	896
05/17	2	1465	553	912
05/17	3	1476	570	906
05/19	1	2857	984	1873
05/19	2	2550	935	1615
05/19	3	2450	931	1519

Note: due to timing issues, the spectrum analyzer would occasionally save two successive data files with the same time stamp. Since this happened so rarely, the analysis programs were not written to accommodate this anomaly and would therefore overwrite the analysis of the first data file with that of the second. A result of this action means that the sum of the number of accepted data files and rejected data files will occasionally be less than the overall total number of data files.

All of the analysis routines were written to process entire runs at a time. Even after culling the data files based on SNR, approximately 9000 files remained to be analyzed—too many files to examine individually. To reduce the number to a more manageable population, a random sample of files was selected from each run. Ten files from each day were chosen based on an observation of the results of TIA test (e) (see Sections 5 and 5.1), the Cumulative Probability Distribution Function (CPDF). An effort was made to equally select files that exceeded the expected CPDF, met the expected CPDF, and were less than the expected CPDF. In addition, the files for three consecutive seconds from Run 1 on May 17th were also selected. All analysis results for these selected files are presented in Appendix E. The same files were also used to compare the signal's actual probability distribution function to several predicted (ideal) distributions. Plots of these comparisons are presented in Appendix D.

4.2 Single File Histograms

The Rayleigh distribution can be described by a single shape variable α, which is also the distribution mode:

$$pdf\,(x,\alpha)=\frac{x}{\alpha^2}e^{-x^2/2\alpha^2}. \tag{1}$$

A family of Rayleigh distributions for various α is shown in Figure 15.

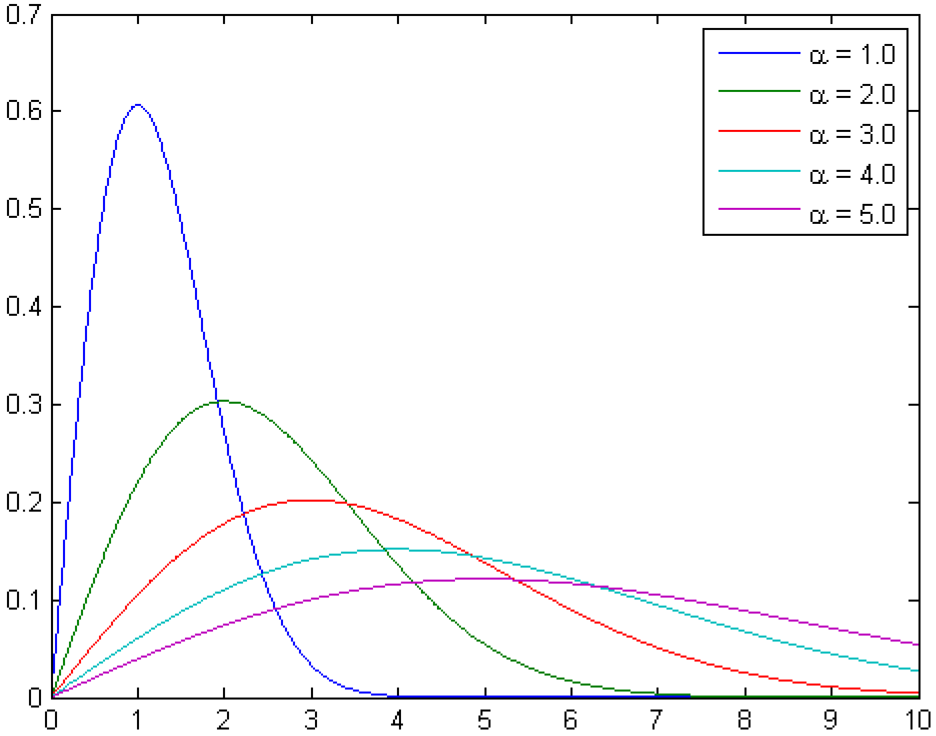

Figure 15. Normalized Rayleigh PDF.

For each data file, a histogram of the voltage envelope (the magnitude of the measured data) was created. The voltage envelope was normalized so it could be compared to the Rayleigh PDF. The 1% quiet period at the beginning of the data file was ignored. Examples of histograms of four randomly selected 400 msec blocks are seen in Figure 16.

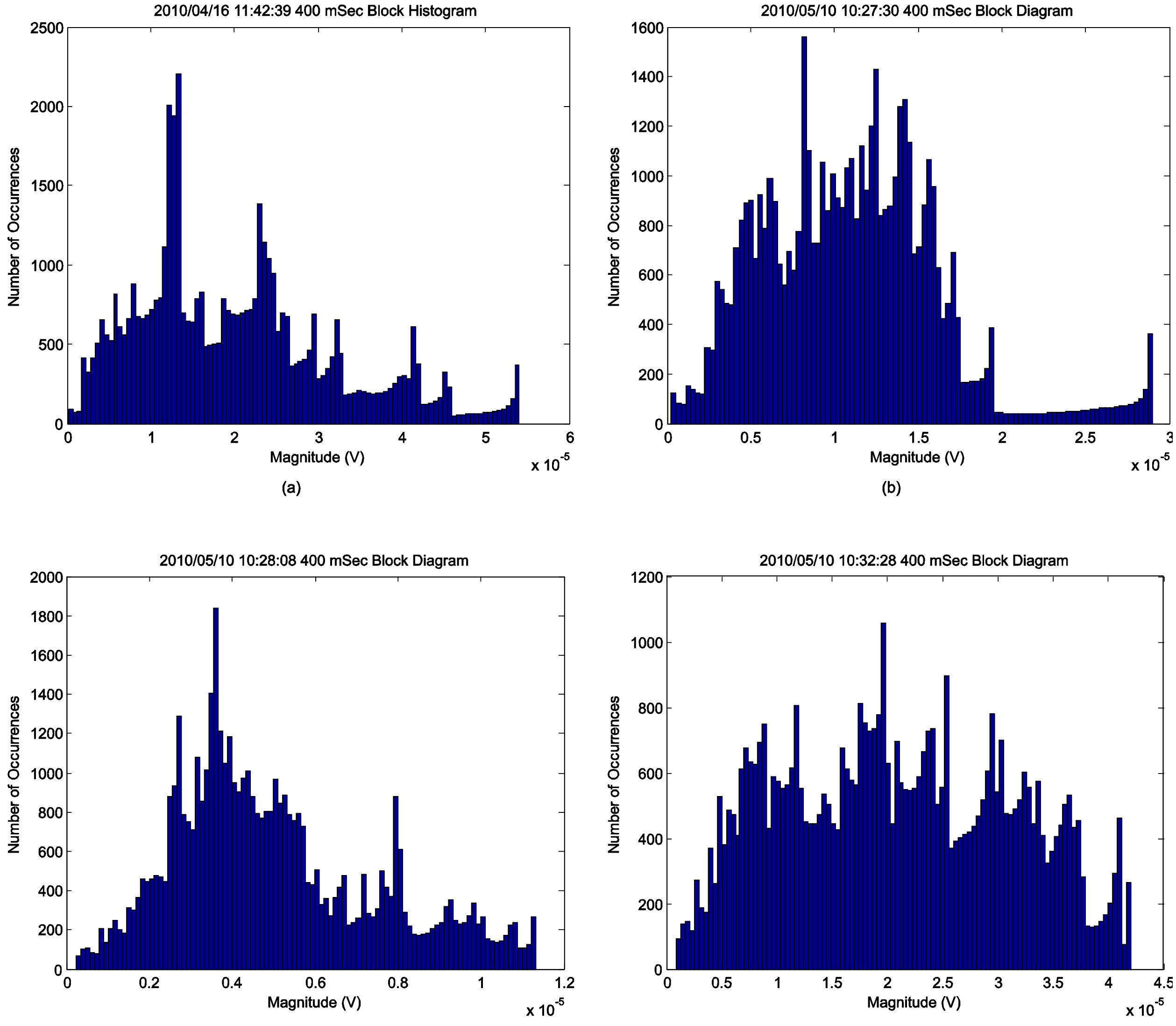

(a) (b) (c) (d)

Figure 16. Histograms of the voltage envelope of sample data files.

These histograms clearly show that a more complex environment was measured than the curves in Figure 15 would predict. There are more than enough points in the data files to render smooth histograms if the measured environment was truly Rayleigh. The evidence for this assertion is based on the level crossing rate equation for a Rayleigh process (see Equation 3 in Section 4.3). Solving this equation for a worst case scenario of 793 MHz and a test taken at 60 mph (corresponding to a Doppler frequency of 70.90 Hz) shows that sampling at 128,000 samples per second should yield a 50% detection probability for fades down to 147 dB below the RMS average, far beyond the dynamic range of our measurement system.

Many of the histograms, like the examples in Figure 16, suggest that the scattering environment is actually multimodal. The scattering sources in the actual environment appear to induce scattered signals with discrete amplitudes. The peaks in these examples that are preceded by a ramp (such as the one on the far right side of Figure 16(b)) indicate that a single fade peak could be resolved in the received signal. This is also true for fading minima.

The filtered time domain voltage envelope for Figure 16(b) can be seen in Figure 17. The major peak that appears at approximately the 50 µsec point of Figure 17 is what causes the final ramp and peak in the PDF for Figure 16(b). A multitude of these types of structures in the histogram indicate that individual fading peaks can be easily resolved.

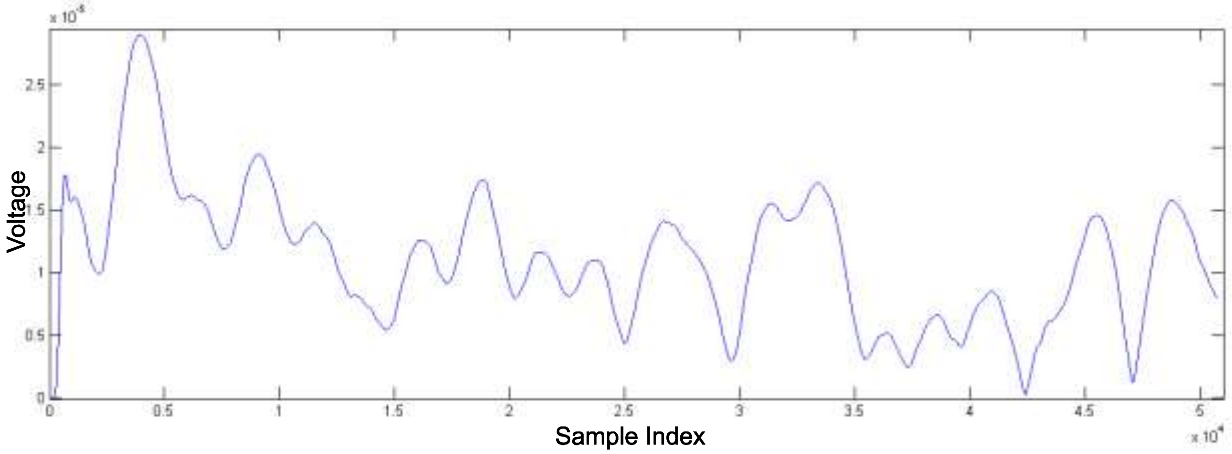

Figure 17. Filtered time domain plot of the voltage envelope for file 2010/05/10 10:27:30 (Figure 16(b)).

Unfortunately, there is no implicit time interval when using the Rayleigh fading model to represent the propagation channel; in other words, the use of a Rayleigh model to describe the fading channel is independent of time. Over all of the intervals the channel should theoretically be Rayleigh. Simply to argue that there is not enough data in these examples is to confirm limitations of the Rayleigh model and affirm the central limit theorem (CLT). Over a long enough time period, the I and Q channels will appear Gaussian because of the CLT. This is exactly what Jakes showed in his examination and modeling of faded channels [7]. If two Gaussian independent and identically distributed (IID) I and Q channels are combined, then the resultant voltage envelope will be Rayleigh. Consequently, for a long enough interval, the voltage envelope would necessarily display a Rayleigh character. But the Rayleigh fading model indicates that the characteristics of fading are the same over all time intervals. Thus, if a Rayleigh distribution adequately describes a real channel it must be independent of the time interval.

The only problem with this reasoning is that, according to the CLT, the distribution of the fades could be seen as a multitude of forms over shorter time intervals, which can cause errors in the transceiver. It is this possibility that is of greatest importance to reliable communications. The time frame of importance here depends on the complexity of the transceivers under test. For a system using a slow symbol rate with simple modulation, Rayleigh may represent an adequate model of the channel. But as the symbol rate increases and the modulation scheme becomes more complex, the time frame necessary to establish Rayleigh statistics in a simulator may cause the channel model to be incorrect. Issues of simulation aside, it is of utmost importance that the real channel be characterized faithfully. By restricting the measurement window to 400 msec, these examples seem to indicate that a Rayleigh distribution of the fading envelope might not be a good representation. To decide if this is really the case, the interval that causes errors in the transceiver must be determined.

There is a danger in basing any decision on histograms alone because many of the real characteristics of the signal, such as those in the time domain, are lost. This is why other statistical measures must be examined.

4.3 Second Order Statistics

Second order statistics are used to examine the more subtle character of signals. Second order statistics were used to refine adherence to the Rayleigh fading model [8], [9]. In this examination, second order statistics can be used to view some of the time characteristics of the signal. In this regard, the level crossing rate (LCR) and the average fade duration (AFD) are most commonly used. The LCR gives an indication of the rate at which fades are occurring in the channel while the AFD gives an indicator of the length of the fade. In the case where the receiver SNR threshold is known, the LCR and AFD can help to explain why particular fading conditions cause a radio to lose lock or generally experience symbol errors. For stochastic models of the channel, the LCR and AFD can be found from the equations that describe the fading distribution.

There are well known equations that describe the second order statistics of Rayleigh distributions [10], [11]. The normalized level crossing threshold for the voltage envelope is defined by:

$$\rho = \frac{R_{Threshold}}{R_{rms}} \tag{2}$$

where R is the amplitude of the signal in volts. The LCR also is a function of the Doppler frequency f_d:

$$LCR = \sqrt{2\pi}\, f_d \rho e^{-\rho^2} . \tag{3}$$

Like LCR, the average fade duration (AFD) of the voltage envelope is both a function of f_d and ρ:

$$AFD = \frac{e^{\rho^2} - 1}{\rho\, f_d \sqrt{2\pi}} . \tag{4}$$

These two equations are the ideal that any Rayleigh-characterized fading channel will approach.

To determine the LCR and AFD from the measurement data, the Doppler frequency must first be calculated from the GPS data. The locations contained in the GPS data were used to calculate the great circle distance between measurement points and, therefore, the instantaneous path velocity. The path velocity can be used to determine the Doppler frequency by $f_d = \nu/\lambda_0$. The path velocity is used rather than the velocity relative to the receiver based on assumptions implicit for Rayleigh scattering.

The LCR is determined by finding the range of values of the normalized voltage envelope (ignoring the 1% noise measurement at the beginning of each file), and then counting the number of times the signal crosses any arbitrary value in the normalized voltage envelope range. The resultant count is then divided by the total time of the measurement. At a given threshold, the rate can be determined from the number of either positive or negative threshold crossings. The LCR is specified in crossings per second.

The AFD is found by examining the measured waveform and determining the average length of time that the signal is below a given threshold. The AFD is given in seconds.

The calculated LCR and AFD can then be compared with the theoretical Rayleigh distribution derived curves (Figure 18). How closely the measured data follows the theoretical curves can be used as an indicator of how closely the channel can be accurately characterized as Rayleigh.

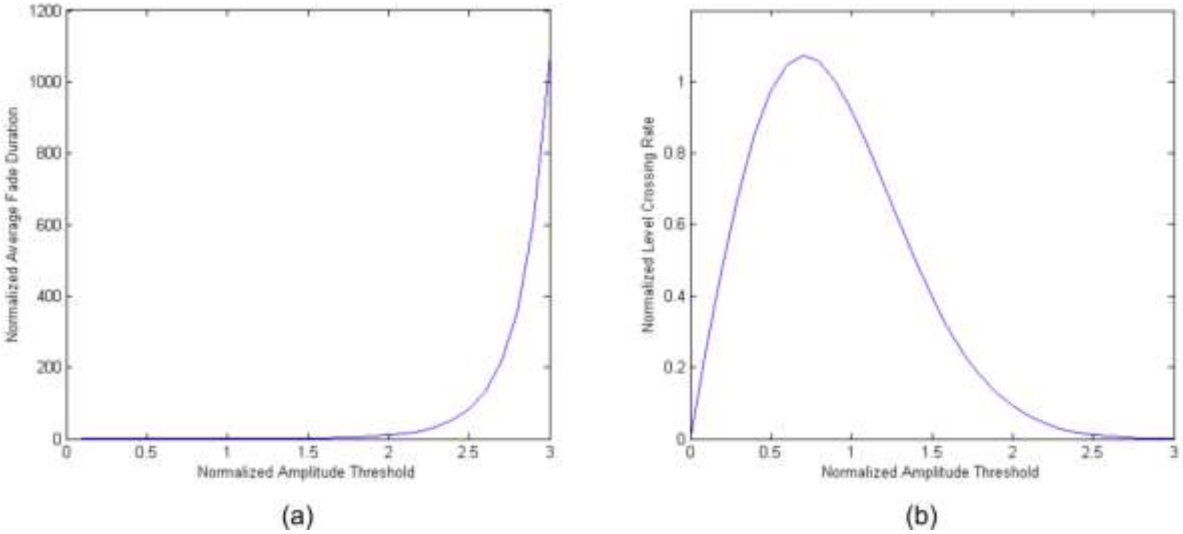

Figure 18. Theoretical Rayleigh curves for AFD and LCR.

5 SIMULATOR SPECIFICATIONS IN TIA-102.CAAA-B FADED CHANNEL CHARACTERISTICS APPLIED TO MEASURED DATA

The Telecommunication Industry Association (TIA) has developed a series of measurement methods for Project 25 radios [12] which include a description of the characteristics for a faded channel simulator that should be used to measure the performance of C4FM/CQPSK transceivers. These characteristics are listed as a series of tests the simulator must meet to qualify under the TIA standard (see Appendix C for the relevant text). Although the tests are defined for simulating a fading environment, they were used in this study to give an indication of how well they characterize the measured channel. In particular, tests (e) through (h) were given the most attention since the other stipulated tests of a TIA-102-based simulator were either trivial or not controllable with the present measurement system design. For instance, the measurement system developed for this study had no way to keep the velocity consistent or limit the fading centers to two rays. The motivation for many of the TIA tests is unclear in the standard; one must assume why they were included.

Results of the TIA tests on selected data files (based on the criteria described at the end of Section 4.1.3) appear in Appendix E. The files were selected because they either represent typical behavior or are anomalous. For each data file, six plots are presented: the voltage histogram, the PDF, the AFD and the results of TIA tests (e) through (g). The results of test (h) were not included in Appendix E because it simply requires that the simulator meet error criteria at two points.

5.1 Test (e)—Cumulative Probability Distribution Function (CPDF)

This test can be considered another aspect of a first order statistic. The CPDF can be used as a statistic to indicate if the channel exceeds the probability that the fading envelope exceeds that predicted by a Rayleigh distribution. The independent variable in this case is the normalized envelope power threshold value P/P_{ave}. The simulation error is stated to be within ±1 dB for 10 dB above to 20 dB below the mean power. Additionally, from 20 to 30 dB below the mean power, the simulation error should be ±5 dB. Measurements that exceed this lower threshold give a good indicator that the measured channel is “worse than Rayleigh.” Of course, these are lower probability events, but this is expected since deep fades are, it is to be hoped, rare occurrences. This is presumably why the threshold is wider in these cases.

5.2 Test (f)—Level Crossing Rate

Unlike typical normalization, the level crossing rate in this test uses the envelope power average instead of the envelope RMS value. It was assumed that for the duration of each individual measurement the speed was constant. The level crossing rate gives an indication of the volatility in the channel. A consistently large level crossing rate indicates that an elevated number of fading events are rapidly moving through the channel. Rayleigh statistics dictate the level crossing rate relative to the Doppler frequency, in other words, the Rayleigh level crossing rate is proportional to Doppler frequency. This is presumably why the threshold for the LCR is given as a function of vehicle speed. The LCR is required to remain in a ±10% velocity threshold between 3 and -30 dB of the mean power.

5.3 Test (g)—Power Spectral Density

The power spectral density gives an indication of how well the simulated, or in this case measured, signal's power is restricted to within a window of ±5% of the theoretical Doppler frequency offset associated with the vehicle speed. In the ideal case, it is well known that a Rayleigh modeled fading signal's power spectrum will not exceed $\pm f_d$. For the Rayleigh fading model at any instant, the receiver can, at the extremes, be traveling directly toward or directly away from any given scatterer at the path velocity. This test gives an indication of how well the simulation has approximated the uniform distribution of scatters around the receiver.

5.4 Test (h)—Correlation Coefficient of the Phase

Test (h) is the only test where the phase of the signal is taken into consideration; all other tests are concerned only with the signal's magnitude (power). Due to the complexity of modern signals and their reliance on multi-level phase modulation, the channel's effect on the signal's phase could be more critical than first- or second-order effects on the signal's power. This test measures the value of the correlation coefficient of the unwrapped phase at two points, lags based on the Doppler frequency ($0.05/f_d$ and $0.15/f_d$).

Because a filter introduces undesirable effects on the signal's phase, test (h) is performed on unfiltered data. As a result, test (h) turned out to be the most problematic of all of the TIA tests, since unwrapping the phase of a noisy signal gives somewhat suspect results. Figure 19 shows two examples of the results of TIA test (h). The left column (a1-a4) shows the results of a data file that passes both requirements of test (h), while the right column (b1-b4) shows the results of a data file that fails both. Plots (a1) and (b1) show the unfiltered amplitude of the signals. Plots (a2) and (b2) show the wrapped phase of the signals, while plots (a3) and (b3) show the unwrapped phase. Plots (a4) and (b4) show the correlation coefficients of the unwrapped phase. The pink bands show the acceptable ranges where the correlation coefficients should lie at the two specified lag points. In (a4), both points fall within the acceptable ranges. In (b4) one point (the $0.05/f_d$ value) falls outside of the range while the other is entirely outside of the range of the calculated correlation coefficient.

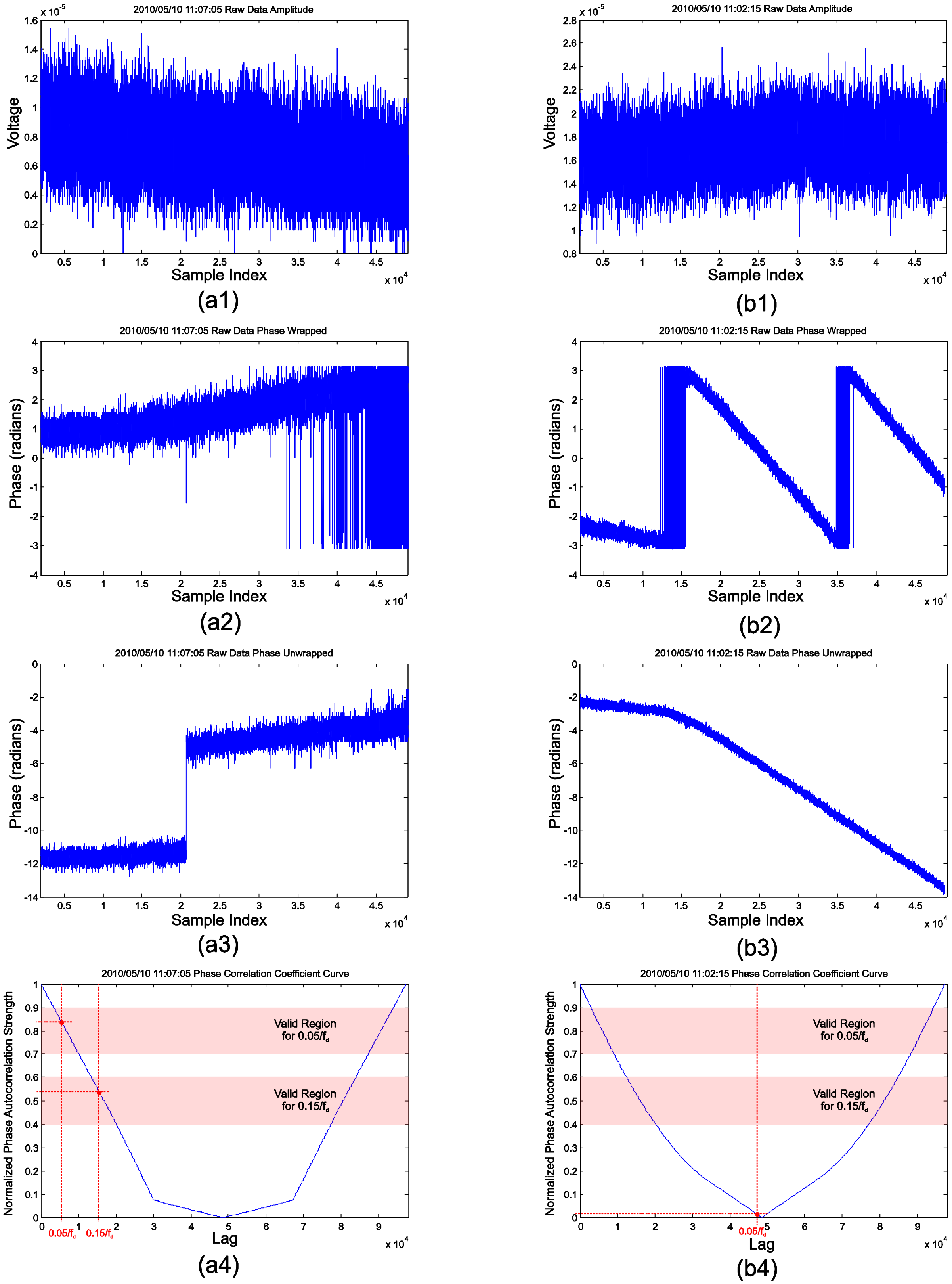

Figure 19. Correlation coefficient curve of sample data files (passing (a1-a4) and failing (b1-b4)) and target value locations.

Two things should be noted. The first is that the trends of the unwrapped phases are opposite in direction. The second is that the step in (a3) cannot be verified; it may be an artifact of the unwrapping algorithm brought on by the spike visible in (a2) at that point. Whether or not these two observations are indicative of the end results was not determined.

Table 3 lists the number of data files that pass TIA test (h) for all 12 measurement runs. As can be seen, the numbers of files that pass are extremely small, but a trend is somewhat apparent, in that more measurements taken in the low-rise urban setting pass the test than measurements taken in the residential setting, and more measurements pass at the 162 MHz frequency than at the 793 MHz frequency. Additional effort must be made to determine the validity and accuracy of the test and to validate the correctness of the phase unwrapping algorithm when used on a noisy signal.

Table 3. Results of TIA test (h) on accepted records

Date	Run #	Frequency (MHz)	Route Setting	Total “accepted” records tested	Number of records where CorrCoeff at 0.05/f_d lag meets requirement	Number of records where CorrCoeff at 0.15/f_d lag meets requirement	Number of records that meet both requirements	Percentage passed
04/16	1	793	residential	436	2	1	0	0%
04/16	2	793	residential	489	5	0	0	0%
04/16	3	793	residential	446	5	0	0	0%
05/10	1	793	urban	1193	98	45	33	2.8%
05/10	2	793	urban	1021	73	30	29	2.8%
05/10	3	793	urban	1228	132	55	44	3.6%
05/17	1	162	residential	629	20	6	5	0.8%
05/17	2	162	residential	553	12	2	2	0.4%
05/17	3	162	residential	570	17	5	5	0.9%
05/19	1	162	urban	984	245	88	72	7.3%
05/19	2	162	urban	935	157	68	62	6.6%
05/19	3	162	urban	931	166	65	56	6.0%

6 CONCLUSION

Section 1 discusses the fact that the Rayleigh fading model has been the most widely used distribution model since it is considered to represent the worst-case propagation condition. A re-evaluation of the fading channel was undertaken to determine if Rayleigh fading model assumptions are valid for digital modulations with ever-increasing bit densities. The results shown in this report indicate that there may be other distributions that more accurately represent fading conditions used for public safety communication.

Section 2 describes how the measurements were conducted in a phased and iterative approach. Sound measurement design principles guided this methodology. Measurement accuracy was accomplished through preliminary data analysis of each measurement, with system improvements suggested by the analysis incorporated into successive versions of the system. Development of the final mobile measurement system proceeded from a lab prototype through two intermediate iterations to a final system design used to take the measurements ultimately analyzed. The lab system consisted of a signal generator, an arbitrary waveform generator, GPS receivers, a real-time spectrum analyzer, and antennas. To improve the accuracy of the system, hardware improvements were integrated into later versions which included more advanced GPS receivers, tuned antennas, tuned cavity filters, and a power amplifier. Equipment configurations were also modified to improve the accuracy of the measurements. In particular, the RTSA was used in several configurations to determine the effects that different spans, sampling rates, acquisition lengths and attenuation levels had on the accuracy of the measured data.

Section 3 describes the measurement environments. Measurements were performed over multiple environments that consisted of rural, residential, and low-density urban locations. These three locations provided a variable scattering environment. The rural environment consisted of a route at the Table Mountain field site, the residential environment was a route in south Boulder, and the low-density urban route was in downtown Boulder. The Table Mountain route was deemed unsatisfactory to evaluate fading because of the lack of fast-fading behavior. Measurements were conducted at test frequencies of 162 MHz and 793 MHz to represent P25 and future public safety communications bands. A fading channel simulator was also used to gather data from a simulated faded signal against which the measured data could be compared. The amount of collected data consisted of 60 measurement runs conducted over the course of 15 days, producing almost 100,000 files equaling 22 GB of data.

Section 4 describes efforts to analyze the data and compare it to Rayleigh characteristics. Processing of the measured data consisted of selecting suitable files for analysis and then applying first and second order statistical analysis using MATLAB® code developed specifically for this task. Data file selection was performed to eliminate measurements taken near or below the measurement system’s noise level. The file selection process was challenging and resulted in multiple attempts to acquire a suitable number of measurements. After the file selection, noise filtering was performed to reduce the noise component in the measurement files. The first order statistics consisted of histograms of the measured data. Second order statistics consisted of the level crossing rate (LCR) and the average fade duration (AFD), which provided evidence to determine if the channel appears Rayleigh in nature.

Section 5 describes how the faded channel simulator characteristics specified in TIA-102.CAAA-B were referenced and compared to the measured data. Four statistical tests were performed on the measured data as well as on the simulator data; specifically the CPDF, LCR, power spectral density, and the correlation coefficient of the phase were calculated. The number of measurement files that passed these tests was very low and future analysis is needed to determine the reasons for this occurrence.

In Appendix B, the P25 error detection and correction coding was analyzed to estimate the limitations of its error correcting capability in the presence of fading. The points at which non-recoverable errors may occur were determined and noted. The principle vulnerability in the P25 signaling is the uncoded frame synchronization sequence, transmitted at the beginning of each data unit.

6.1 Fading is a More Complicated Phenomenon than is Perceived

Multipath fading is typically modeled as a Rayleigh distribution in the absence of LOS propagation. The Rayleigh distribution assumes a combination of multiple signals with various identical signal strengths and uniform phase distributions. Implicit in the physical realization of a Rayleigh faded channel is the physical presence of enough scatterers so that the Central Limit Theorem assures that the combination of the individual distributions results in Gaussian distributions of the I and Q signals. In turn, the presence of Gaussian distributed IID [13] quadrature components results in a Rayleigh distributed magnitude. Constructive and destructive interference of the multiple scattered wavefronts results in a Rayleigh faded voltage envelope occurring at the receiver.

Why is real-world fading more complicated? In the measured data presented in this paper, there are indicators that the number of scatterers is too small to assure the CLT assumption is satisfied. Many of these distributions exhibit a multimodal nature that indicates a small number of individually resolvable scatters. Also, instead of the smooth variation of magnitude versus frequency in the Doppler region that is predicted by the Rayleigh model, these data often exhibit distributions with recognizable fine structure.

In contrast to previous examinations over longer time regimes—periods during which the receiver traverses distances of 40 to 100 wavelengths are not uncommon—this work has concentrated on shorter time regimes characteristic of high speed data radios. Within these short time regimes, the small number of scatters visible to the receiver appears to lead to distributions with a significantly greater number of deep fades than those predicted by the Rayleigh model.

6.1.1 Fading over Short Time Regimes is Different than That over Longer Time Regimes

In short time regimes these data indicate that multimodal fading distributions are not uncommon. We hypothesize that the multimodal nature of the observed distributions is the result of summing distributions from individual scatterers that are significantly different in modal value (i.e., the reflection coefficients of the resolvable scatterers are significantly different from one another).

6.1.2 Fading over Longer Time Regimes Converges to Rayleigh Because of the Central Limit Theorem

Assuming that a moving receiver passes through a region that is sparsely populated with scatterers, at any given instant the receiver will see fewer scatterers than the CLT assumption would dictate. Consequently, the contributions associated with each scattering source resolve into separable distributions over the short period of time during which the receiver sees only these scatterers (Figure 20(a)). In the next instant of time, the receiver position changes and a new collection of scatterers become visible. Over time, the receiver perceives an increasing number of individual scattering distributions (Figure 20(b) and Figure 20(c)) until, eventually, the CLT assumptions are met. At this point, the I and Q components exhibit a Gaussian amplitude distribution and the magnitude distribution of the signal is Rayleigh (Figure 20(d)).

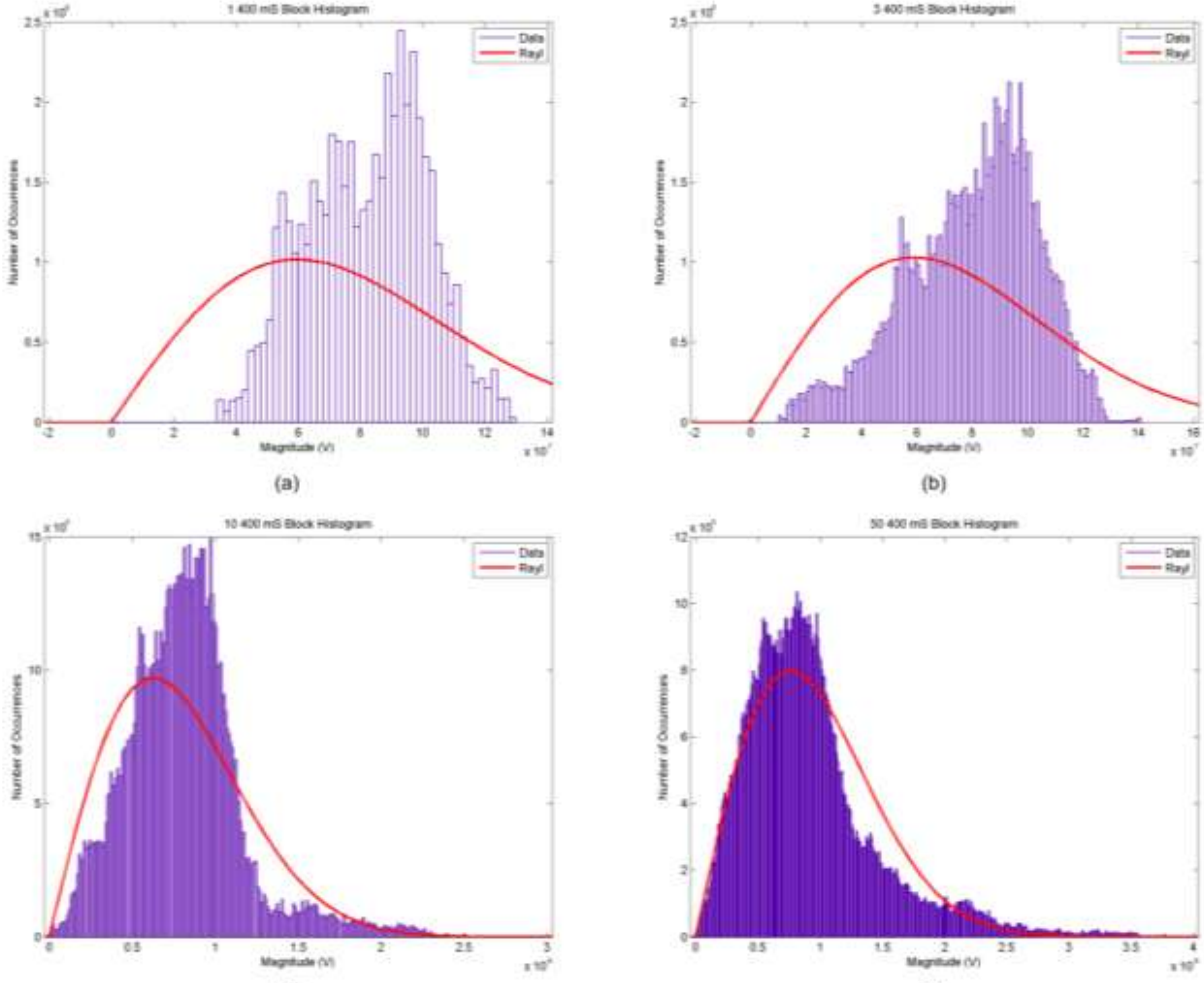

(a) (b) (c) (d)

Figure 20. Examples showing how, over an increasing length of time (1, 3, 10, and 50 blocks), the signal’s power distribution approaches the predicted Rayleigh distribution.

To determine the second order statistics and compare them to the theoretical curves for a given Rayleigh distribution, each data file must be normalized against its Doppler frequency. The LCR and AFD are dependent on the Doppler frequency since they are an indication of the time behavior of the fading activity. Each data file was collected while the measurement system was travelling at different velocities; this made the processing of second order statistics difficult. For a given velocity and transmitted frequency, the received signal bandwidth is theoretically bounded between the carrier frequency plus or minus the Doppler frequency. To compare differing channel time intervals under the assumption that the scattering environment remains similar, the data needed to be collated relative to the Doppler frequency.

Collation proved to be the easiest method to examine large numbers of data files with approximately the same Doppler frequency. Unfortunately, the data processed in this manner is not spatially or temporally contiguous; this should be taken into account when interpreting this statistic.

Nonetheless, over a large number of data files, the effect of the CLT can be seen from the LCR statistic; over longer time intervals, the data moved closer to the LCR curve predicted by Rayleigh fading theory. Figure 21 shows this case, at least in terms of the qualitative character of the curve. Note that this figure represents 175 data files collected over a period of 1295 seconds. This is a long time period relative to a radio symbol or frame. Considering the qualitative character of the data, the shape of the LCR is approximately that of the theoretical LCR over this long time period; this means that the radio would experience short term LCRs that are substantially different from theory. What remains unexplained is that the data quantitatively exceeds the LCR of Rayleigh theory by approximately a factor of three (the data’s vertical axis is on the left and the theoretical LCR’s axis is on the right of the graph). The data maximum is approximately 25 level crossings per second while the theoretical curve maximum is approximately eight crossings per second. This may imply that the channel fading events are occurring three times more often than Rayleigh fading predicts. This potentially means that if a radio is designed based on Rayleigh assumptions it will typically experience lowered performance relative to the design criteria.

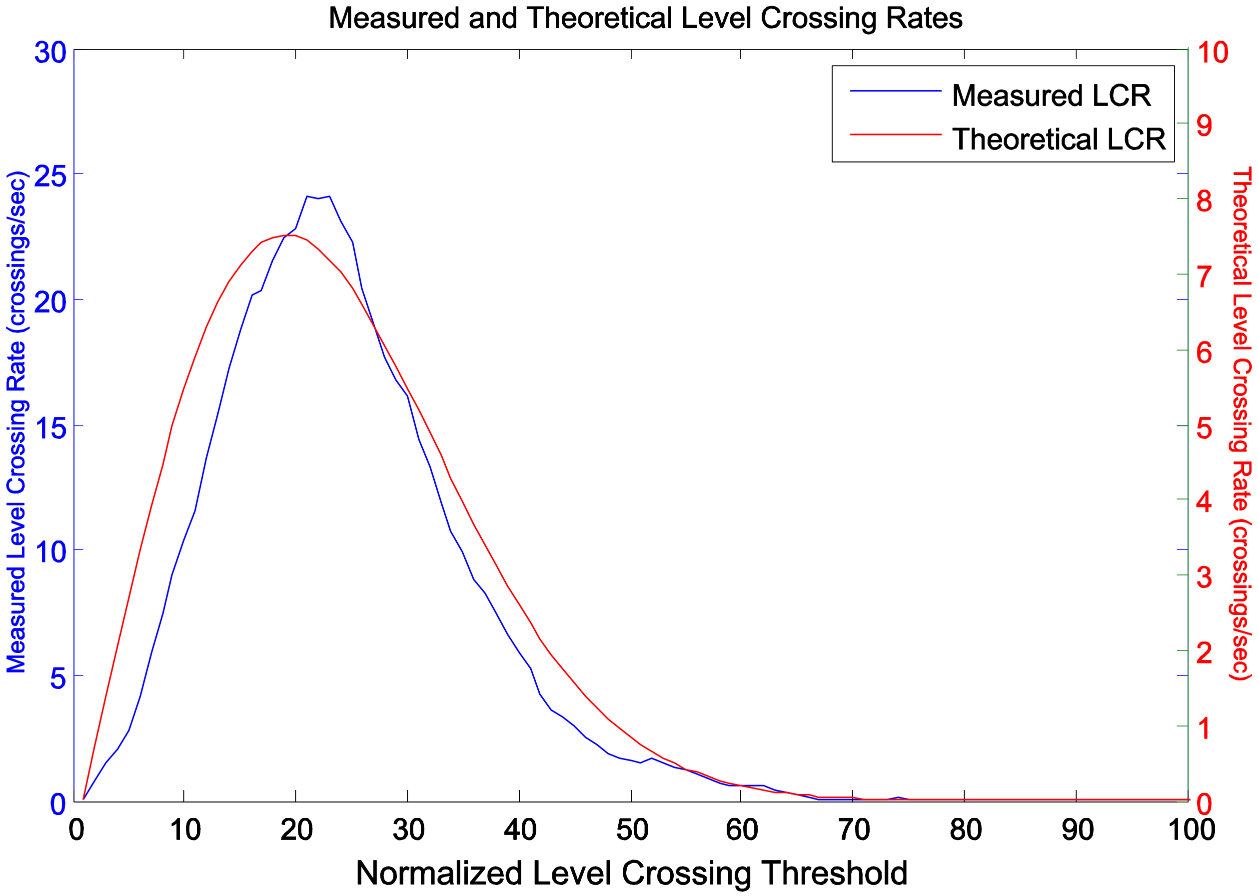

Figure 21. Theoretical and measured level crossing rates versus the normalized level crossing threshold of 175 data files from 17 May 2010 (residential, 162 MHz) that had a Doppler frequency between 6.5 and 7.5 Hz.

6.2 Alternative Distributions

A number of alternative distributions to the Rayleigh model exist for fading measurements. For example, if a direct line-of-sight path exists, or if one ray from the scattering distribution is dominant, then a Rician distribution is appropriate. If the fading model is to represent behaviors over a long path (on the order of hundreds of wavelengths), then a lognormal distribution is often used to represent “slow fading.” To distinguish between large and small fading events, single measurements are typically conducted to emphasize the mean channel behavior; typically, this requires 50 acquisitions within a distance of 40 wavelengths. Measurements conducted in this manner are an expression of Lee’s criterion, which is often used to remove the effects of fast fading so that only the effects of slowly-varying features of the radio channel remain.

It is also possible to statistically express the combination of Rayleigh/Rician behavior in short term fading with lognormal behavior over longer time/distance regimes—this is known as the Suzuki distribution. In the present measurements, each individual acquisition happens over a time period of 400 msec and a distance of less than 20 wavelengths at maximum velocity. Therefore, slow fading effects were not considered in these analyses.

Another distribution that is of interest is the Nakagami-m distribution. Unlike the Rayleigh distribution, which is completely described by a single parameter, the Nakagami-m has two degrees of freedom. The second parameter is called the shape factor and is typically identified as the m in Nakagami-m. The equation for this distribution is given as:

$$p(\gamma) = \left(\frac{m}{\Omega}\right)^m \frac{\gamma^{m-1}}{\Gamma(m)} \exp\left(\frac{-m\gamma}{\Omega}\right) \tag{5}$$

where Γ is the Gamma function.

The Nakagami-m distribution is of particular interest because of the meaning of the m parameter. When m = 1 the Nakagami-m distribution can be shown to be equivalent to the Rayleigh distribution. Similarly, when m = 0.5, the Nakagami-m distribution collapses to a one-sided Gaussian (Normal) distribution. When the fading channel is described by a Nakagami-m distribution with m < 1 the channel is known as “worse than Rayleigh,” or WTR.

The Rayleigh distribution is often assumed to describe the worst fading condition that a radio receiver can experience, but this is an incorrect assumption. In WTR fading, the proportion of deep fades exceeds the fraction predicted by the Rayleigh probability distribution curve. An example case from actual data is given in Figure 22.

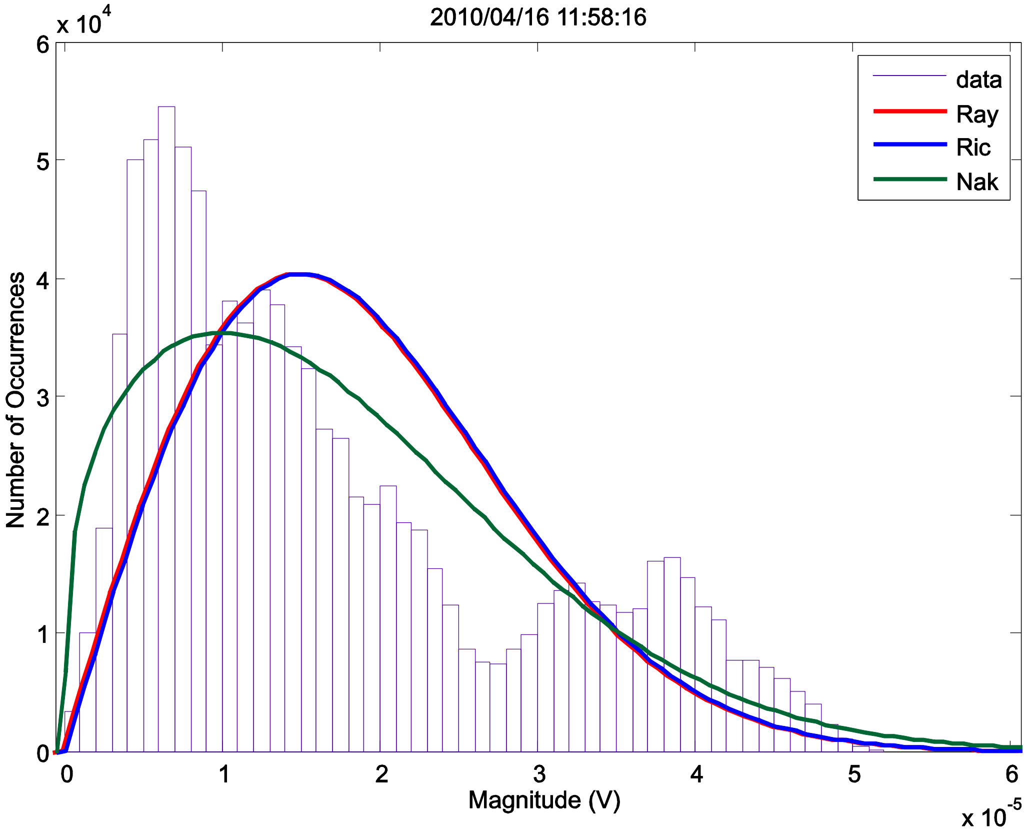

Figure 22. Example probability distribution of worse-than-Rayleigh (WTR) fading evident in a single 400 msec block (residential, 793 MHz).

In this figure, the probability distribution function from one 400 msec acquisition is fit to Rayleigh, Rician and Nakagami-m distribution curves at the 95% confidence level. The bimodal distribution of the measured data is evident, and it is clear that a much greater proportion of the data occupies the portion of the graph to the left of the peak (mode) of the red Rayleigh curve (coincident with the blue Rician curve in this example) than the fitted curve would predict. This indicates a considerably higher number of deep fades in the actual data than the theoretical Rayleigh model would anticipate. The green curve shows the Nakagami-m fit, where the m parameter is 0.62.

In this research approximately 26,000 measurements of this type were investigated, representing two different propagation environments at two different frequencies. Each was fitted with a Nakagami-m distribution curve at the 95% confidence level. In over half of the cases (51.2%) the m parameter was less than one, indicating worse than Rayleigh conditions (Figure 23). The high incidence of this channel behavior argues for more study using the fast sampling short time regime conditions suggested by these experiments. It is clear that, in the time regimes characteristic of high speed data radio operation, the incidence of worse than Rayleigh conditions is much higher than previously suspected.

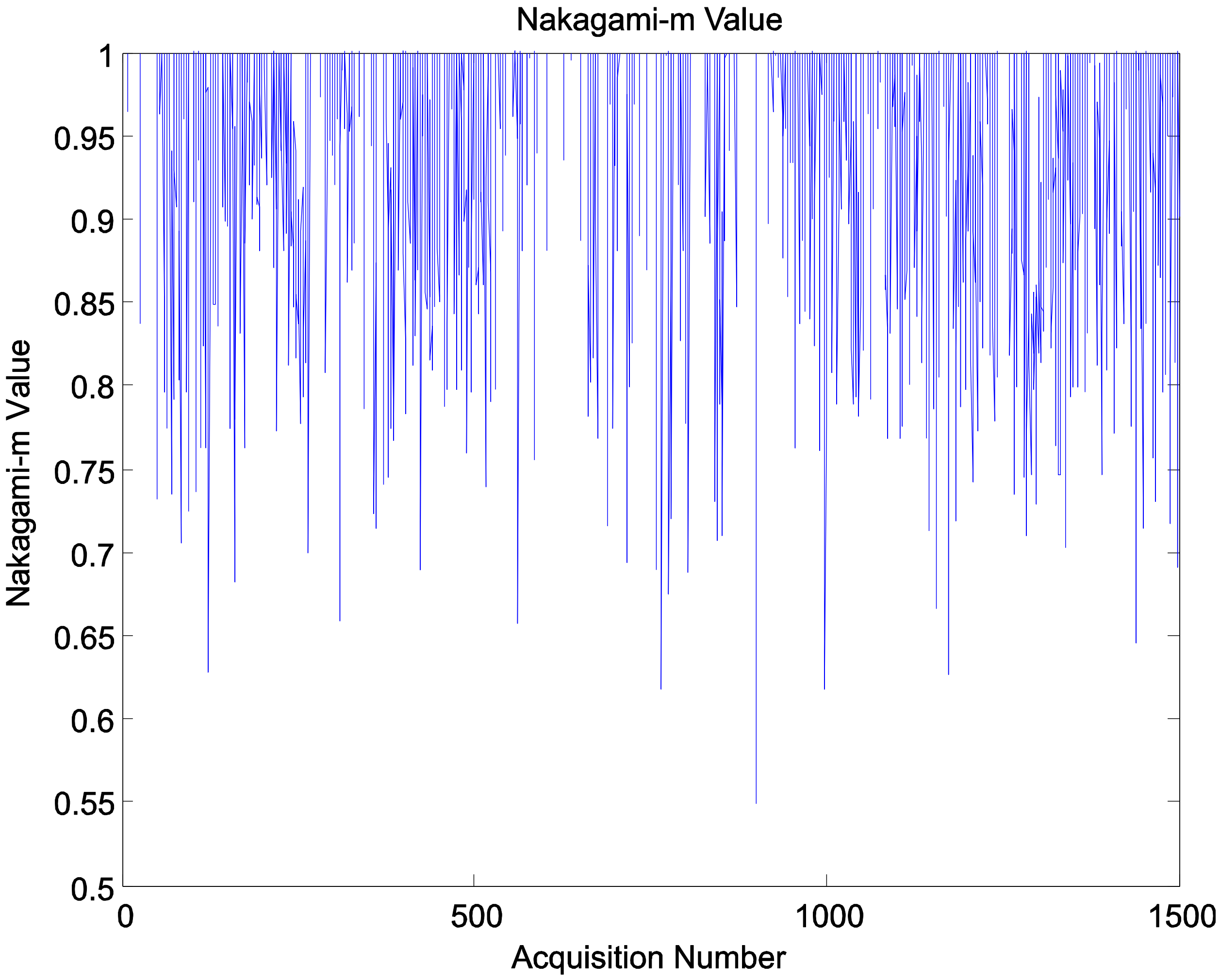

Figure 23. Plot of Nakagami-m values <1.0 for all data files in a single run.

6.3 Fading Effects on Radio Receiver Performance

In the Rayleigh case, expressions for the LCR and AFD give an indication of the time behavior of the fading channel. An extension of current analyses would involve plotting these second order statistics for the empirical data versus the expected Rayleigh second order statistics to determine if the channel is worse than Rayleigh. For example, if the Rayleigh faded channel AFD indicates that the received signal level for a P25 radio is less than the receiver's minimum threshold for 2.5 msec (24 P25 bits or half of the frame synchronization), then the P25 radio will presumably fail. In situations where this exists, a longer synchronization sequence is needed to maintain synchronization.

Several radio design parameters are obviously dependent on the channel time statistics. If fade durations are long, then the interleaving interval may need to be increased. Similarly, the frame sync interval is dependent on the length of the average fade duration. If the behavior of the channel leads to deeper fades than originally anticipated, this may require a change in the AGC design to achieve greater dynamic range.

These experiments indicate that a radio would experience deeper fades than the Rayleigh model would predict within time regimes significant to radio performance. The excess deep fading occurs because the number of scatterers seen during the short-term measurement does not produce the uniform phase distribution required by the assumption of the Rayleigh fading model. More analysis is needed to determine if second order statistics are similarly impacted.

Without further study of second order effects it is impossible to say whether changes to the P25 protocols or modulation are necessary. Our studies do indicate that level crossing rates within typical radio time regimes are more than an order of magnitude greater than the Rayleigh models predict. This effect may be a strong argument for more robust P25 error correction coding. If similar effects are present in the AFD behaviors, interleaving distance and the length of the synchronization sequence will need to be re-evaluated.

These experiments suggest that the P25 radios are being designed for channel conditions more benign than those encountered in real world situations. In all probability, improved performance could be maintained if radio designers were made more aware of the detrimental conditions these experiments have revealed.

These effects are likely to be even more pronounced at the faster symbol rates characteristic of LTE signals. The LTE symbol rate is approximately three times that of P25, which may exacerbate the problems noted. These experiments include measurements in the 700 MHz band to address possible effects on LTE signals as well as to ascertain if these effects are a function of wavelength. Under the analyses performed in this effort, the measurements do not show a strong frequency dependence. However, LTE uses phase dependant modulation; an analysis of this data from the perspective of phase behavior is potentially valuable to future LTE usage in the public safety band.

7 REFERENCES

[1] Sen, I.; Matolak, D.W.; Xiong, W., “Wireless channels that exhibit ‘Worse than Rayleigh’ fading: analytical and measurement results” in *Proc. IEEE Military Communications Conference, 2006, MILCOM 2006*, pp.1-7, 2006

[2] “Coverage prediction for mobile radio systems operating in the 800/900 MHz frequency range,” *IEEE Transactions on Vehicular Technology*, Committee on Radio Propagation, Vol. 37, No. 1, Appendix III: Received Signal Fading Distribution, pp. 57-60, Feb. 1988

[3] Ossanna, J. F., “A model for mobile radio fading due to building reflection: theoretical and experimental fading waveform power spectrum,” *Bell Syst. Tech. J.*, 43, pp. 2935-2971, 1964

[4] Clarke, R. H.,”A statistical theory of mobile radio reception,” *Bell Syst. Tech. J.*, 47, pp. 957-1000, 1965

[5] Parsons, J. D (Ed.), *The Mobile Radio Propagation Channel*, Chichester, UK: John Wiley &Sons. LTD., 2000

[6] Xiao, C.; Zheng, Y.R.; Beaulieu, N.C., “Statistical Simulation models for Rayleigh and Rician Fading” in *Proc. IEEE International Conference on Communications, 2003. ICC '03.*, vol.5, pp. 3524-3529, May 2003

[7] Jakes Jr., W. C. (Ed.), *Microwave Mobile Communications*, John Wiley & Sons LTD., New York, NY, 1974

[8] Zheng, Y.R.; Xiao, C., “Simulation models with correct statistical properties for Rayleigh fading channels,” *IEEE Transactions on Communications*, Vol. 51, No. 6, pp. 920-928, Jun. 2003

[9] Hadzi-Velkov, Z., **“**On the second order statistics of the multihop Rayleigh fading channel,” *IEEE Transactions on Communications*, Volume 57, Issue 6, pp.1815-1823, Jun. 2009

[10] Rappaport, T. S. *Wireless Communications Principles and Practice*, Upper Saddle River, New Jersey: Prentice Hall PTR, 1999

[11] Fontan, F. P. (Ed.). *Modeling the Wireless Propagation Channel*, New York, NY: John Wiley & Sons LTD., 2008

[12] *Digital C4FM/CQPSK Transceiver Measurement Methods*, TIA-102.CAAA-B, Telecommunications Industry Association, 2004

[13] Rusek, F., “Mutual Information of IID Complex Gaussian Signals on Block Rayleigh-faded Channels” in *Proc. 2010 IEEE International Symposium on Information Theory (ISIT)*, pp.300-304, 2010

[14] Proakis, J. G.; Manolakis, D. G. *Digital Signal Processing*, New York, NY: Macmillan Publishing Co., 1992

APPENDIX A: TEST EQUIPMENT SET-UP AND CONFIGURATION FOR FADING MEASUREMENTS

I. Receiver test equipment and configuration

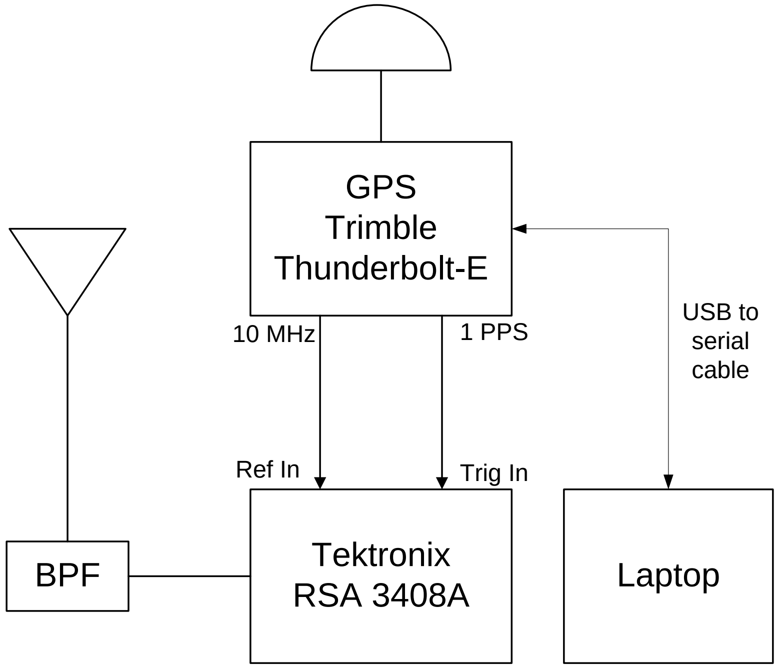

Figure A-1. Receiver test equipment configuration.

Test Equipment	
Spectrum Analyzer	Tektronix RSA 3408A
GPS	Trimble Thunderbolt-E
GPS Antenna	Trimble Bullet antenna
Receive antenna	Antenna for 162 and 793 MHz frequencies
Band pass filter (BPF)	TX RX Systems cavity for 162.0275 and 793 MHz
Laptop	Asus Eee with Trimble GPS Studio
USB to Serial cable	FTDI USB to serial cable with driver

Test Equipment configuration

1. Connect the test equipment as indicated in Figure A-1.

    a. Use the appropriate antenna and cavity filter for the frequency of interest

2. Configure the RSA 3408A

    a. Press the PRESET button
    b. Press the LOAD button
    c. Select LOAD STATE
    d. Select SELECT FILE button
    e. Scroll to fading receiver config ref 0dB.sta date (5/14/2010)

f. Select LOAD FILE NOW (screen shot in Figure A-2 displayed)
g. Press INPUT button. Press Reference Source softkey and toggle until Ext is highlighted. This sets the 10 MHz external reference source from the GPS unit.

RSA 3408A fading receiver configuration file consists of the following:
AMPLITUDE
  Ref Level: 0
  RF Attn: 30
SPAN: 100 kHz
TRIG
  Mode: Triggered
  Repeat: Continuous
  Source: External
  Level: 0.5 V
  Slope: Rise
  Position: 1 %
TIMING
  Acq Length: 400 msec

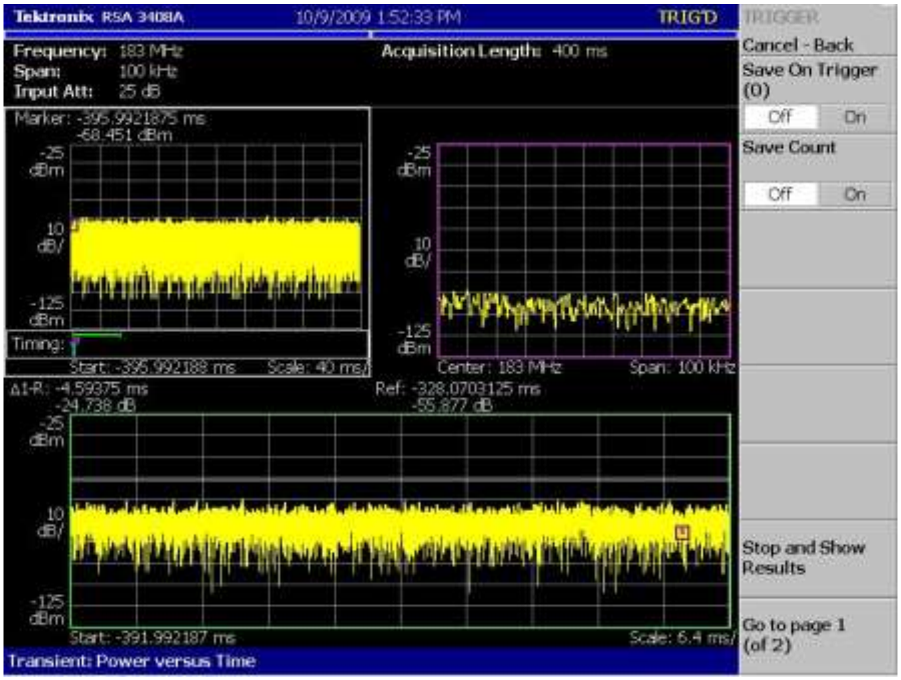
Tektronix RSA 3408A 10/9/2009 1:52:33 PM TRIG'D
Frequency: 183 MHz
Span: 100 kHz
Input Att: 25 dB
Acquisition Length: 400 ms
Marker: -395.9921875 ms
-68.451 dBm
Start: -395.992188 ms Scale: 40 ms/
Center: 183 MHz Span: 100 kHz
Δ1-R: -4.59375 ms
-24.738 dB
Ref: -328.0703125 ms
-55.877 dB
Start: -391.992187 ms Scale: 6.4 ms/
Transient: Power versus Time

Figure A-2. Screen shot of RSA 3408A in the receive measurement mode.

3. Configure the Trimble Thunderbolt-E

  a. Connect the GPS antenna, 10 MHz out, 1 PPS, and USB to serial cables as indicated in the Receiver Test Equipment Configuration diagram (Figure A-1)
  b. Boot the Trimble GPS Studio software (ver. 1.01.1) on the laptop
  c. Left click on the Connections tab and select Auto-Detect
  d. Select the appropriate COM Port from drop down menu

e. Hit Start button and select YES when prompted to connect and start monitoring
f. Left click on the Receiver tab and select Configure
g. In the Receiver Configuration Menu, Left click on the GPS Configuration tab (see Trimble GPS Studio screen shot in Figure A-3)
    i. Set Receiver Mode to Auto 2D/3D
    ii. Set Dynamics to Land
    iii. Hit SET button

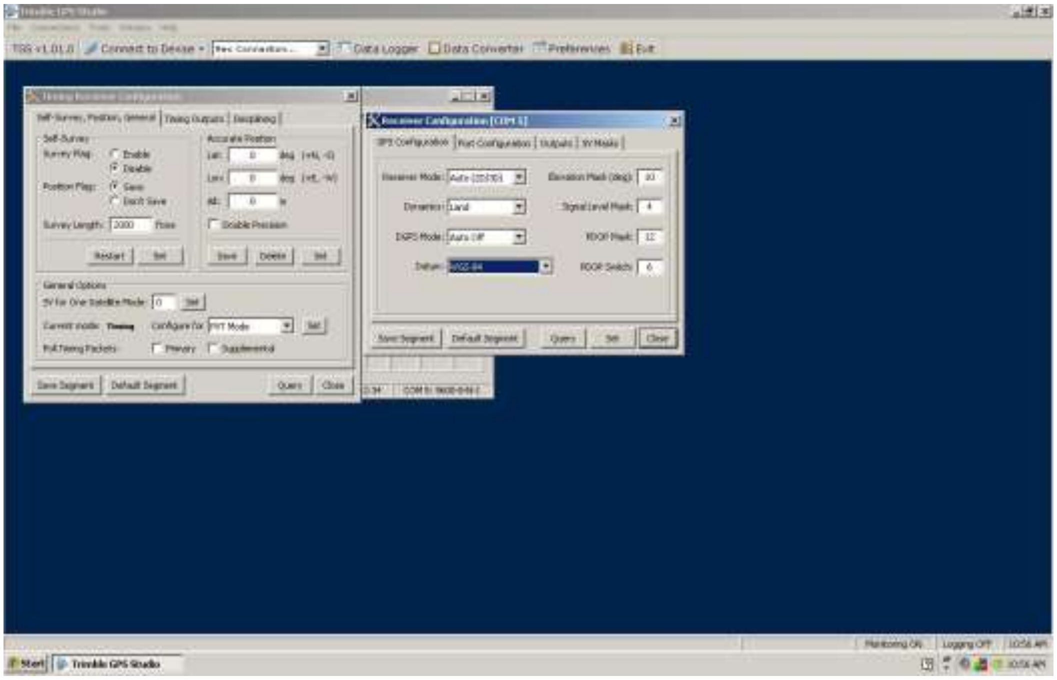

Figure A-3. Trimble GPS Studio receiver configuration window.

4. Manually sync the RSA and laptop clocks

    a. Go to date and time properties and manually sync clocks with each other

5. To log data on RSA

    a. Press TRIG button
    b. Select Go to Page 2 button
    c. Select SAVE ON TRIGGER button
    d. Note that the Save on Trigger count increments to indicate that data is being logged
    e. To stop logging Select SAVE ON TRIGGER button (see Figure A-2)

6. To log GPS data with the Trimble GPS Studio software

    a. Left click on the Data Logger
    b. Create a filename and location to log data
    c. Left click on Start Logging tab

d. In the Status Info box the Activity line indicates “Logging Started” and the Received line will increment the log file size (see Figure A-4)
e. The RX and TX buttons will be blinking green to indicate log data activity
f. To stop logging left click on the Stop Logging tab

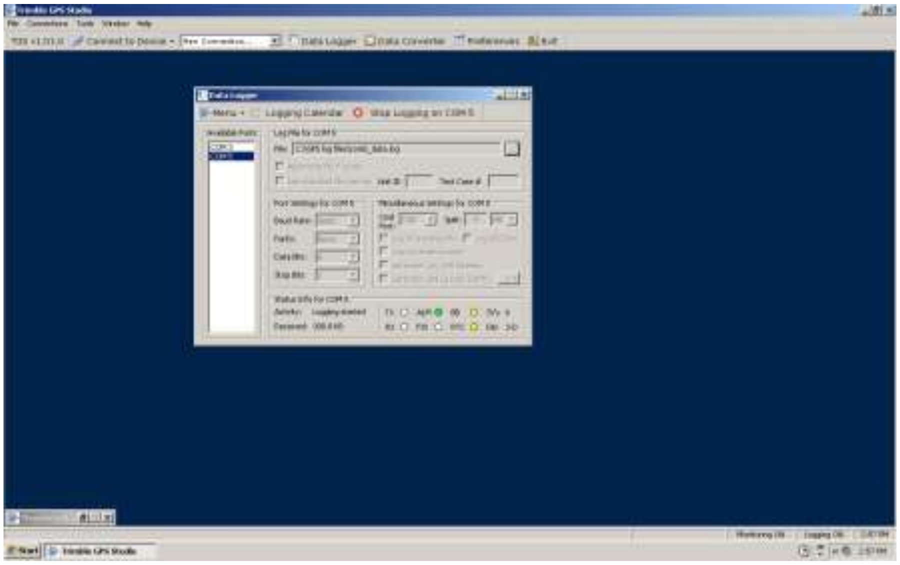

Figure A-4. Trimble GPS Studio data logging window.

II. Transmitter test equipment and configuration

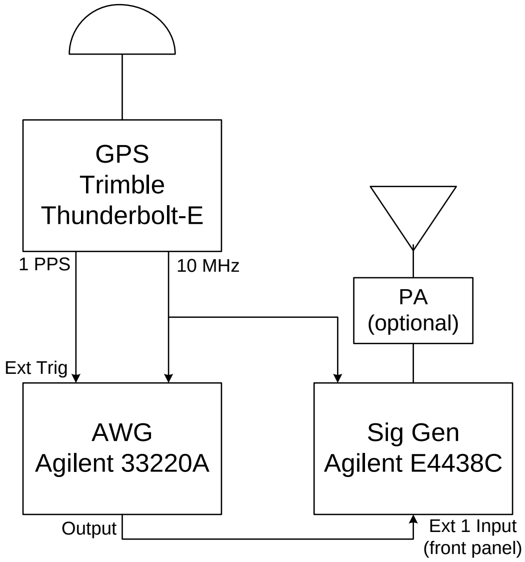

Figure A-5. Transmitter test equipment configuration.

<u>Test Equipment</u>	
Signal Generator	Agilent E4438C
GPS	Trimble Thunderbolt-E

GPS Antenna	Trimble Bullet antenna
Antenna	Diamond Antenna model D-130N
AWG	Agilent 33220A

Test Equipment configuration

1. Connect the test equipment as indicated in the transmitter test equipment configuration diagram (Figure A-5) above.

2. Configure the Agilent 33220A

    a. Press the STORE/RECALL button
    b. Select RECALL STATE button
    c. Select STATE 1 and press RECALL STATE button
    d. Instrument should indicate:
        i. Freq Period: 1.2 Hz
        ii. Ampl High Level: 5.0 V P-P
        iii. Offset Lo Level: 2.5 V DC
        iv. Duty Cycle: 50%
        v. External Trigger highlighted

3. Configure the Agilent E4438C (SN SG42080115)

    a. Press the RECALL button
    b. Press Select Seq softkey and scroll to 0
    c. Press Select Reg softkey and scroll to 25 (date 11/13/09)
    d. Press Recall softkey
    e. Press the FREQUENCY button and enter the desired frequency via the keypad
    f. Press the AMPLITUDE button and enter the desired amplitude via the keypad
    g. For dB units
        i. Press the AMPLITUDE button
        ii. Select MORE button
        iii. Select AMPL REF SEL button
        iv. Set amplitude to dB units
    h. Push the RF ON/OFF button and toggle power **on**. Note front panel indicator.
    i. Push the MOD ON/OFF button and toggle **on**. Note front panel indicator.
    j. Verify that output power is being produced and the signal toggles on and off.

4. Configure the Trimble Thunderbolt-E

    a. Connect the GPS antenna, 10 MHz out, 1 PPS, and USB to serial cables as indicated in the Receiver Test Equipment Configuration diagram
    b. Boot the Trimble GPS Studio software (ver. 1.01.1) on the computer. This is only needed to verify GPS operation and can be disconnected when completed.
    c. Left click on the Connections tab and select Auto-Detect
    d. Select the appropriate COM Port from drop down menu
    e. Hit Start button and select YES when prompted to connect and start monitoring
    f. Left click on the Receiver tab and select Configure

g. In the Receiver Configuration Menu, Left click on the GPS Configuration tab (see Trimble GPS Studio screen shot in Figure A-6)
    a. Set Receiver Mode to O-D Clock mode
    b. Set Dynamics to Stationary
    c. Hit SET button
h. Verify that the unit has entered the Over-determined (O-D) clock mode before conducting measurements

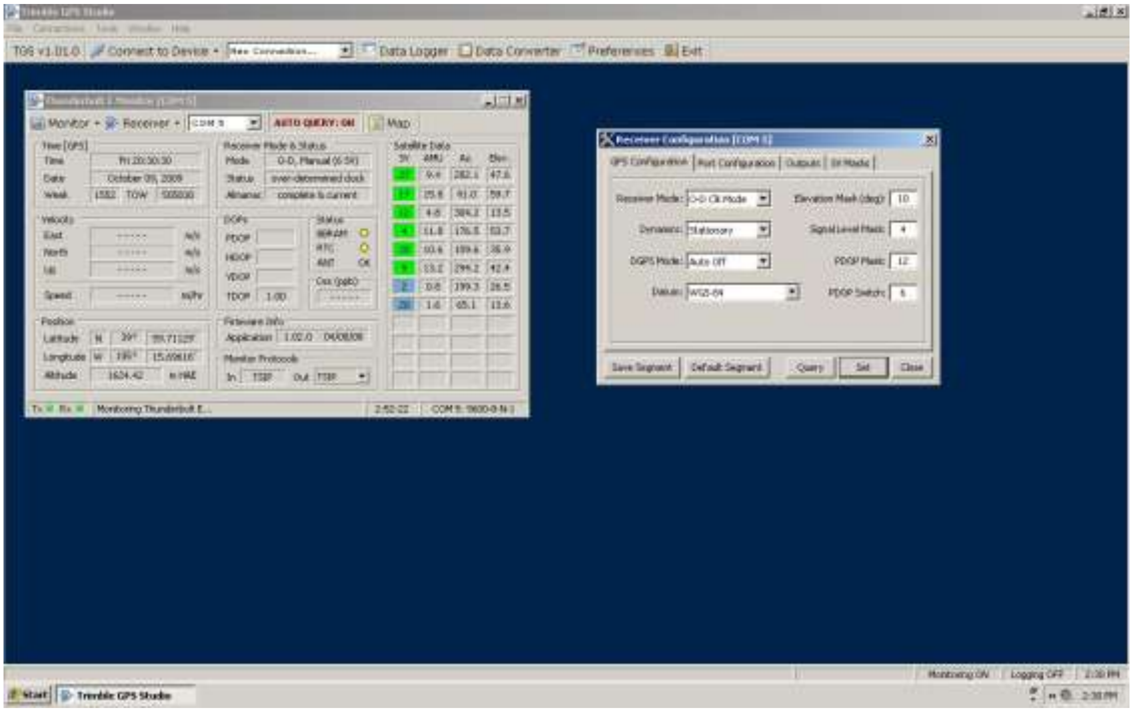

Mode: O-D, Manual (6 SV)
Status: over-determined clock
Almanac: complete & current

Receiver Mode: O-D Clk Mode
Dynamics: Stationary
DGPS Mode: Auto Off
Datum: WGS-84
Elevation Mask (deg): 10
Signal Level Mask: 4
PDOP Mask: 12
PDOP Switch: 6

Figure A-6. Trimble GPS Studio receiver configuration window.

5. For Fading Simulator tests with the Agilent E4438C

    a. Scroll to DIGITAL MOD and Select
    b. Scroll to SOURCE and Select
    c. Scroll to SOURCE and Select
    d. Scroll to PATTERN and Select
    e. Press RETURN
    f. Scroll to PATTERN and Select
    g. Scroll to 0 and Select
    h. Scroll to FREQ and Select and enter desired freq
    i. Scroll to LEVEL and Select and enter desired level

APPENDIX B: THE POTENTIAL FADING CHANNEL EFFECT ON P25 PROTOCOL STRUCTURE

The mobile radio channel presents a harsh environment for radio communication. To illustrate the effect that the measured data imposes on a radio, a theoretical analysis of the P25 protocol was conducted with intent to compare it with the measured data. The P25 standard specifies error detection and correction techniques to combat the effects of fading and other channel impairments. Of particular interest are the average fade duration (AFD) and the fade rate (referred to as level crossing rate or LCR). These statistics could be used to determine the frequency with which the fading channel would impact the radio receiver’s ability to withstand burst errors. The P25 protocol timing structure will be examined to show the potential limitations of the error correcting codes and indicate the fading channel events that would produce non-recoverable errors. This analysis uses a P25 Phase 1 system operating in 12.5 kHz channels and employing C4FM modulation. The channel rate is 9.6 kbps with a symbol rate of 4800 symbols per second, or 2 bits per symbol.

The P25 common air interface (CAI) specifies a messaging protocol between subscriber units and system infrastructure (i.e., base station). A typical voice transmission consists of a Header Data Unit (HDU) followed by multiple superframes of logical data unit (LDU) pairs (LDU1/LDU2) and a terminator data unit (TDU) as shown in Figure B-1. The HDU provides the frame synchronization, link control, encryption initialization, and addressing. LDU1 and LDU2 each provide nine frames of coded voice words as well as frame synchronization, addressing, and encryption synchronization. Together, LDU1 and LDU2 pairs are referred to as a superframe. Following the completion of all transmitted superframes, a terminator data unit (TDU) is sent to signify the end of the message exchange. The TDU contains frame synchronization, Network ID, and associated coding. Status symbols, consisting of 2 bits, are periodically inserted into the data stream to indicate busy, idle, talk-around or unknown channel conditions. Each of the HDU, LDU1/LDU2, and TDU data units incorporate error detection and correction coding consisting of a combination of Reed Solomon, Golay, BCH, Hamming, and interleaving.

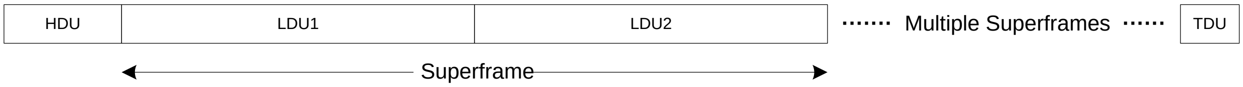

Figure B-1. P25 voice transmission from subscriber to base station.

The HDU, shown in Figure B-2, consists of an unencoded 48 bit frame synchronization (FS) sequence, a 16 bit Network ID (NID) field that is BCH encoded to 64 bits, and a 120 bit header field that has Reed Solomon and Shortened Golay codes applied to produce a 648 bit Header Code Word (HCW). The header field consists of a 72 bit Message Indicator (MI), an 8 bit Manufacturer’s ID (MFID), an 8 bit Algorithm ID (ALGID), a 16 bit Key ID (KID) a 16-bit Talk-group ID (TGID). Appended to the end is a 10 bit null field to create a 770 bit word. The last step inserts a 2-bit status symbol after every 70 bits to create a 792 bit HDU. At 9600 bps, an 82.5 msec HDU transmission is produced.

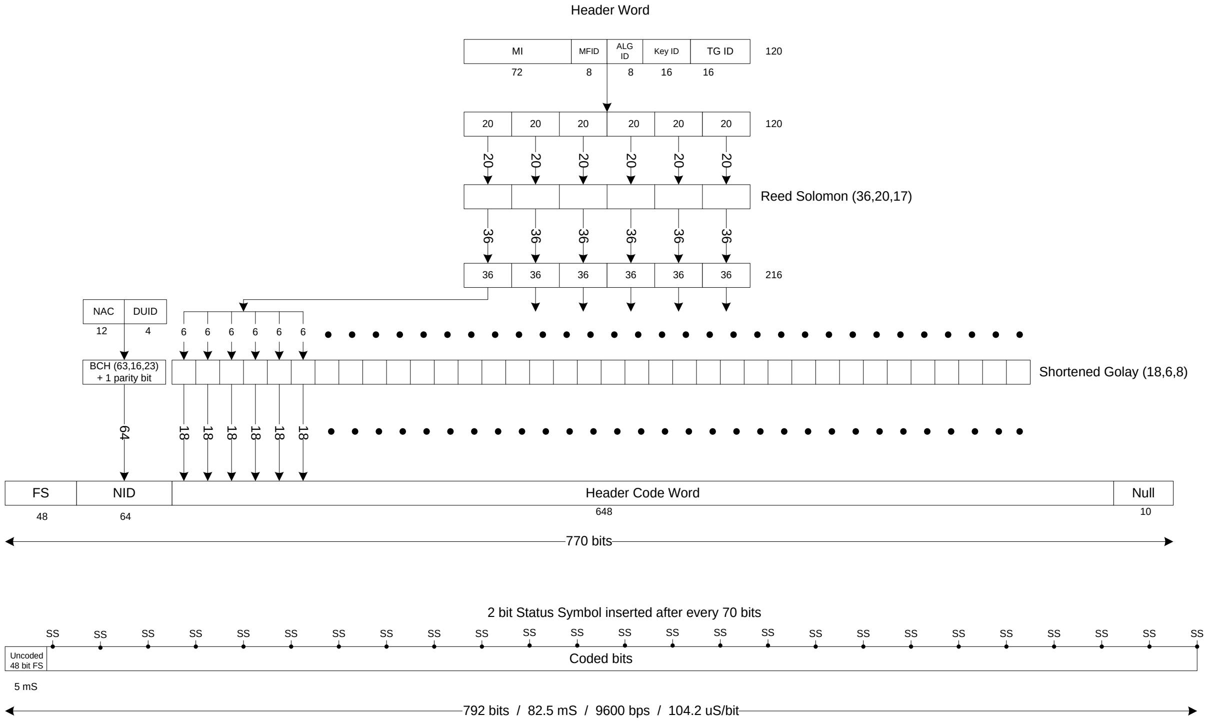

Figure B-2. HDU message structure.

LDU1, the first half of a superframe, contains a 48 bit FS, a 16 bit NID, 9 coded voice words, a 240-bit Link Control word, and 32 bits of Low Speed Data (LSD) as shown in detail in Figure 20. P25 systems specify the IMBE vocoder, which produces an 88 bit uncoded voice word for every 20 msec of speech. The uncoded voice words are divided into 8 voice frames, U0-U7, and protected using Golay and Hamming codes. U0-U3 are Golay encoded (23, 12, 7) while U4-U6 are Hamming coded (15, 11, 3) to form C0-C6. U7 is not error protected. C0-C6 are then concatenated to form a 114 bit sequence and exclusive-ORed with a 114 bit PN sequence. The resultant word is concatenated with C0 and U7 to form a 144 bit sequence, which is interleaved to form a coded voice word for each voice frame (i.e., VC1-VC9). VC1-VC9 are inserted into LDU1 as shown in Figure B-3.

The FS and NID are encoded in the same manner as the HDU. The Link Control word is a 72 bit field that is subdivided into an 8 bit Link Control Format (LCF) field, an 8 bit Manufacturer's ID (MFID) field, an 8 bit reserved field, a 16 bit Destination ID and a 16 bit Source ID. The 72 bit field is broken into six 12 bit fields, and a Reed Solomon (24, 12, 3) code is applied to produce a 144 bit sequence. This 144 bit sequence is first broken into six 24 bit fields, with each 24 bit field further divided into four 6 bit fields. A Hamming (10, 6, 3) code is applied to each of the 6 bit fields, producing a 240 bit sequence. This 240 bit word is broken into six 40 bit coded Link Control Words (LC1-LC6). The 16 bit Low Speed Data is encoded with a short cyclic code (16, 8, 5) to form a 32 bit coded word. LC1-LC6 and LSD are inserted into LDU1 as shown in Figure B-3. A 2 bit status symbol is inserted into the stream after every 70 bits to create a 1728 bit LDU1. The resultant coding produces an LDU1 transmission of 180 msec.

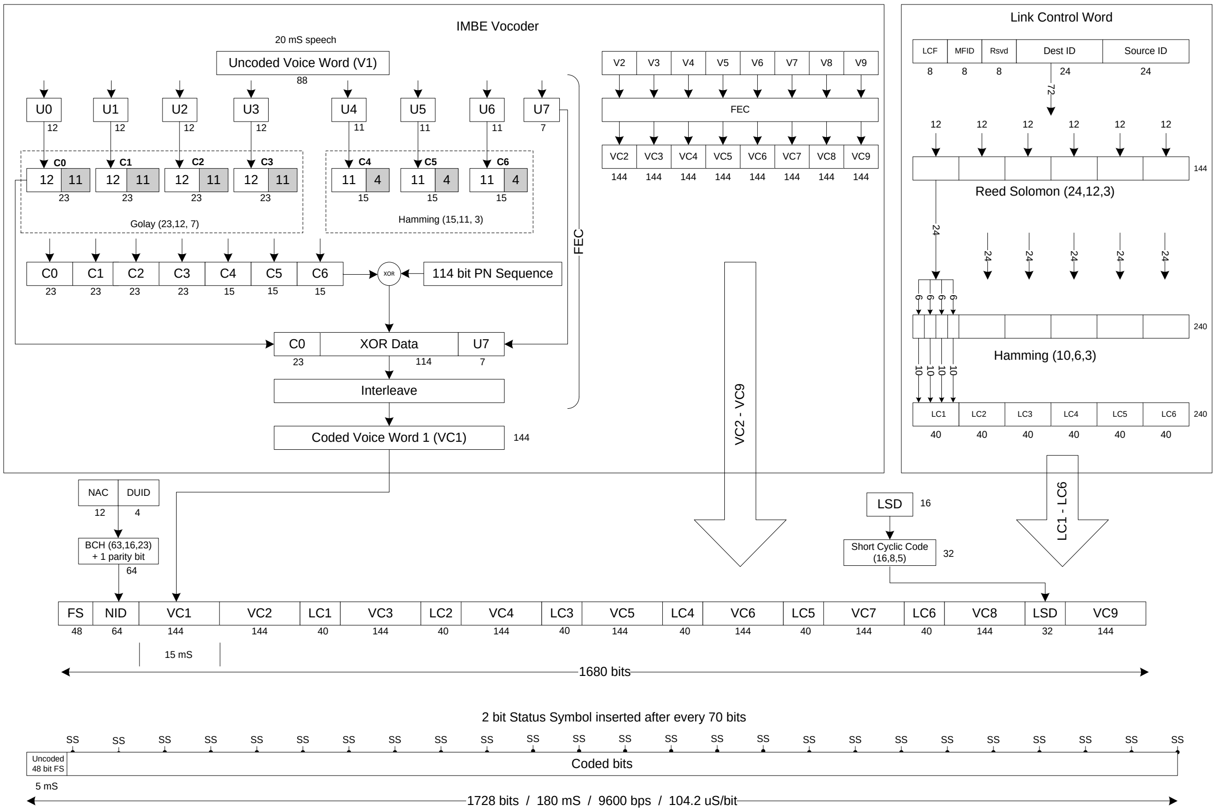

Figure B-3. LDU1 message structure.

LDU2, the second half of a superframe, also contains nine coded voice words (VC10-VC18) as well as an FS, NID, and an Encryption Synchronization word (ESW). The FS and NID are encoded in the same manner as the HDU. The ESW is a 96 bit field that is subdivided into a 72 bit Message Indicator (MI) field, an 8 bit Algorithm ID (ALGID) field and a 16 bit Key ID (KID) field. The 96 bit field is broken into six 16 bit fields, and a Reed Solomon (24, 16, 9) code is applied to produce a 144 bit sequence. This 144 bit sequence is first broken into twenty-four 6 bit fields, with a Hamming (10, 6, 3) code applied to each of the 6 bit fields, producing a 240 bit sequence. This 240 bit word is broken into six 40 bit coded ESWs. Voice coding is applied in the same manner as previously described and LDU2 is assembled as shown in Figure B-4. LDU2 transmissions are 180 msec.

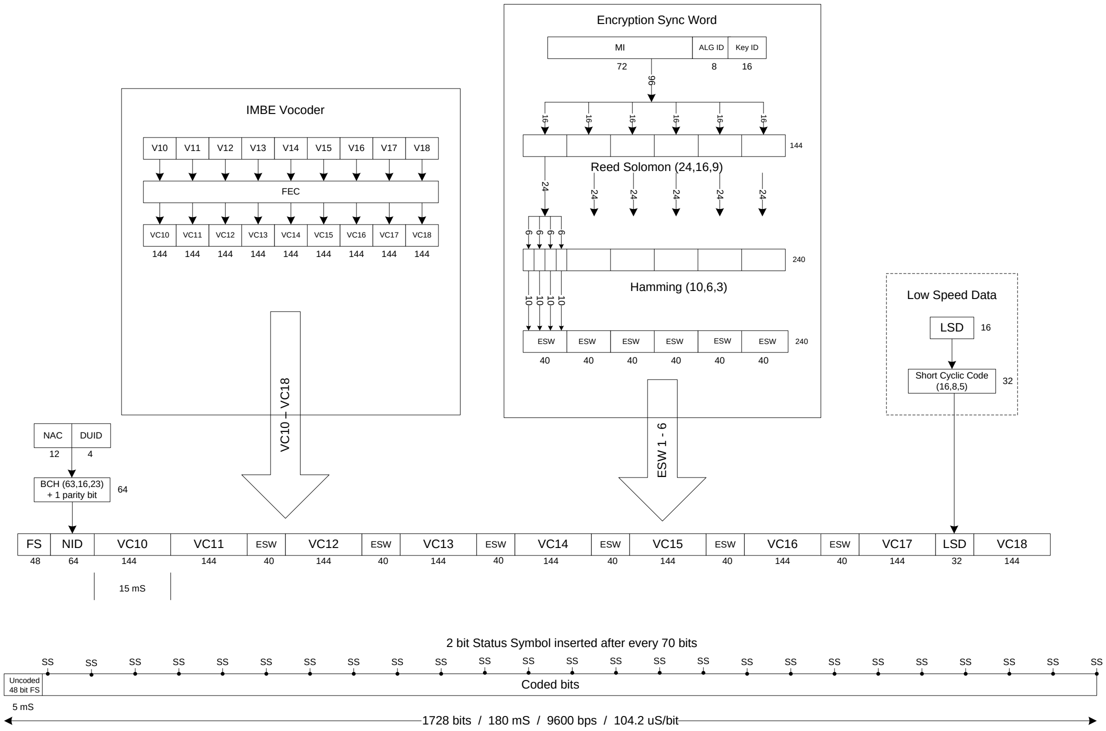

Figure B-4. LDU2 message structure.

The simple Terminator Data Unit (TDU) consists of a 48 bit FS, a 16 bit NID that is BCH encoded to 64 bits and a 28 bit Null field as shown in Figure B-5. A 2 bit status symbol is inserted into the stream after every 70 bits to create the 144 bit TDU, producing a 15 msec transmission.

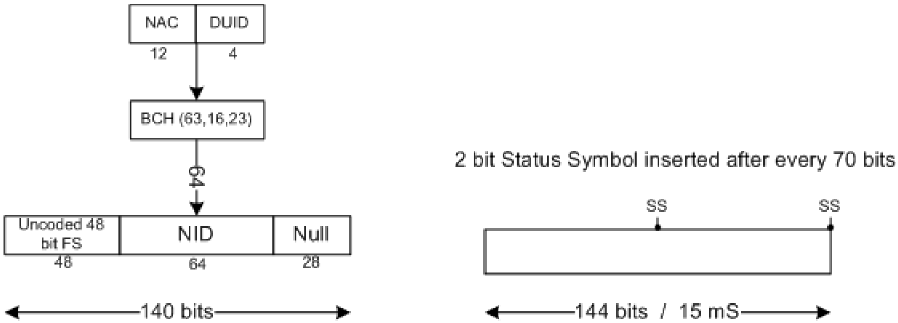

Figure B-5.TDU message structure.

B.1 Estimates of Channel-induced Non-recoverable Errors

A theoretical analysis to determine the degree of fading that can be tolerated by an actual P25 radio system was performed. We make the implicit assumption that a fade that creates continuous errors over half of the synchronization time would result in a loss of synchronization and the incorrect reception of the frame. P25 contains error detection and correction coding that is capable of correcting a finite number of errors in received data bits. When the number of block errors exceeds the radio's error correcting threshold, errored bits are produced and subsequently propagated through the receivers' protocol stack. As a result of the varying number of error-correction bits and different interleaving techniques in each sub-frame, the continuous bit-errors necessary for a frame loss will vary; this number is shown in Tables B-1 through B-3.

The AFD and LCR are two key parameters that are considered for their effect on the received data. Separate AFDs and LCRs are calculated for each type of data unit, as well as for the vocoder, since each contains different packet lengths and error coding schemes.

Fade duration becomes a factor when it exceeds the length (the number of bits multiplied by the bit length (104.2 µsec)) of the minimum number of continuous bit errors that will produce a block error. For example, 24 continuous bit errors would be produced by a 2.5 msec fade duration, causing the loss of an FS sub-frame.

The critical fade rate is calculated by taking the reciprocal of the length of the data unit under analysis. For example, the HDU is 82.5 msec long and would be corrupted by a fade occurring at 12.1 Hz (or fades/sec).

B.2 Vocoder

P25 vocoder frames are encapsulated within the P25 protocol and include error coding and interleaving. The vocoder error detection and correction coding is complex and not discussed here. Fundamentally, when errored frames are received the vocoder corrects errors within its capability with respect to the error code used. When the number of errors in a particular frame exceeds the vocoder's ability to correct them, the vocoder algorithm can repeat the previous frame, mute the errored frame, or perform adaptive smoothing between the adjacent frames. Given that voice frames are 20 msec long, a single frame loss will be minimally perceived by the listener.

Status symbols are continuously transmitted after every 70 bits in each of the data units. Since the codes are repeated at this high rate, a fade duration of 208 µsec and a fade rate in excess of 133 fades/sec would be needed to affect the status symbol reception.

B.3 HDU

An HDU is 82.5 msec in length and contains the 48 bit FS field containing uncoded data, NID, and header word. It is assumed that a 50% loss of FS will prevent the receiver from synchronizing. This equates to a 24 bit loss that could be caused by a minimum fade duration of 2.5 msec. The NID field would also be affected by a 24 bit fade. The header word is capable of withstanding a fade of 5.5 msec due to its robust error correction coding. When a fade in excess of 5.5 msec is encountered, the MI, MFID, Algorithm ID, Key ID, and TGID could be affected and potential crypto sync and talk group addressing will be adversely affected. Since the length of the HDU is short compared to that of LDU1 and LDU2, a higher fade rate is required to affect the HDU.

Table B-1 shows the fading effects on the HDU subframes.

Table B-1. Fading Effects on HDU.

HDU Subframe	Affects	Continuous Bit-Errors to Cause a Loss	Fade Duration	Fade Rate (fades/sec)
FS	Frame Synchronization	24	2.5 msec	12.1
NID	Network Access Code (NAC) Data Unit ID (DUID)	24	2.5 msec	12.1
Header Word	MI Manufacturer ID (MFID) Algorithm ID Key ID Talk Group ID (TGID)	53	5.5 msec	12.1

B.4 LDU1

An LDU1 is 180 msec in length. FS and NID fade data is the same as that of the HDU. A 2.5 msec fade affects the Link Control Word. Table B-2 shows the fading effects on the LDU1 subframes.

Table B-2. Fading Effects on LDU1.

LDU1 Subframe	Affects	Continuous Bit-Errors to Cause a Loss	Fade Duration	Fade Rate (fades/sec)
FS	Frame Synchronization	24	2.5 msec	5.6
NID	Network Access Code (NAC) Data Unit ID	24	2.5 msec	5.6
Link Control Word	Manufacturer ID Source ID Destination ID	7	0.7 msec	2.8
Low Speed Data	User data	22	2.3 msec	2.8

B.5 LDU2

An LDU2 is 180 ms in length. FS and NID fade data is the same as that of the HDU. Table B-3 shows the fading effects on the LDU2 subframes.

Table B-3. Fading Effects on LDU2.

LDU2 Subframe	Affects	Continuous Bit-Errors to Cause a Loss	Fade Duration	Fade Rate (fades/sec)
FS	Frame Synchronization	24	2.5 msec	5.6
NID	Network Access Code (NAC)	24	2.5 msec	5.6
Encryption Synchronization Word	MI Algorithm ID Key ID	7	0.7 msec	2.8
Low Speed Data	User data	22	2.3 msec	2.8

B.6 TDU

The TDU contains FS and NID data only, therefore the loss of this data will have the same effect as the loss of the HDU and LDUs.

The precise timing of the catastrophic consecutive errors fading events (CCEFE) is, of course, asynchronous with a P25 transmission. CCEFE of the channel might momentarily be dangerous to the P25 signal but there is still only a statistical probability that they will happen in such a way as to cause unrecoverable protocol errors. It is the purpose of this analysis to determine the fade rate and duration that would be required to cause CCEFE. Further study is necessary to determine how to identify CCEFEs in the measurements.

APPENDIX C: SIMULATOR SPECIFICATIONS IN TIA-102.CAAA-B FADED CHANNEL CHARACTERISTICS

The following text was taken from the TIA standard *Digital C4FM/CQPSK Transceiver Measurement Methods* [12]. It describes the required characteristics for a faded channel simulator.

The faded channel simulator shall have the following characteristics:

a) Capable of operation at the desired channel frequency.

b) Simulate a flat fading channel for simulated vehicle speeds of 8 km/h and 100 km/h.

c) Simulate two rays with independent fading statistics. Each Rayleigh faded ray shall have a time delay of up to 50 µs with delay resolution of 0.1 µs.

d) Generation of the Rayleigh fading conditions shall conform to the following:

e) The measured Rayleigh Cumulative Probability Distribution Function (CPDF) shall be compared against a calculated CPDF. The calculated Rayleigh CPDF, F(P), is as follows:

> *for* $P<0$*:* $F(P) = 0$*; for* $P\geq 0$*:* $F(P) = 1 - \exp(-P/P_{ave})$*, where P is the signal power level and* P_{ave} *is the mean power level.*

Measured CPDF of power shall be within ±1 dB of the calculated CPDF of power for 10 dB above the mean power level to 20 dB below the mean power level.

Measured CPDF of power shall be within ±5 dB of the calculated CPDF of power for 20 dB below the mean power level to 30 dB below the mean power level.

f) The level crossing rate (LCR) shall be compared against a calculated LCR. The calculated Rayleigh level crossing rate, L(P), is as follows:

> *For* $P<0$*:* $L(P) = 0$*; for* $P\geq 0$*:* $L(P) = (2\pi P/P_{ave})^{0.5} f_d \exp(-P/P_{ave})$*, where P is the signal power level,* P_{ave} *is the mean power level, and* f_d *is the Doppler frequency offset associated with the simulated vehicle speed. The Doppler frequency is given by the following:*
>
> $f_d = (v/c)f_c$
>
> *where v is the simulated vehicle speed, c is the speed of light in a vacuum (*2.997925×10^{8} *m/s), and* f_c *is the assigned channel frequency. The measured LCR curve shall not deviate from the calculated LCR curve by more than ±10% of the simulated vehicle speed. This shall hold for 3 dB above the mean power level to 30 dB below the mean power level.*

g) The measured power spectral density, S(f), shall meet the requirements specified below. The power spectrum measurement shall be made on an unmodulated carrier (frequency f_c*) applied to the input of the channel simulator.*

The maximum power spectral density level, S_{max}*, shall exceed* $S(f_c)$ *by at least 6 dB.*

The simulated Doppler frequency offset, f_d*, shall be within ±5% of the theoretical Doppler frequency offset associated with the vehicle speed. The simulated Doppler* *frequency offset shall be calculated from the measured power spectral density as follows:*

$f_d = (1/2\pi)(2b_2/b_0)^{0.5}$,

where:

$$b_n = (2\pi)^n \int_0^{\infty} S(f)(f - f_c)^n \, df$$

b_n *is the* n^{th} *moment of* $S(f)$.

$S(f)$ *shall be at least 30 dB below* $S(f_c)$ *for* $|f-f_c| > 2f_d$.

h) *The correlation coefficient of the unwrapped phase of the simulated, received signal shall be compared against the calculated theoretical correlation coefficient of the phase of the Rayleigh faded signal. The theoretical correlation coefficient,* $p(\tau)$*, is approximated by the following:*

$$\rho(\tau) = \frac{3}{2\pi}\sin^{-1}(h(\tau)) + 6(\frac{1}{2\pi}\sin^{-1}(h(\tau)))^2$$

$$-\frac{4}{4\pi^2}\sum_{n=1}^{\infty}\frac{(h(\tau))^{2n}}{n^2}$$

where:

$$h(\tau) = J_0(2\pi f_d \tau) * \frac{\sin(2\pi f_d \tau)}{2\pi f_d \tau}$$

*and * is the convolution function.*

The measured correlation coefficient of the phase shall be 0.8 ±0.1 at a lag of $0.05/f_d$, *and 0.5 ±0.1 at a lag of* $0.15/f_d$.

APPENDIX D: HISTOGRAMS OF SELECTED MEASURED DATA FILES WITH EXPECTED NAKAGAMI-M, RAYLEIGH AND RICIAN CURVES

All of the analysis routines were written to process entire runs at a time. Even after culling the data files based on SNR, approximately 9000 files were still left to analyze—too many files to examine individually. To reduce the number to a more manageable population, a random sample of files from each run was selected. The selected results are presented because they either represent typical behavior or are anomalous. Ten files from each day were chosen based on an observation of the results of TIA test (e), the Cumulative Probability Distribution Function (CPDF) (see plots (d) in Appendix E). An effort was made to equally select files that exceeded the expected CPDF, met the expected CPDF, and were less than the expected CPDF. In addition, the files for three consecutive seconds from Run 1 on May 17th were also selected.

For each one of these selected files, plots were generated to show a comparison between the actual probability distribution function and several predicted (ideal) distributions. In each figure, the probability distribution function from one 400 msec acquisition is fit to Rayleigh (red line), Rician (blue line), and Nakagami-m (brown line) distribution curves at the 95% confidence level. For the Nakagami-m distribution, the m parameter is 0.62 (see Section 6.1.2 for more information).

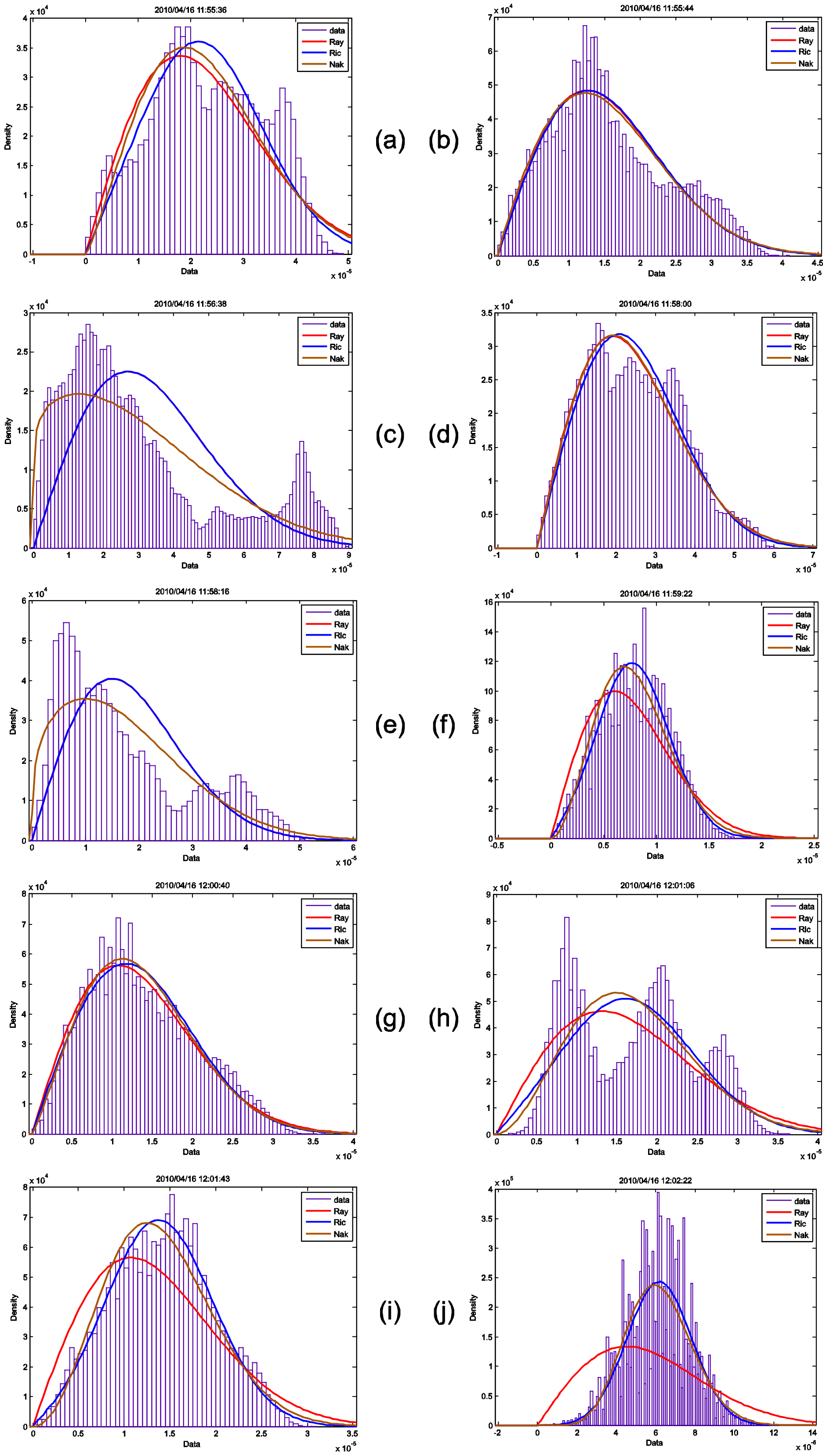

Figure D-1. Data from 16 April 2010 (residential environment, 793 MHz).

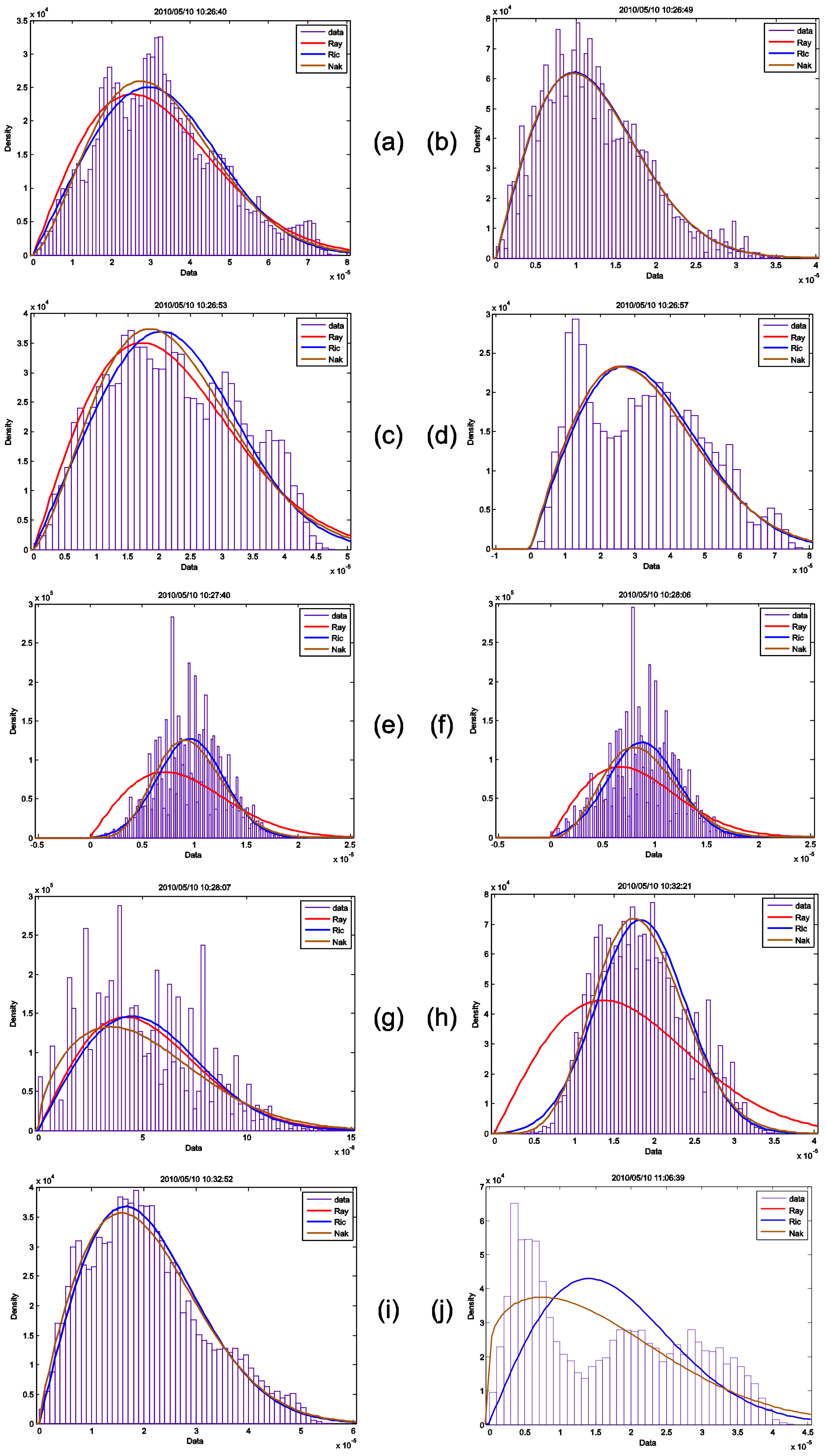

Figure D-2. Data from 10 May 2010 (low-rise urban environment, 793 MHz).

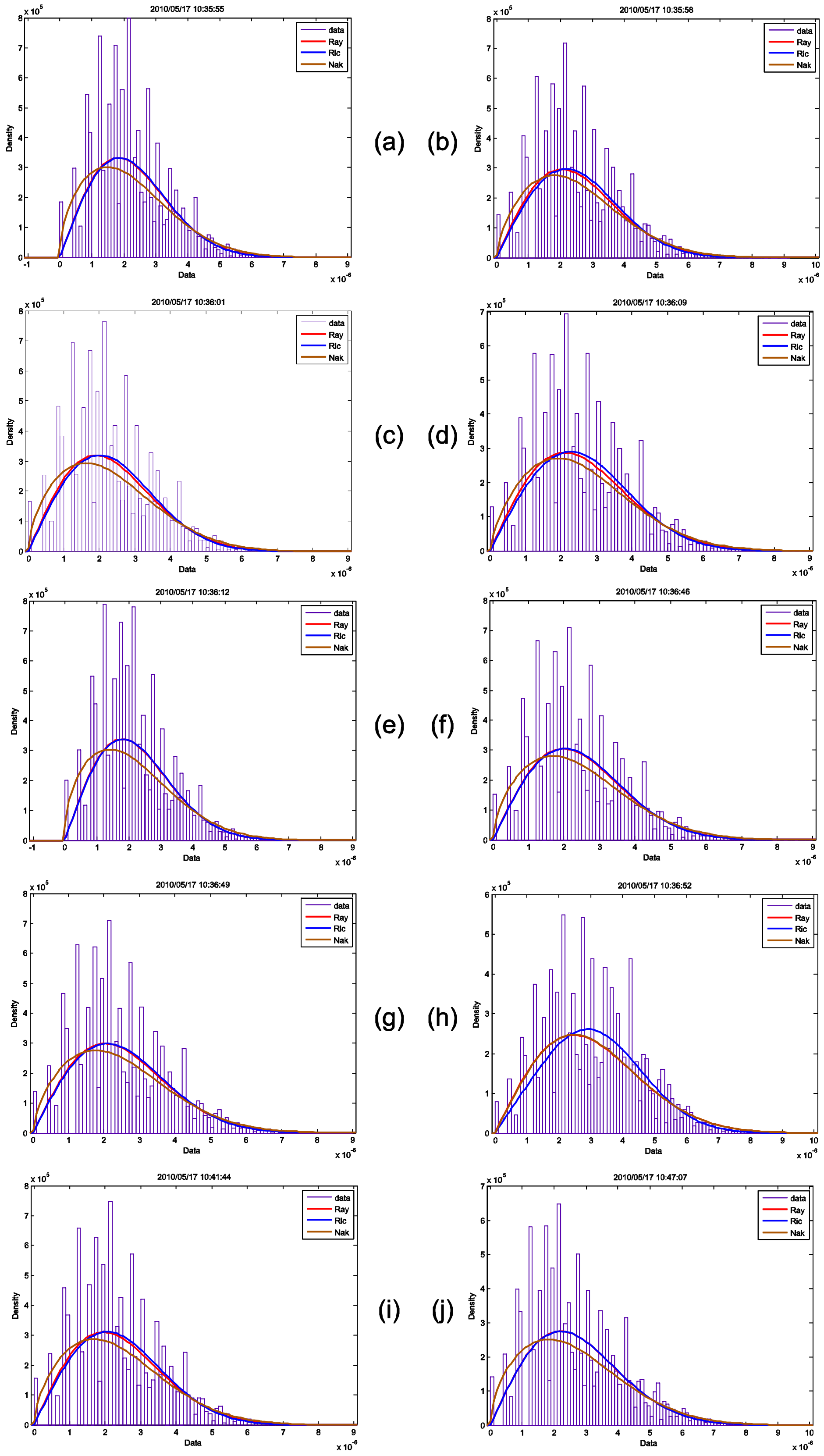

Figure D-3. Data from 17 May 2010 (residential environment, 162 MHz).

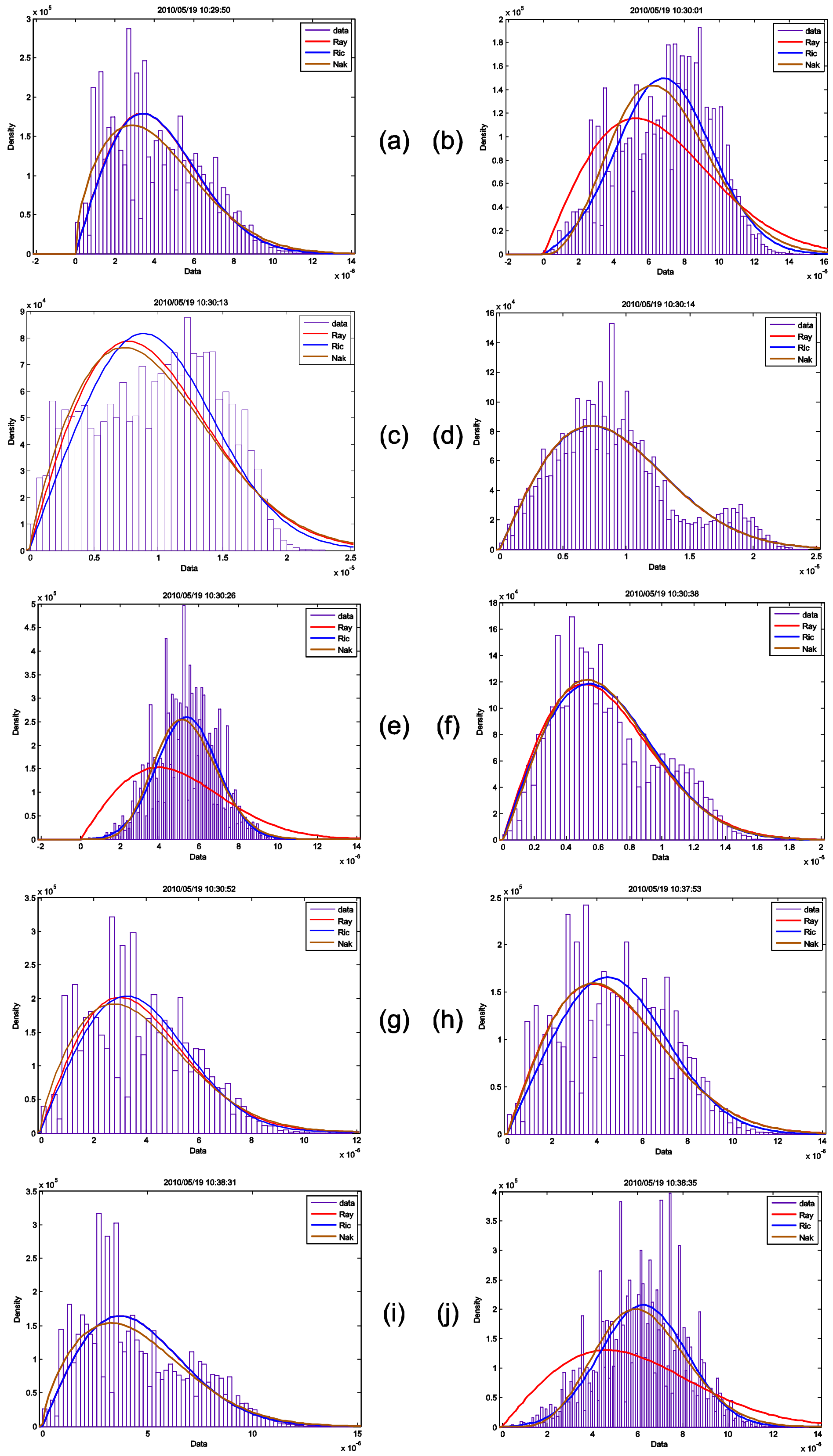

Figure D-4. Data from 19 May 2010 (low-rise urban environment, 162 MHz).

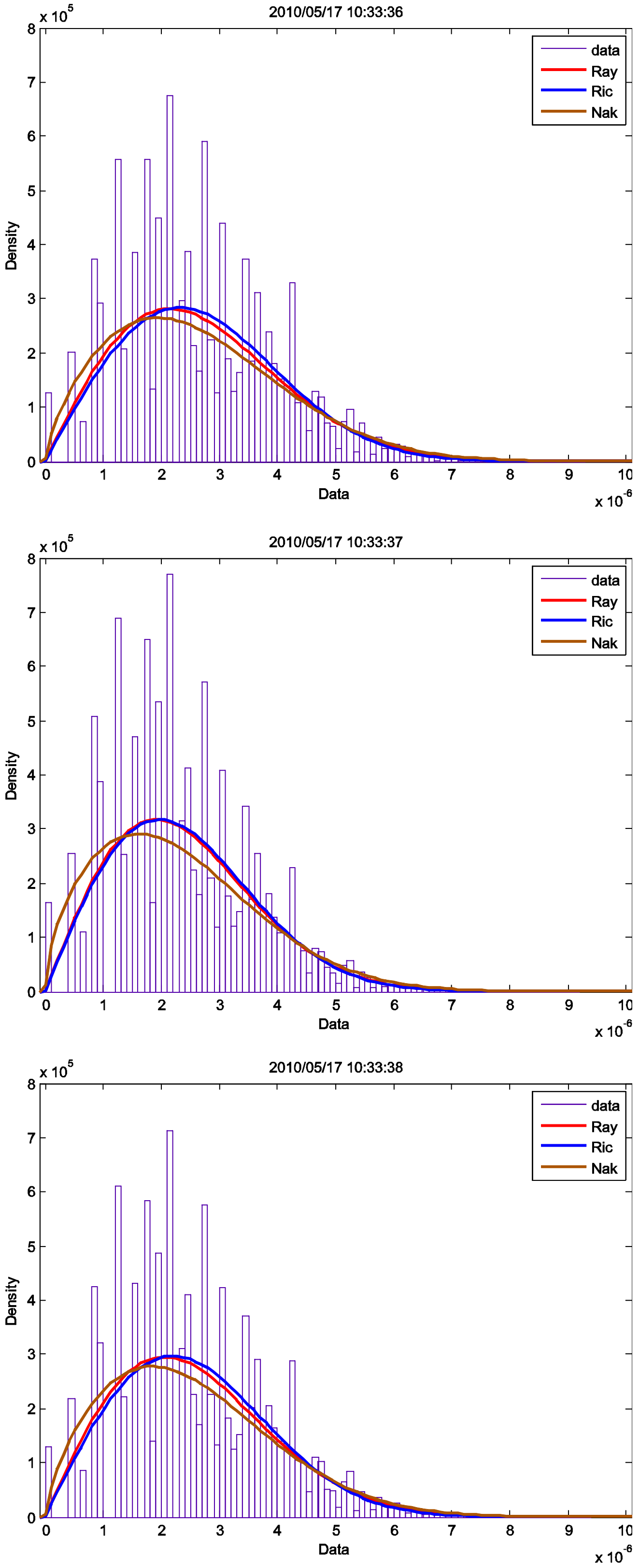

Figure D-5. Data from three successive seconds for 17 May 2010 (residential environment, 162 MHz).

APPENDIX E: ANALYSIS PLOTS FOR ALL SELECTED DATA FILES

For each file selected by the criteria described at the beginning of Appendix D, six plots are presented:

(a) a histogram of the signal’s voltage—see Section 4.2
(b) the average fade duration (AFD)—see Section 4.3
(c) level crossing rate (LCR)—see Section 4.3
(d) cumulative probability distribution function (CPDF)—see Section 5.1
(e) normalized LCR—see Section 5.2
(f) power spectral density (PSD)—see Section 5.3

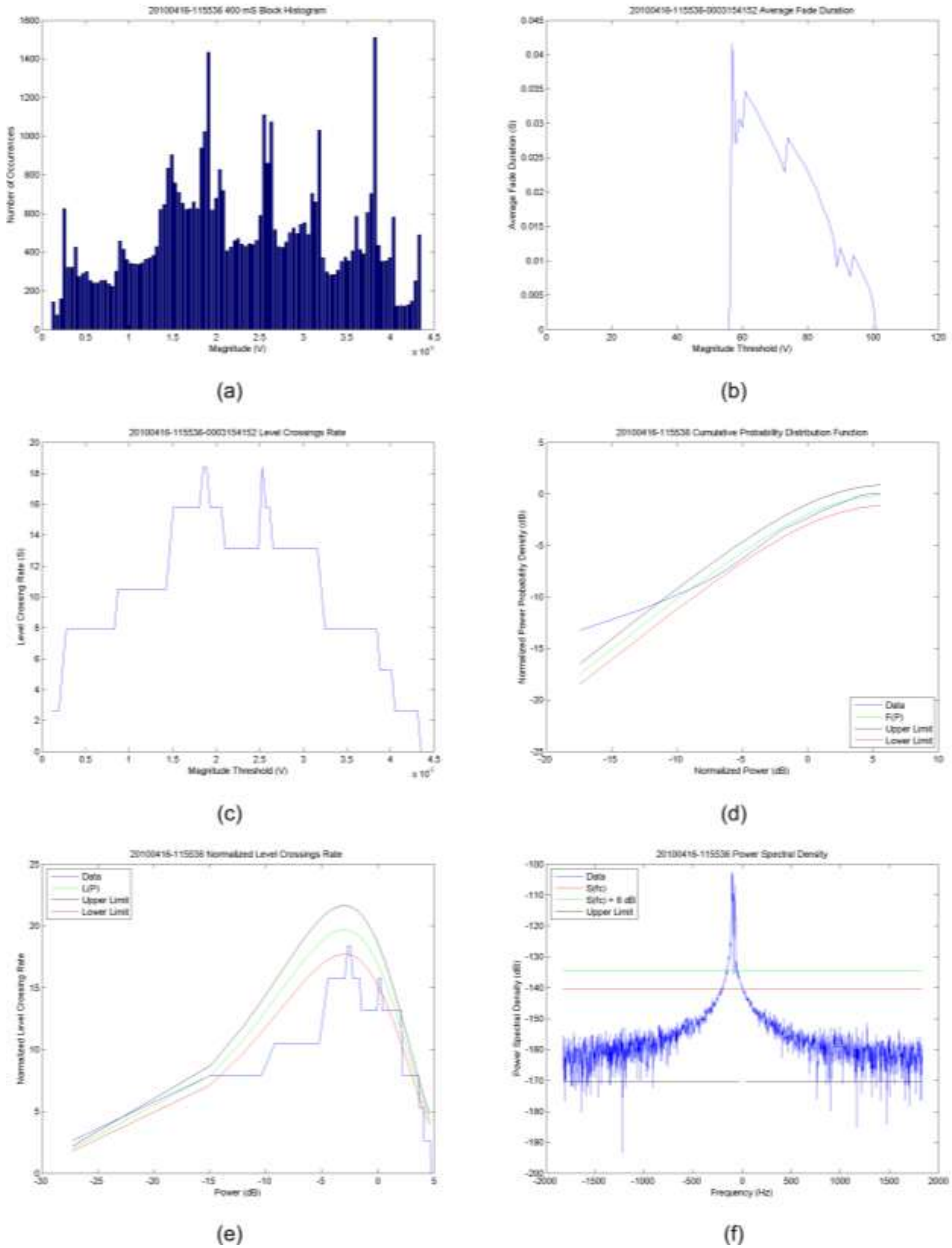

(a) (b) (c) (d) (e) (f)

Figure E-1. Plots for data file 2010/04/16 11:55:36 (residential environment, 793 MHz).

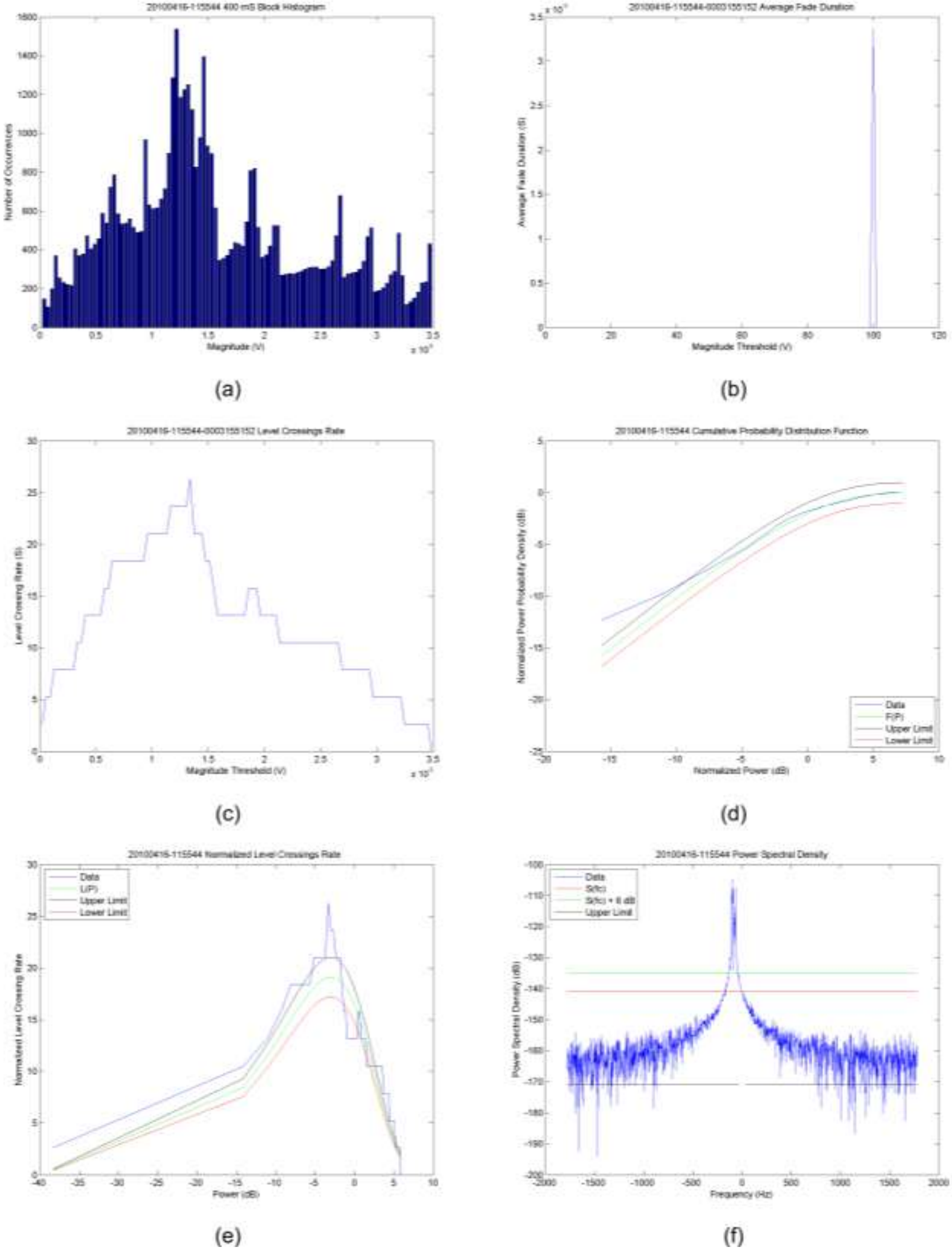

(a) (b)

(c) (d)

(e) (f)

Figure E-2. Plots for data file 2010/04/16 11:55:44 (residential environment, 793 MHz).

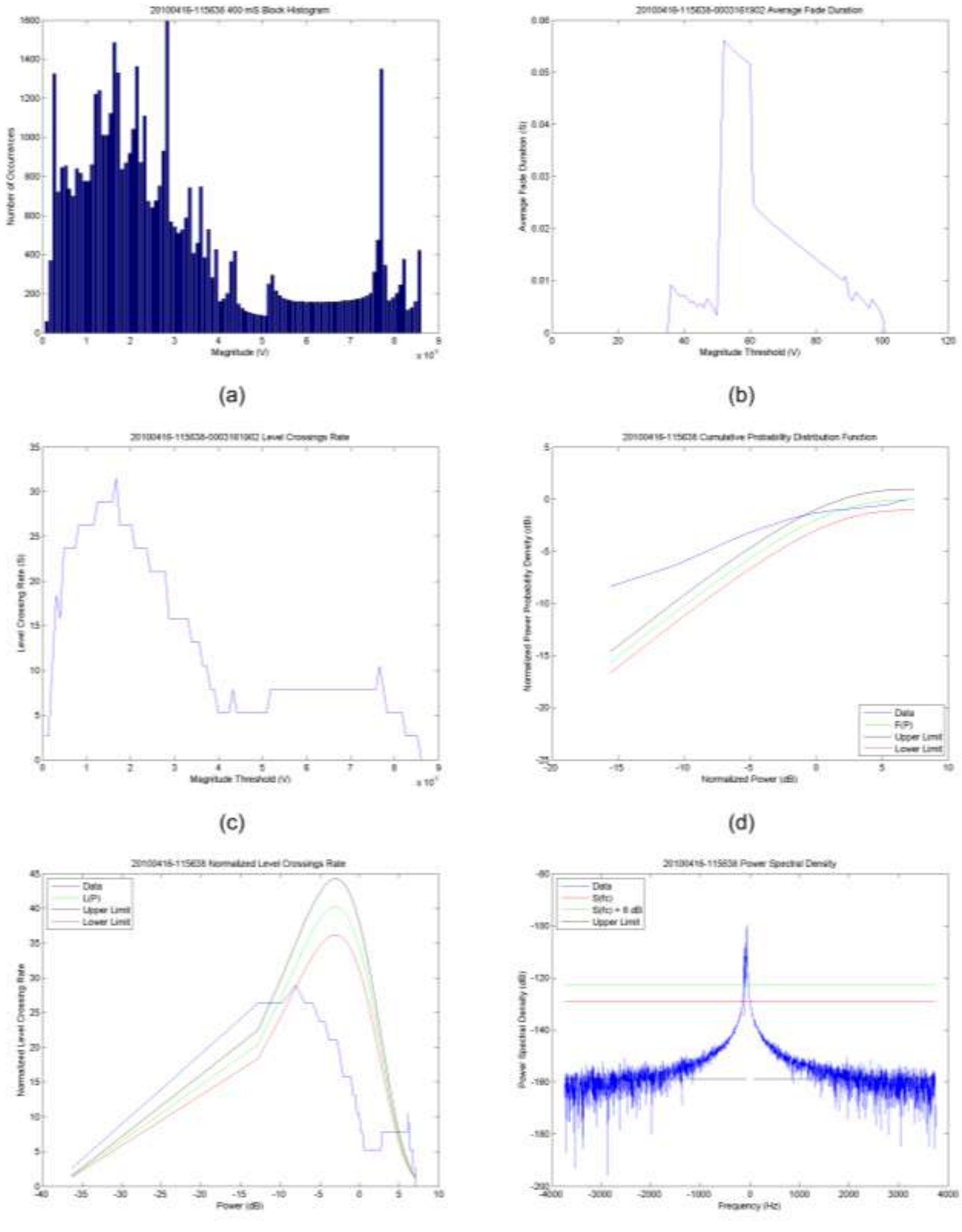

(a) (b)

(c) (d)

(e) (f)

Figure E-3. Plots for data file 2010/04/16 11:56:38 (residential environment, 793 MHz).

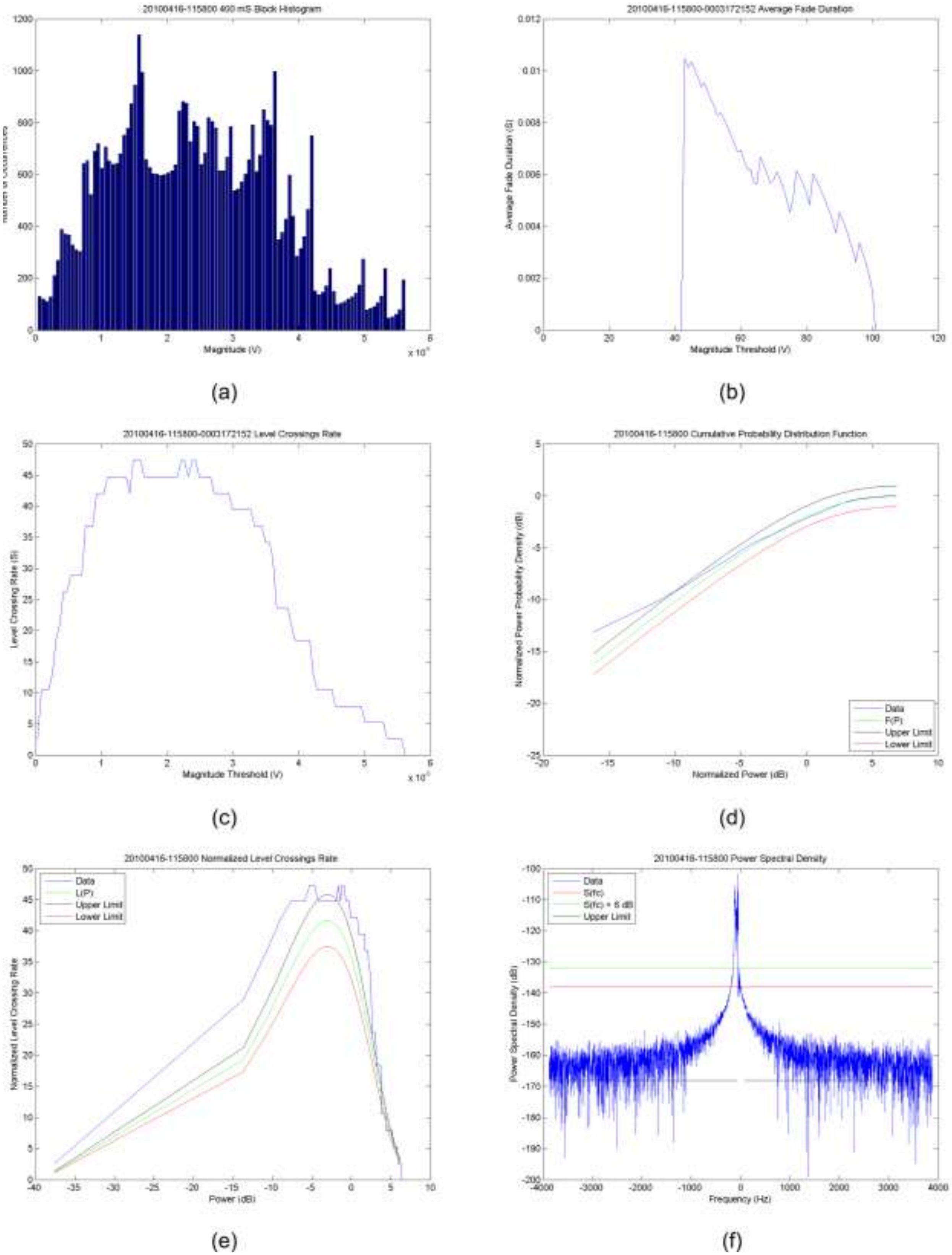

(a)

(b)

(c)

(d)

(e)

(f)

Figure E-4. Plots for data file 2010/04/16 11:58:00 (residential environment, 793 MHz).

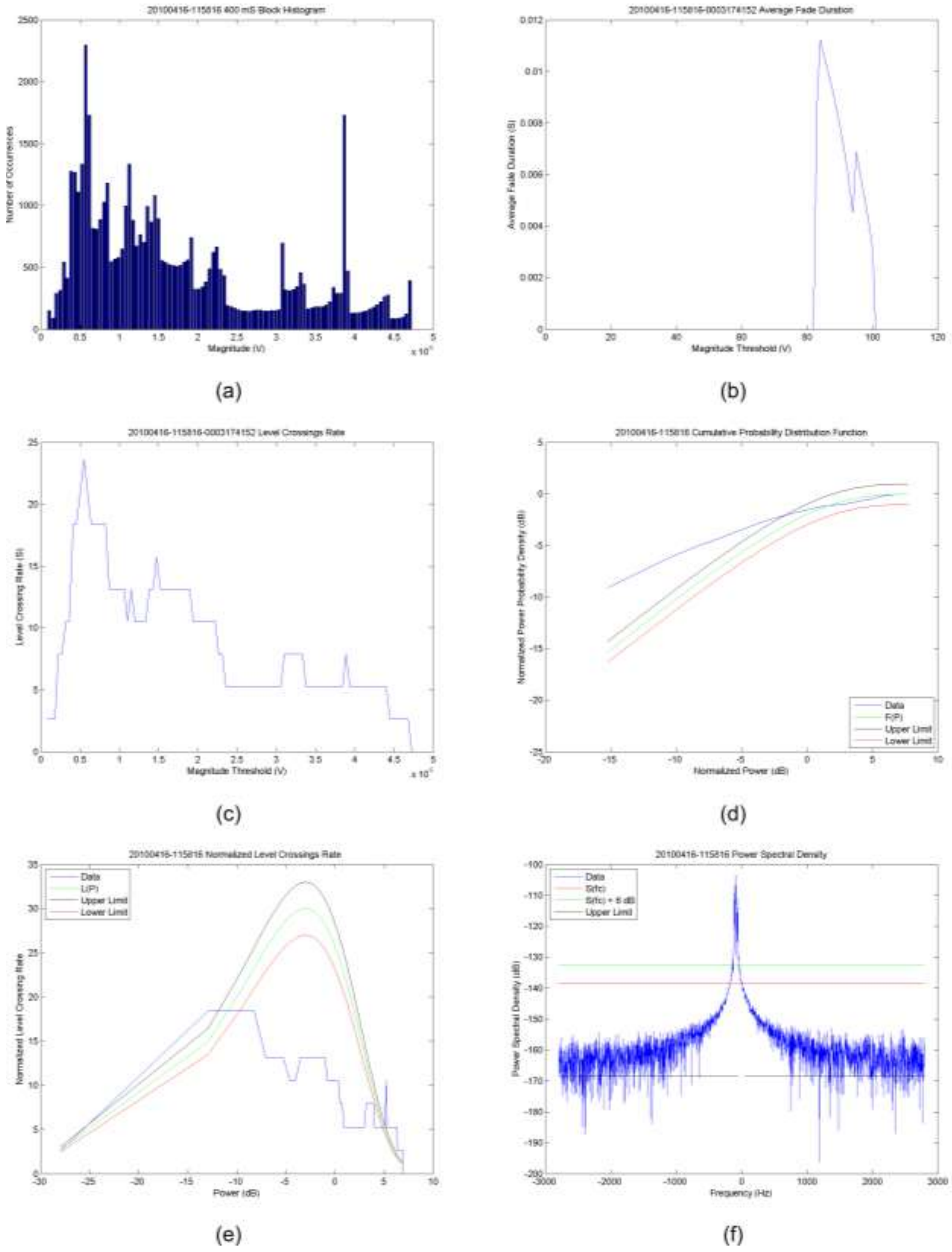

Figure E-5. Plots for data file 2010/04/16 11:58:16 (residential environment, 793 MHz).

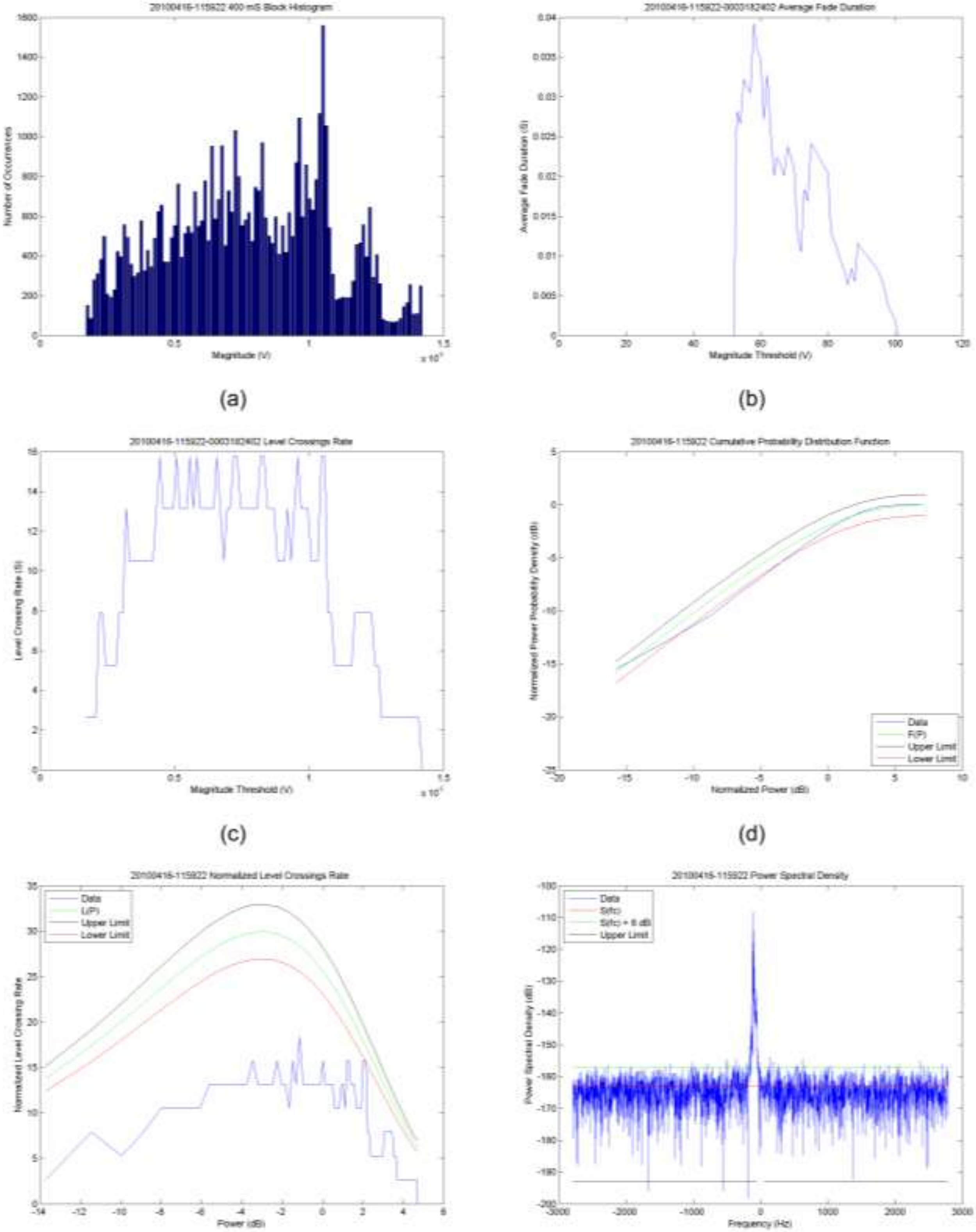

(a)

(b)

(c)

(d)

(e)

(f)

Figure E-6. Plots for data file 2010/04/16 11:59:22 (residential environment, 793 MHz).

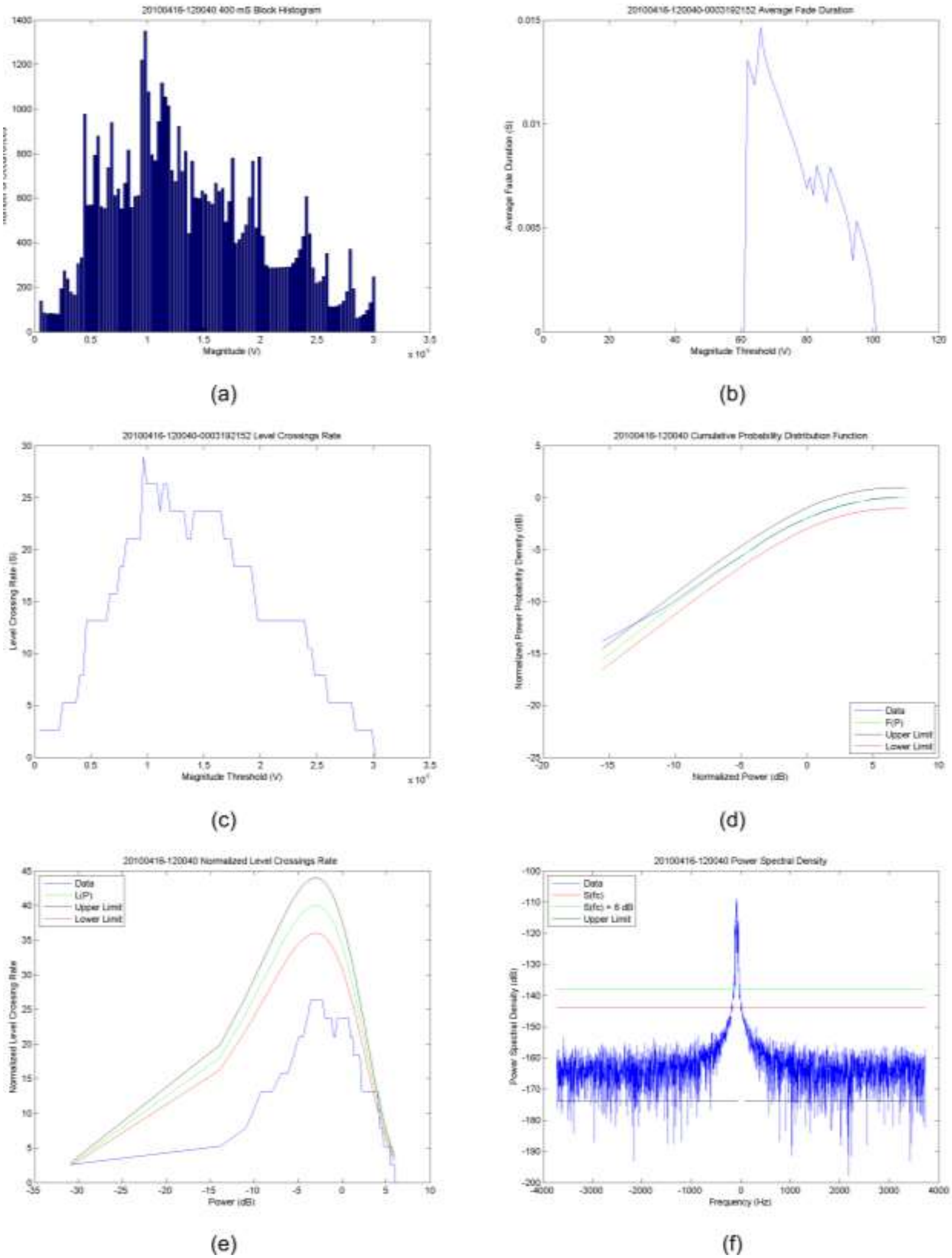

(a) (b)

(c) (d)

(e) (f)

Figure E-7, Plots for data file 2010/04/16 12:00:40 (residential environment, 793 MHz).

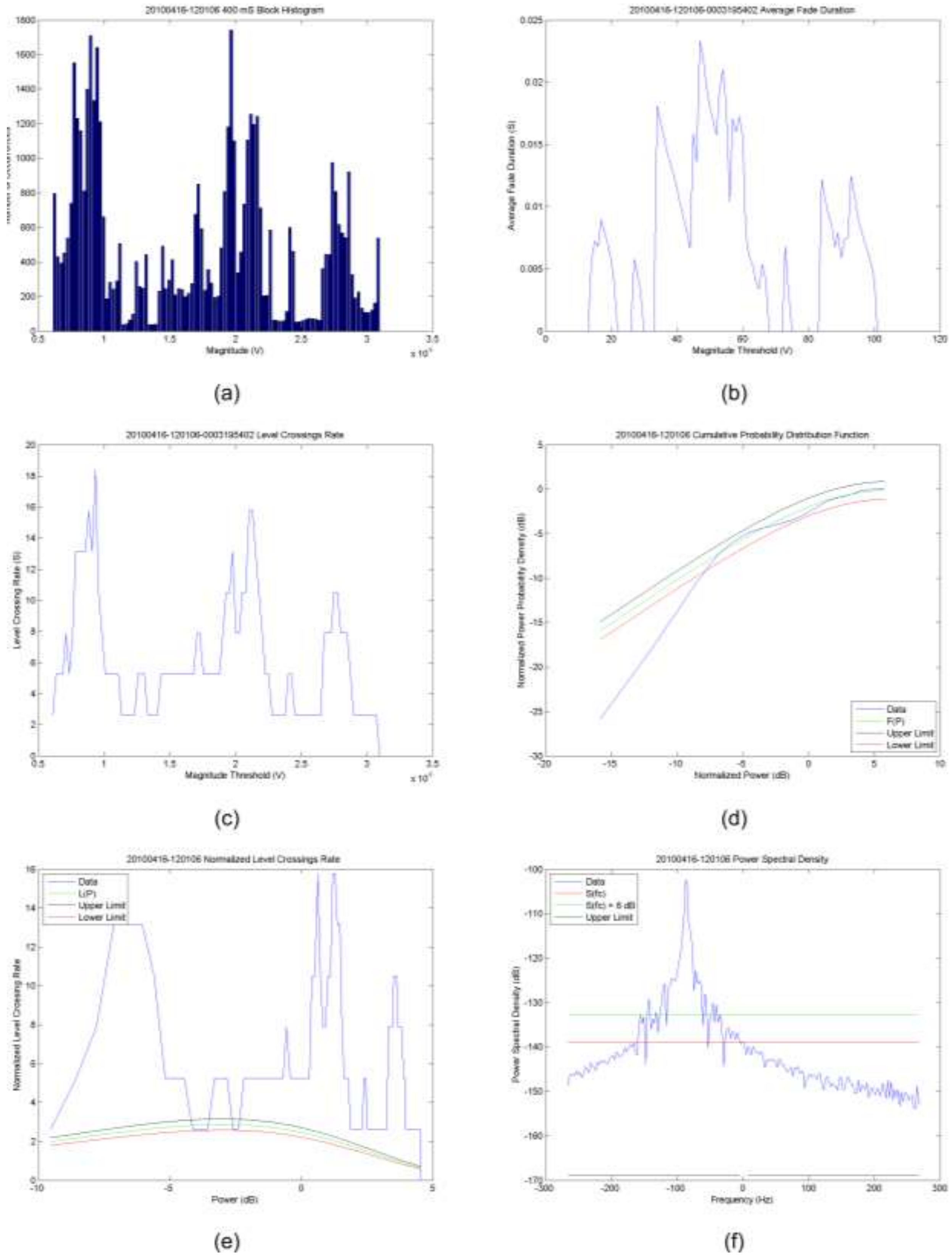

(a) (b)

(c) (d)

(e) (f)

Figure E-8. Plots for data file 2010/04/16 12:01:06 (residential environment, 793 MHz).

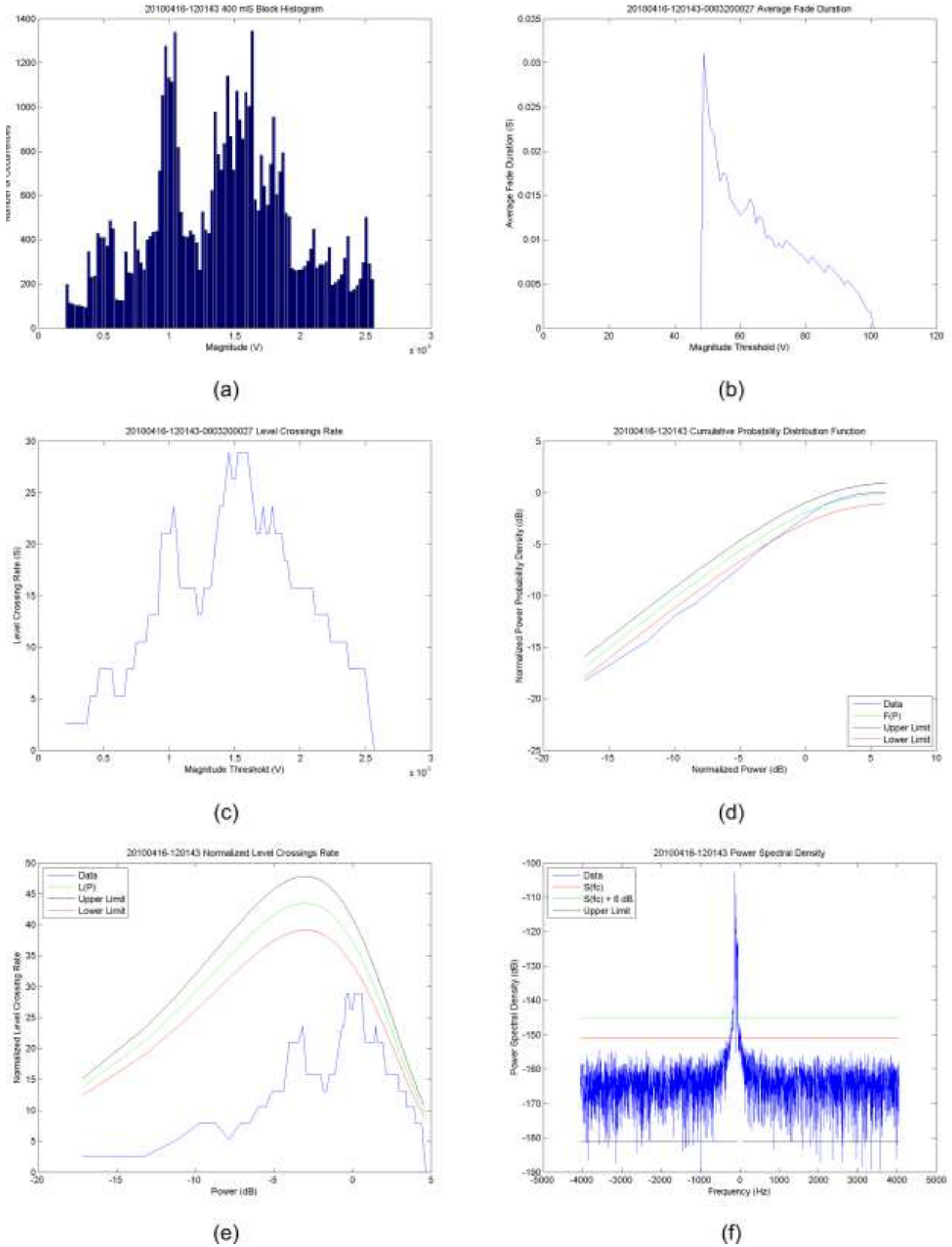

(a) (b)

(c) (d)

(e) (f)

Figure E-9. Plots for data file 2010/04/16 12:01:43 (residential environment, 793 MHz).

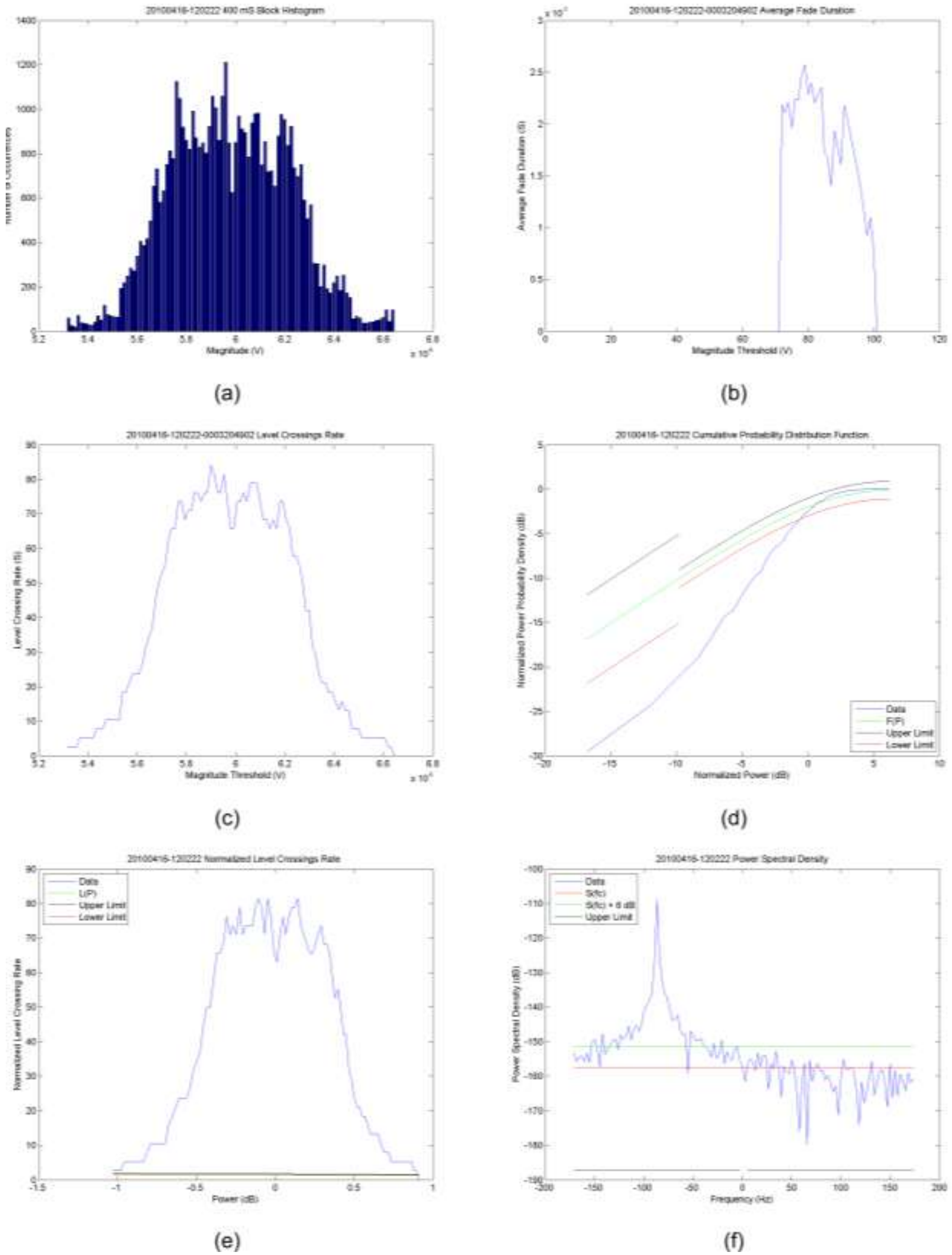

(a) (b) (c) (d) (e) (f)

Figure E-10. Plots for data file 2010/04/16 12:02:22 (residential environment, 793 MHz).

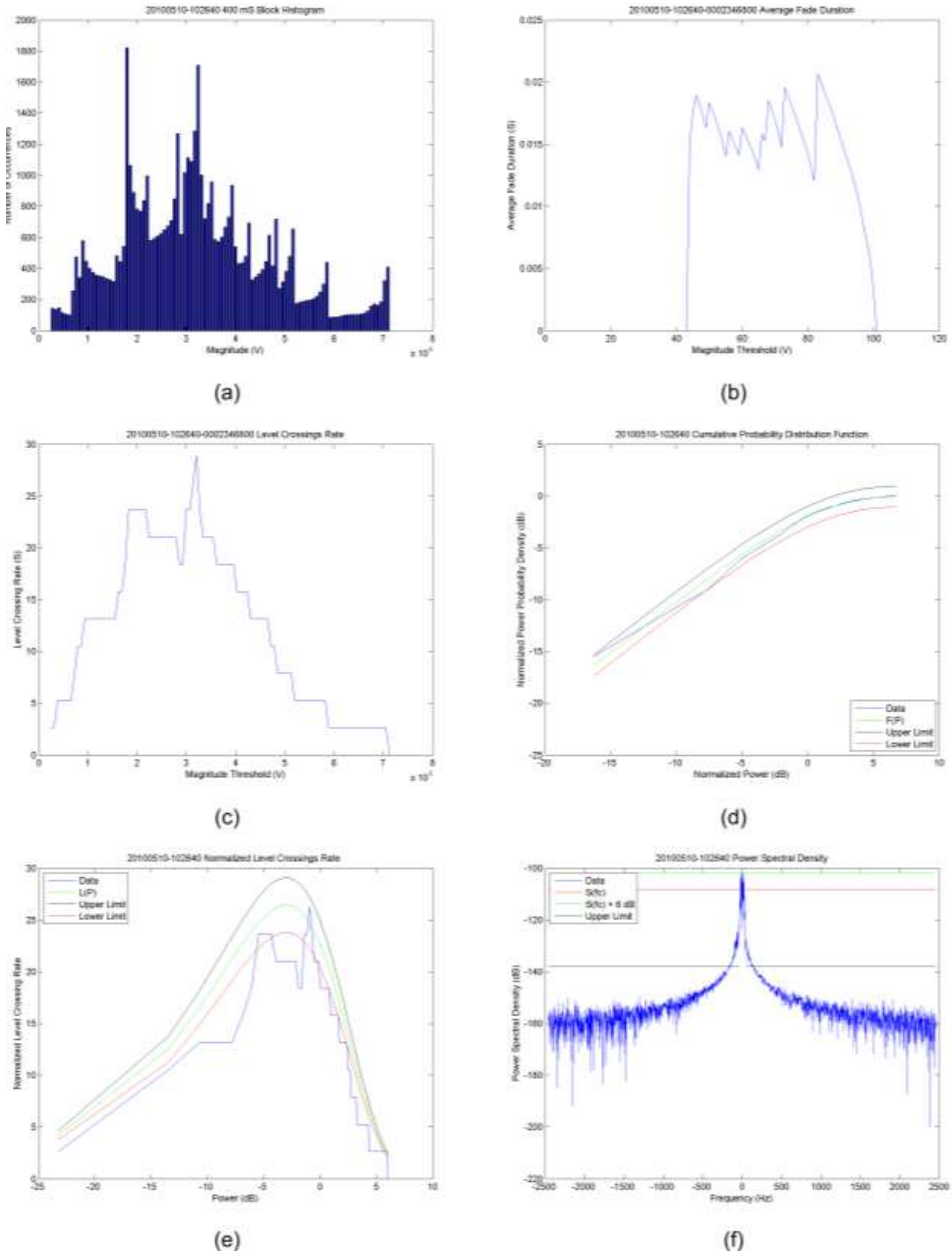

Figure E-11. Plots for data file 2010/05/10 10:26:40 (low-rise urban environment, 793 MHz).

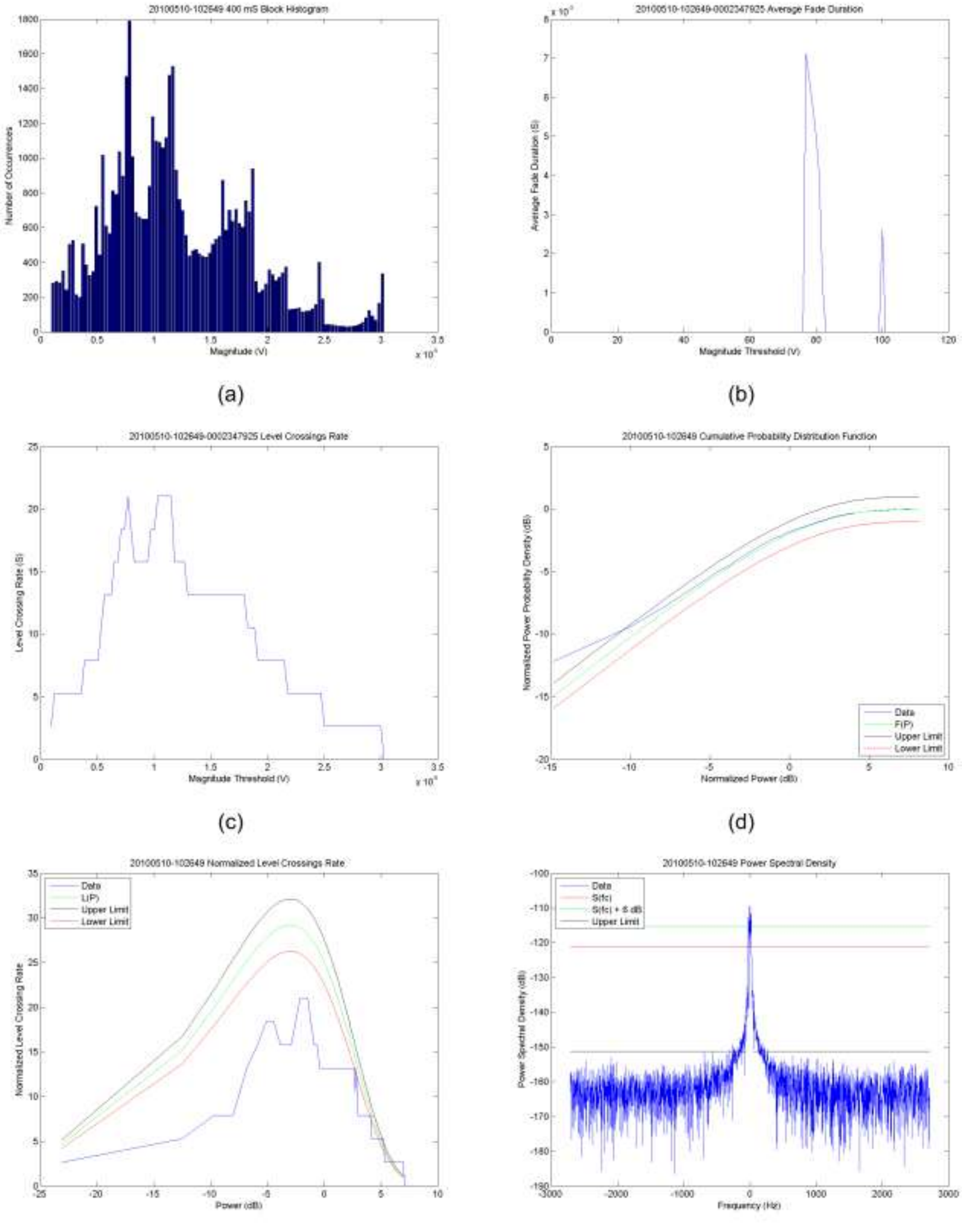

(a) (b)

(c) (d)

(e) (f)

Figure E-12. Plots for data file 2010/05/10 10:26:49 (low-rise urban environment, 793 MHz).

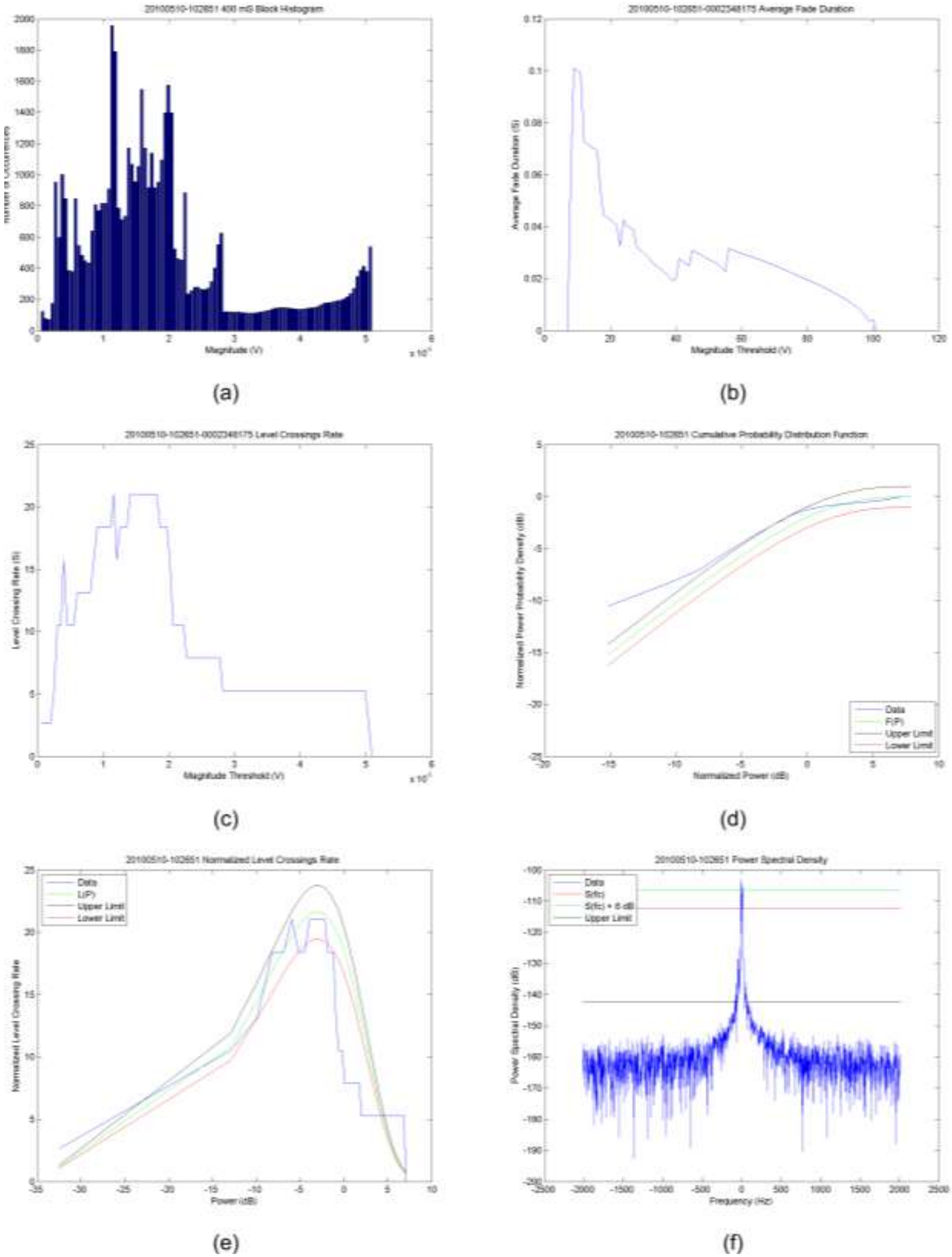

(a) (b)

(c) (d)

(e) (f)

Figure E-13. Plots for data file 2010/05/10 10:26:53 (low-rise urban environment, 793 MHz).

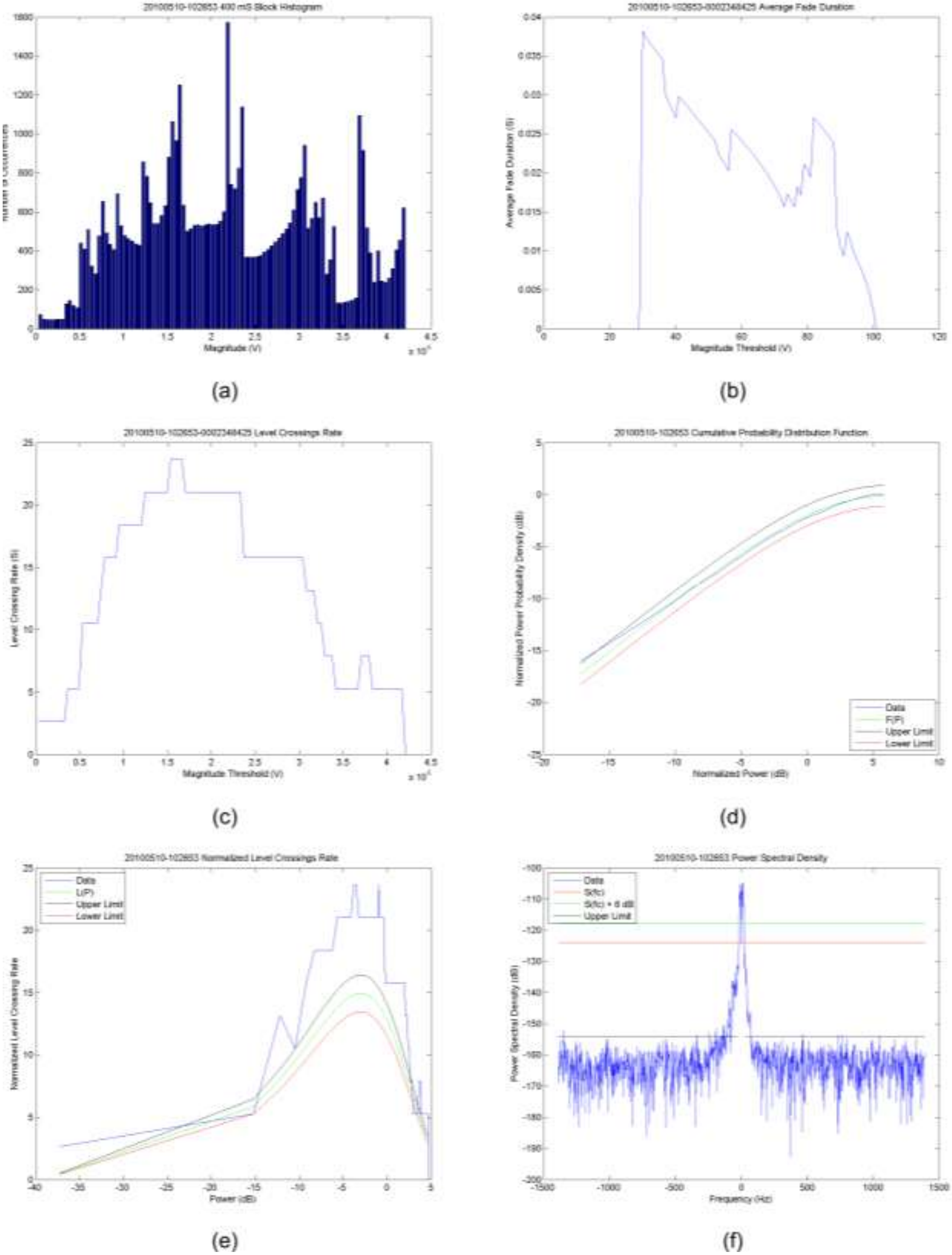

Figure E-14. Plots for data file 2010/05/10 10:26:57 (low-rise urban environment, 793 MHz).

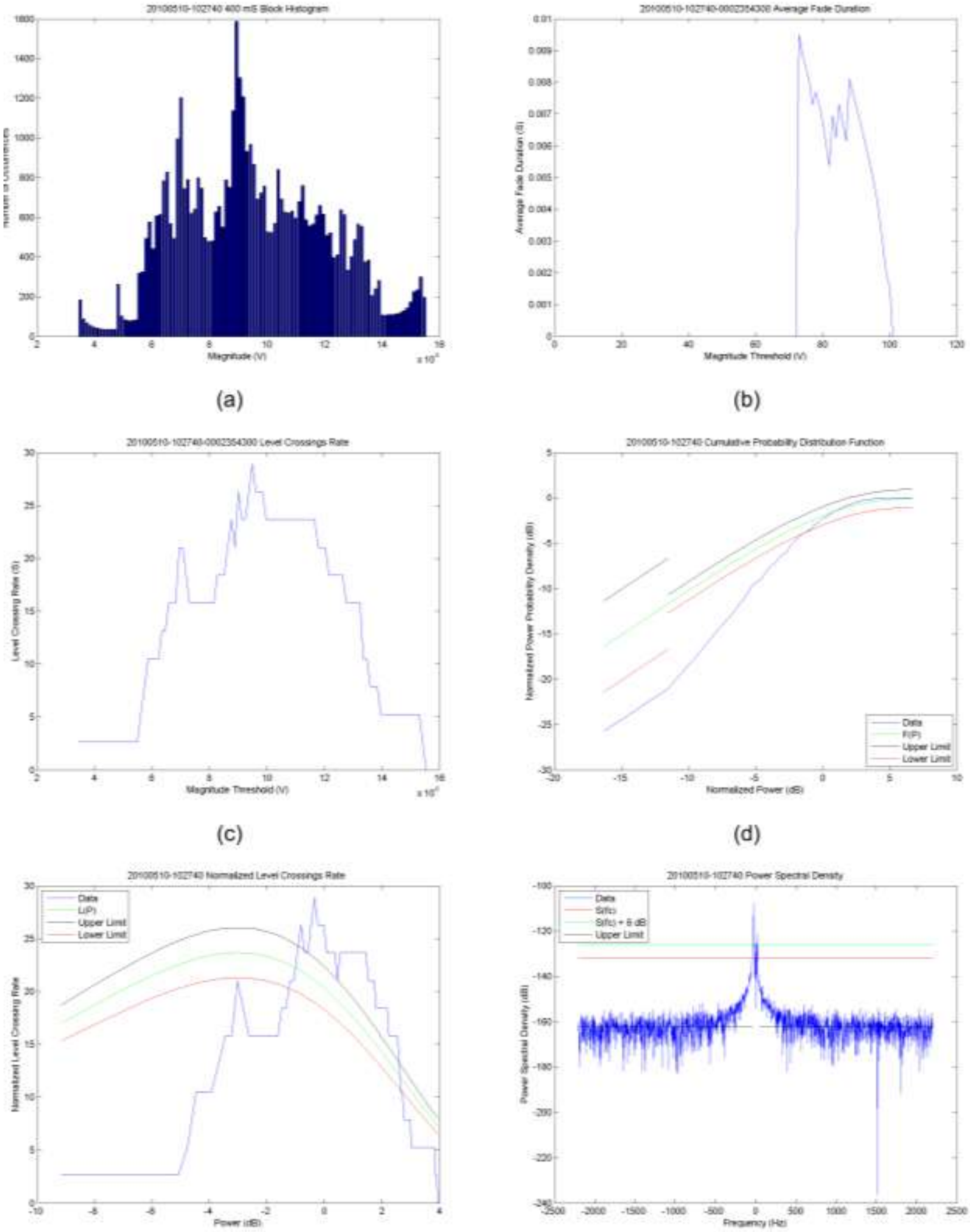

(a) (b)

(c) (d)

(e) (f)

Figure E-15. Plots for data file 2010/05/10 10:27:40 (low-rise urban environment, 793 MHz).

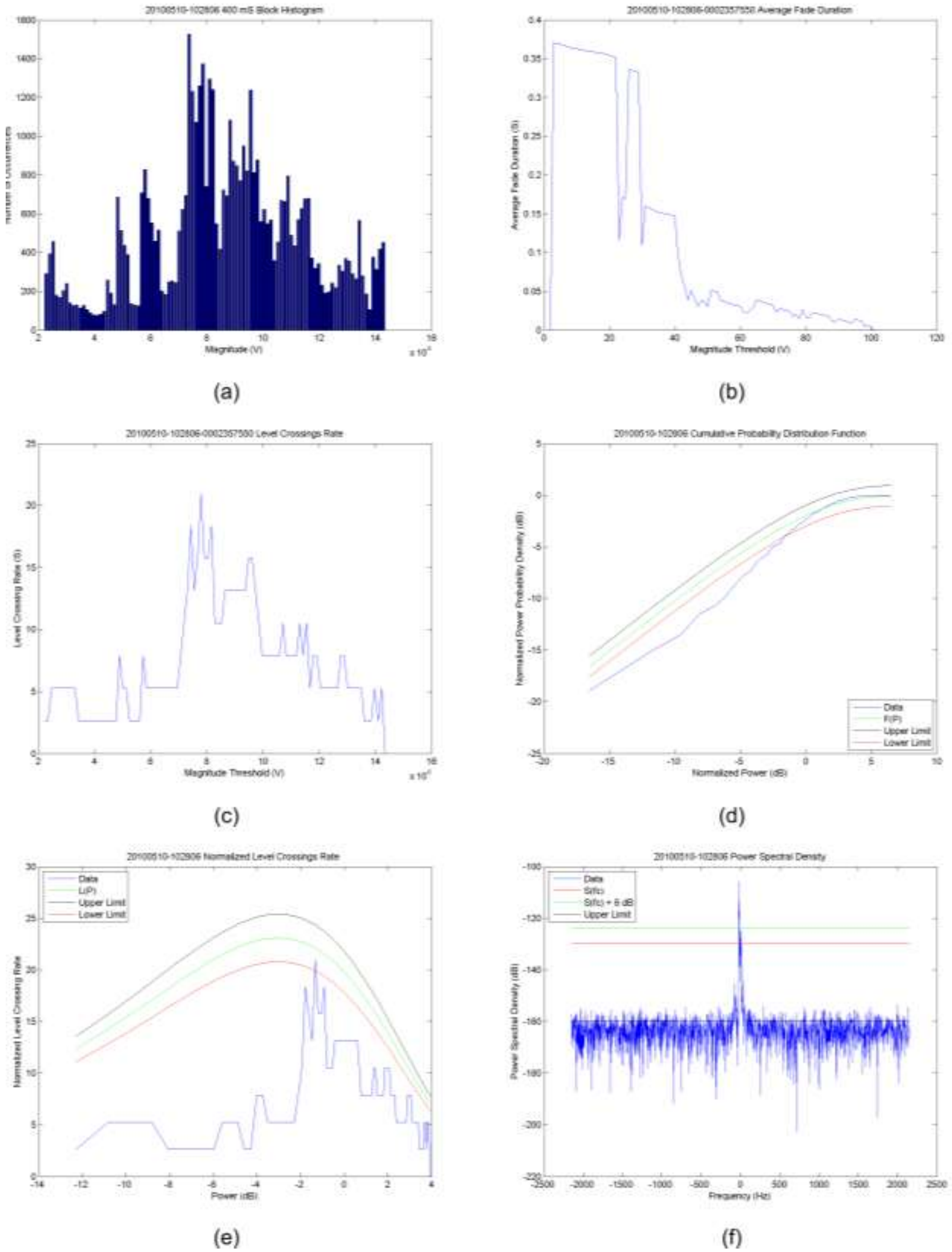

(a) (b) (c) (d) (e) (f)

Figure E-16. Plots for data file 2010/05/10 10:28:06 (low-rise urban environment, 793 MHz).

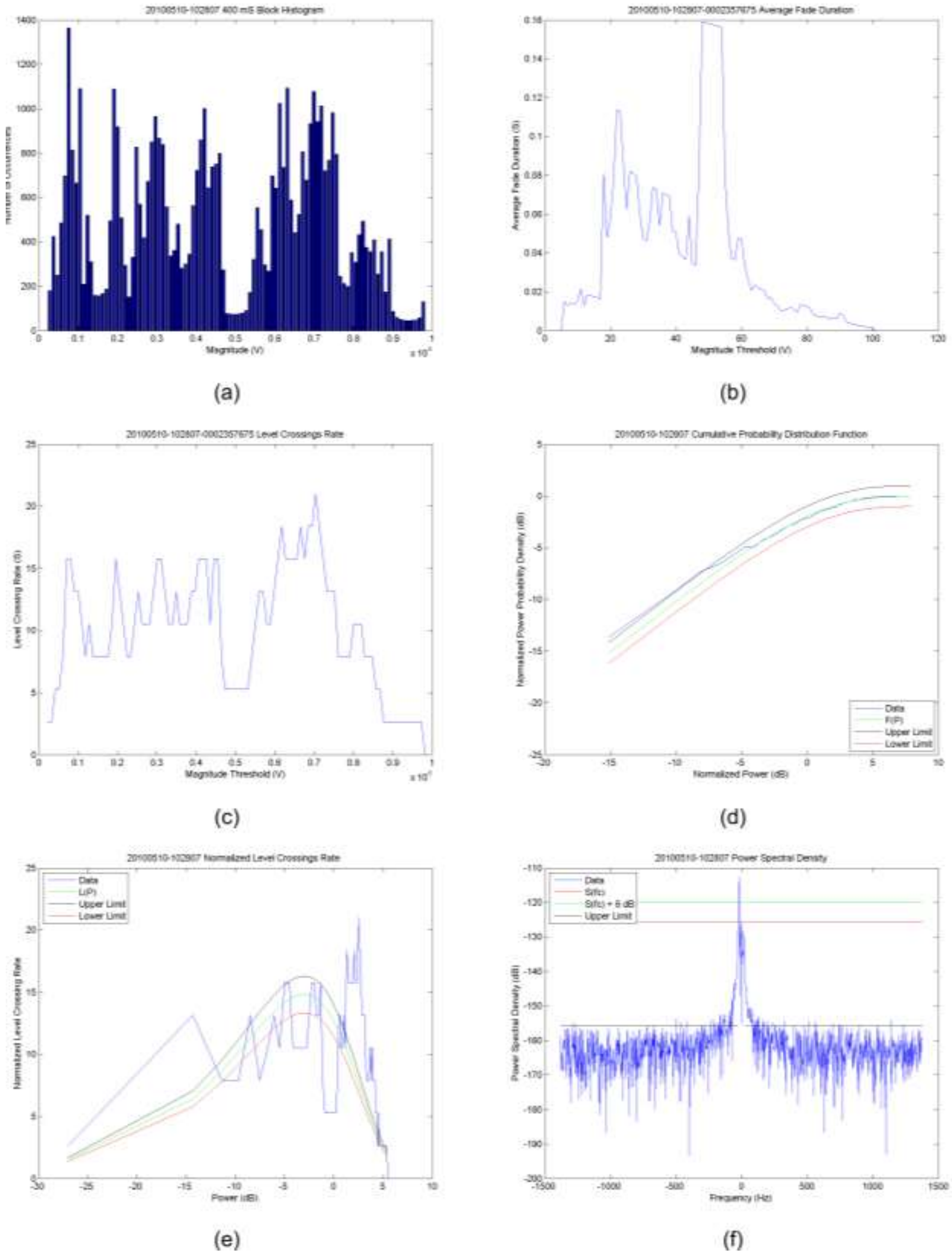

(a)

(b)

(c)

(d)

(e)

(f)

Figure E-17. Plots for data file 2010/05/10 10:28:07 (low-rise urban environment, 793 MHz).

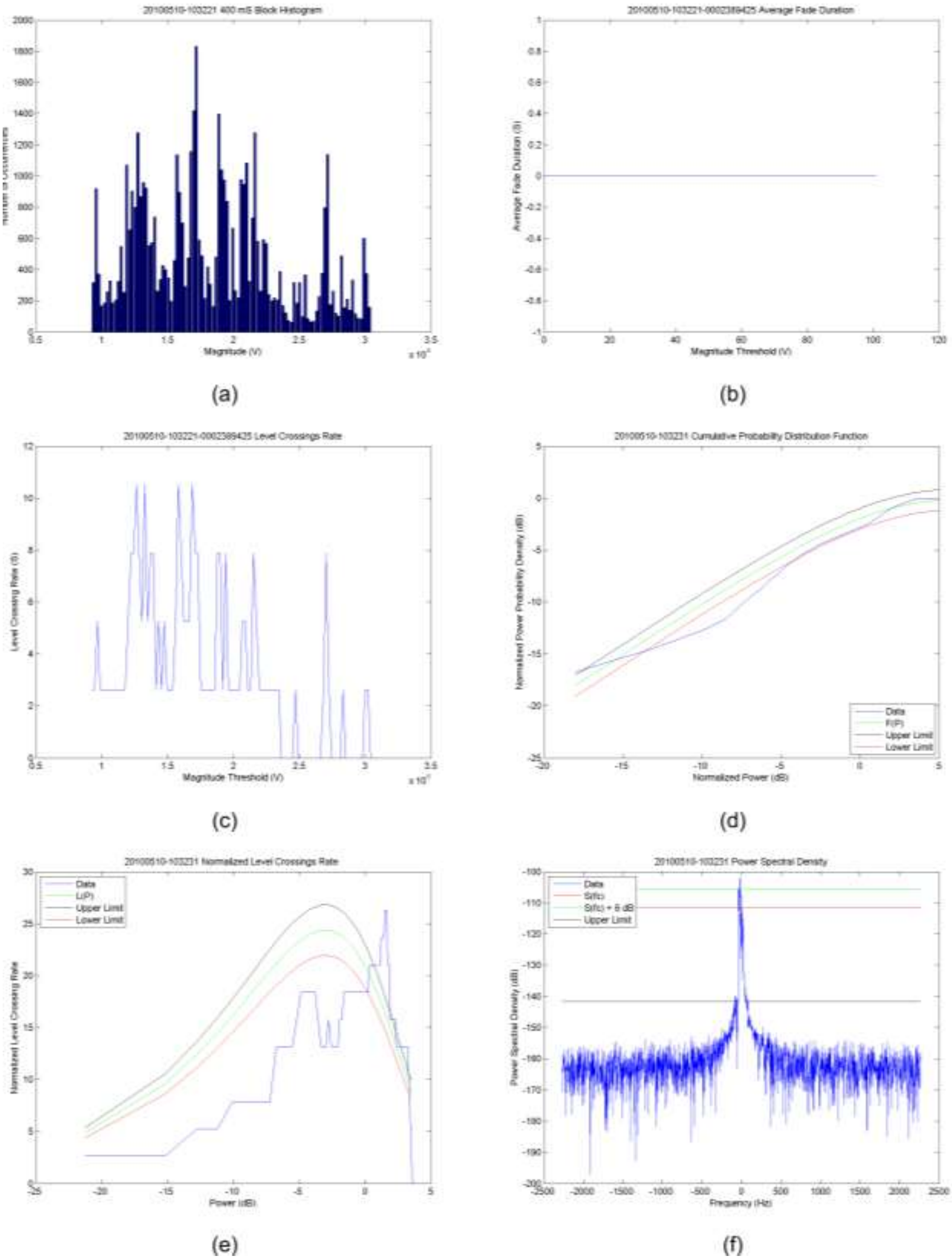

(a) (b) (c) (d) (e) (f)

Figure E-18. Plots for data file 2010/05/10 10:32:21 (low-rise urban environment, 793 MHz).

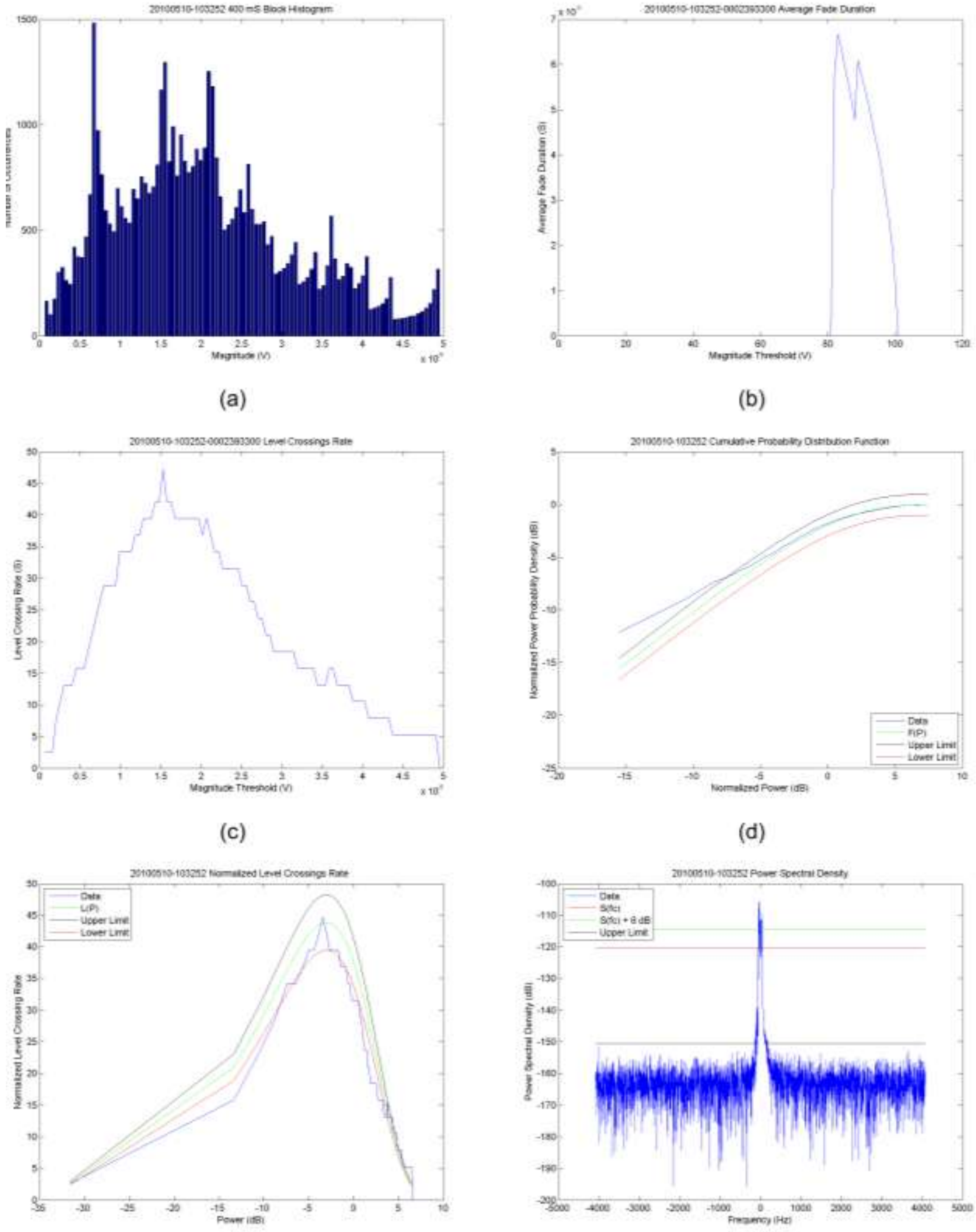

(a) (b)

(c) (d)

(e) (f)

Figure E-19. Plots for data file 2010/05/10 10:32:52 (low-rise urban environment, 793 MHz).

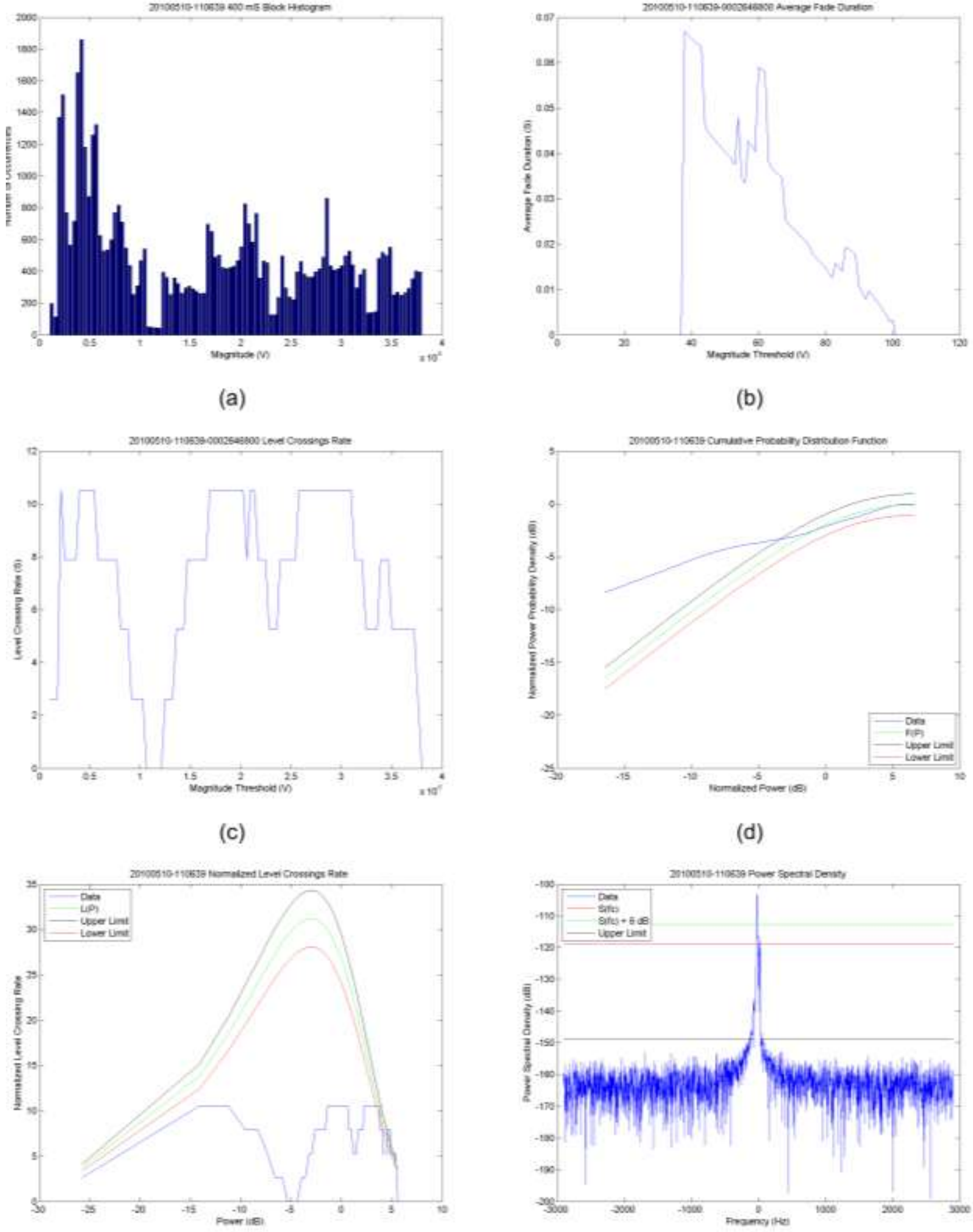

(a) (b)

(c) (d)

(e) (f)

Figure E-20. Plots for data file 2010/05/10 11:06:39 (low-rise urban environment, 793 MHz).

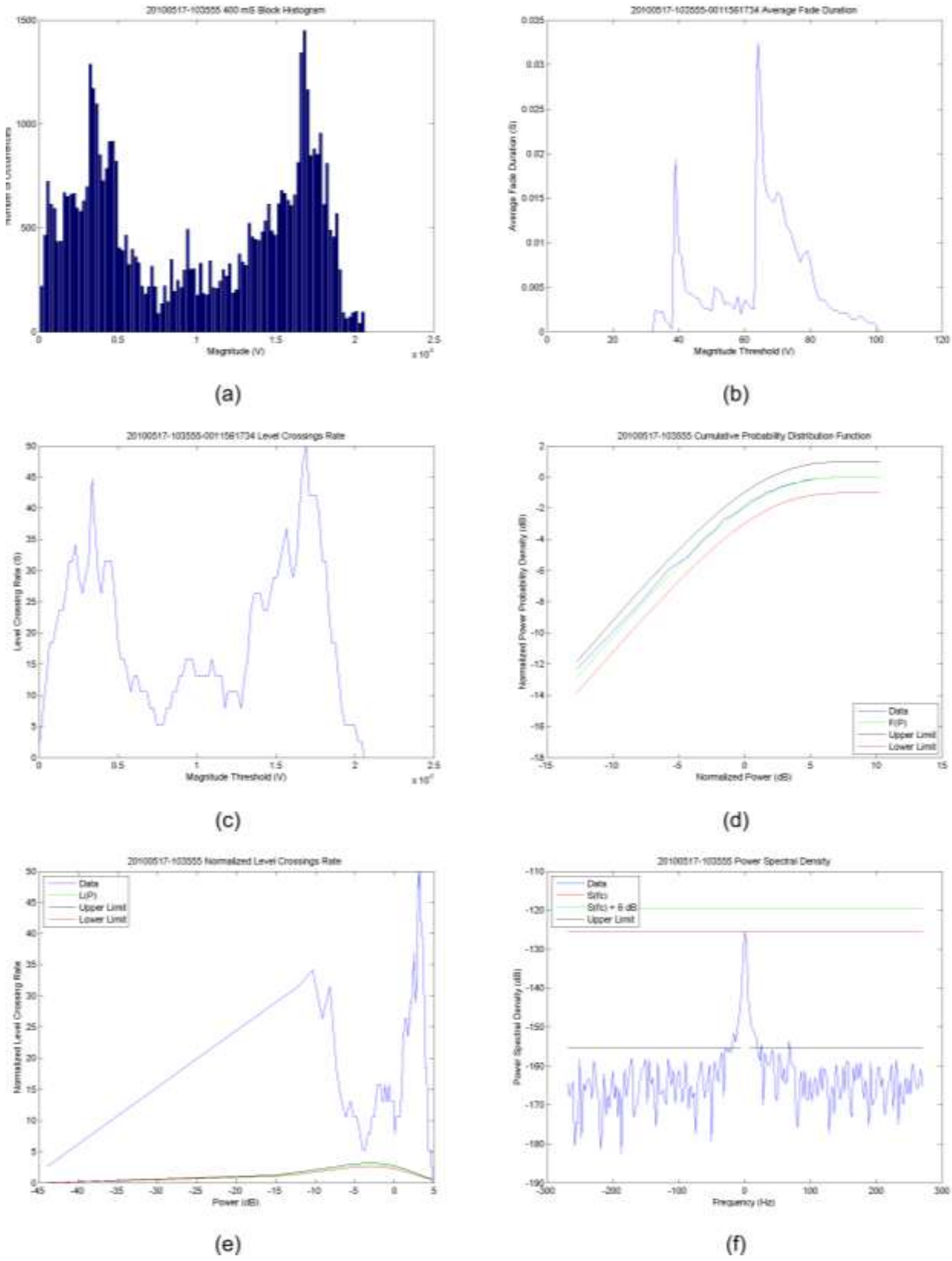

Figure E-21. Plots for data file 2010/05/17 10:35:55 (residential environment, 162 MHz).

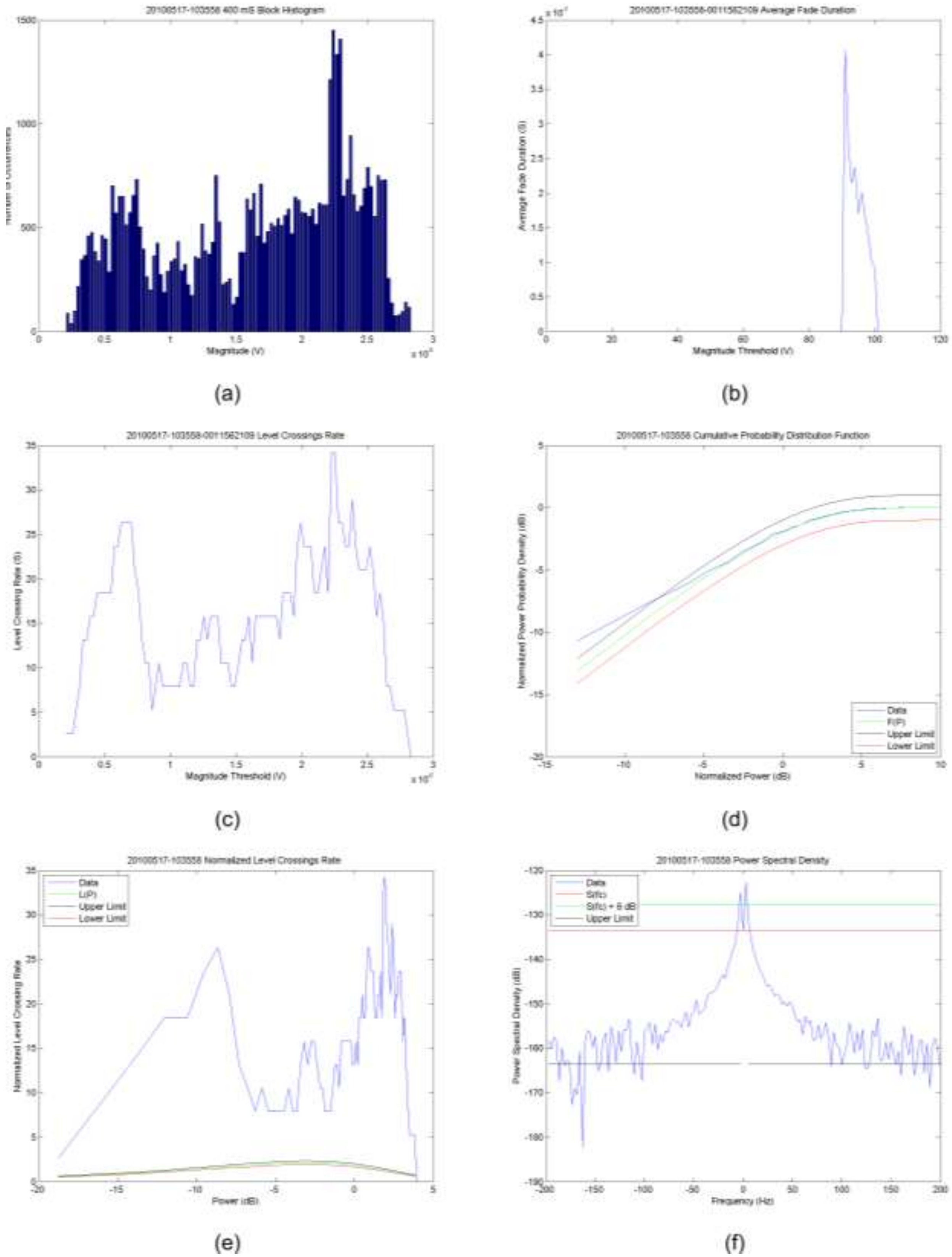

(a) (b) (c) (d) (e) (f)

Figure E-22. Plots for data file 2010/05/17 10:35:58 (residential environment, 162 MHz).

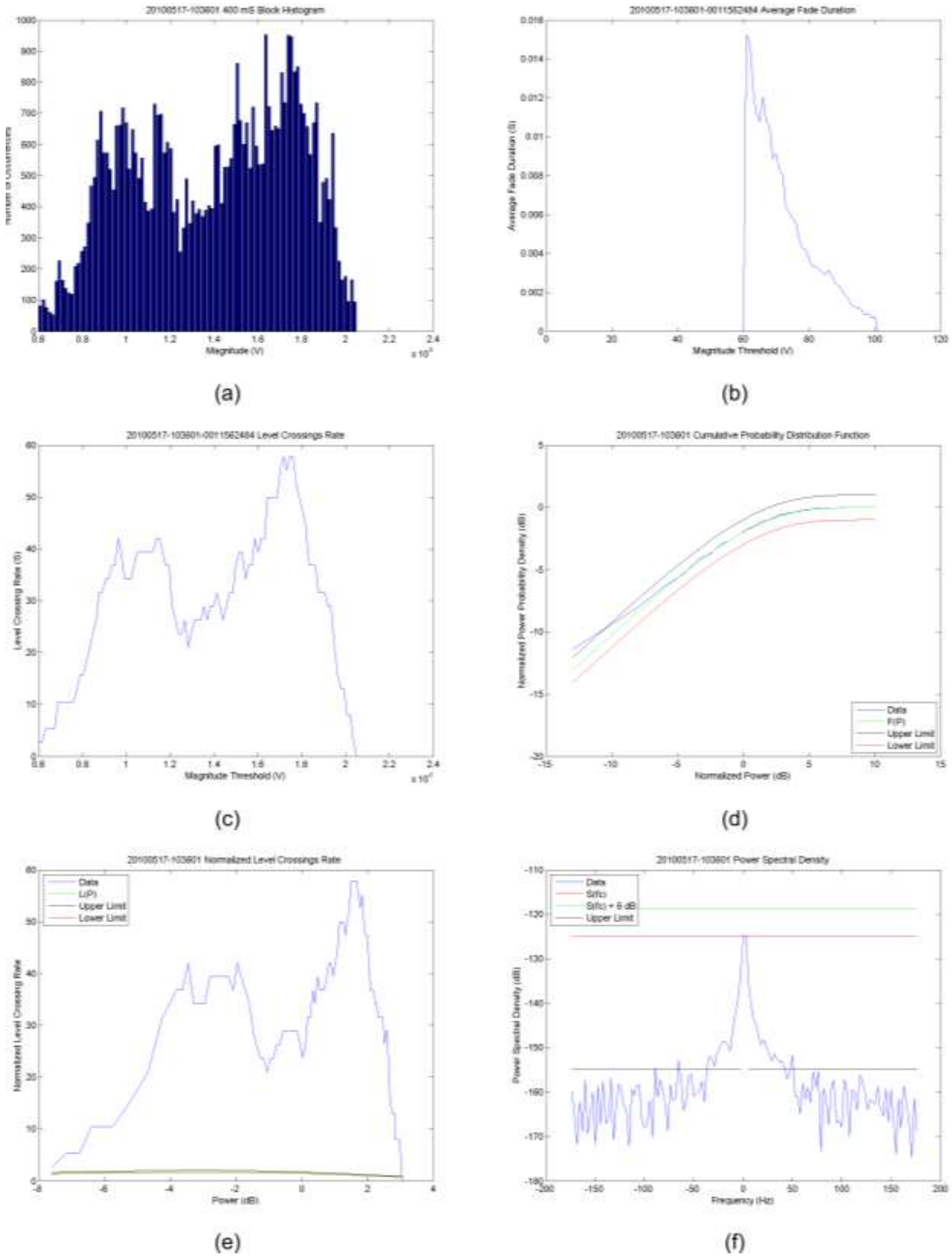

(a) (b) (c) (d) (e) (f)

Figure E-23. Plots for data file 2010/05/17 10:36:01 (residential environment, 162 MHz).

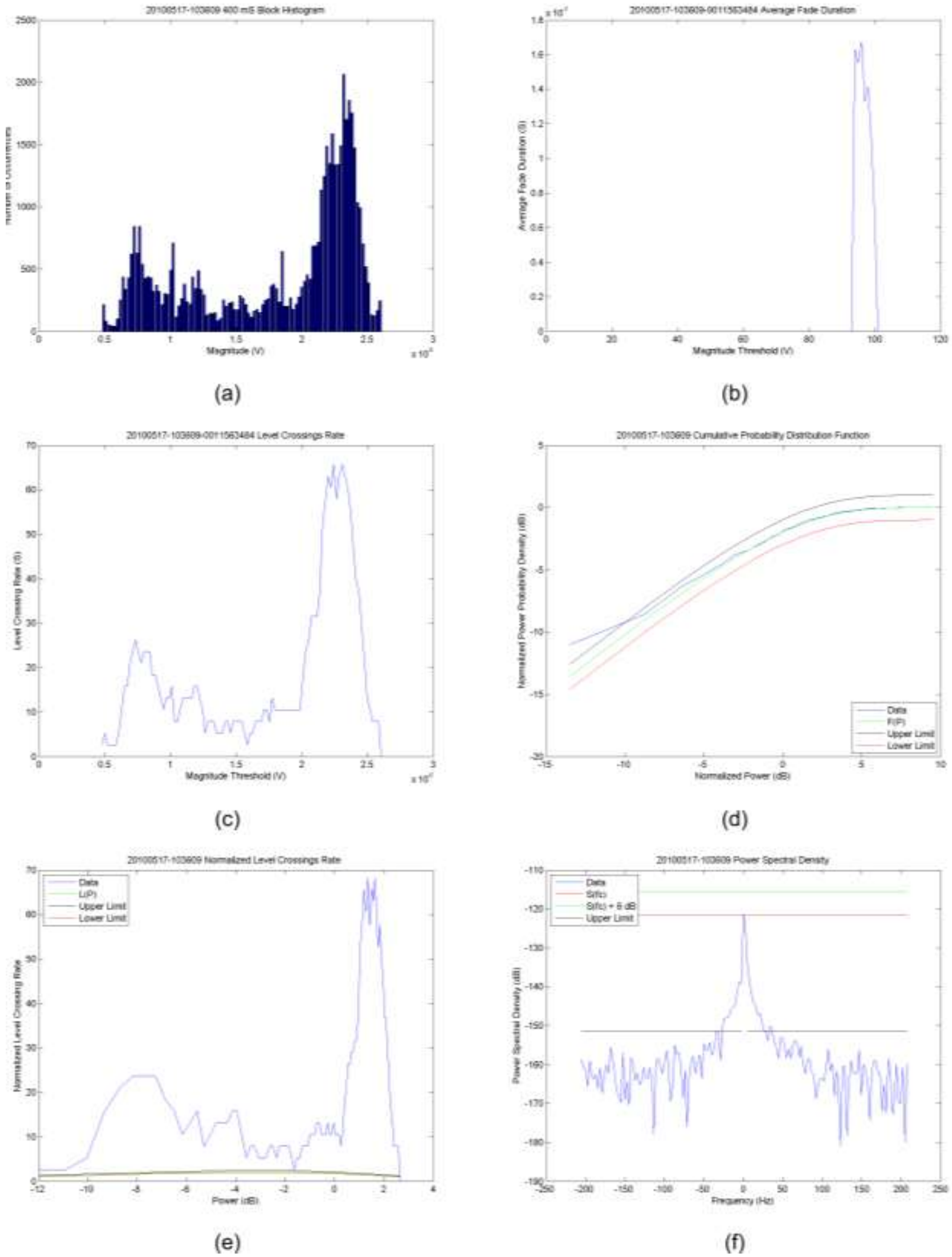

(a) (b) (c) (d) (e) (f)

Figure E-24. Plots for data file 2010/05/17 10:36:09 (residential environment, 162 MHz).

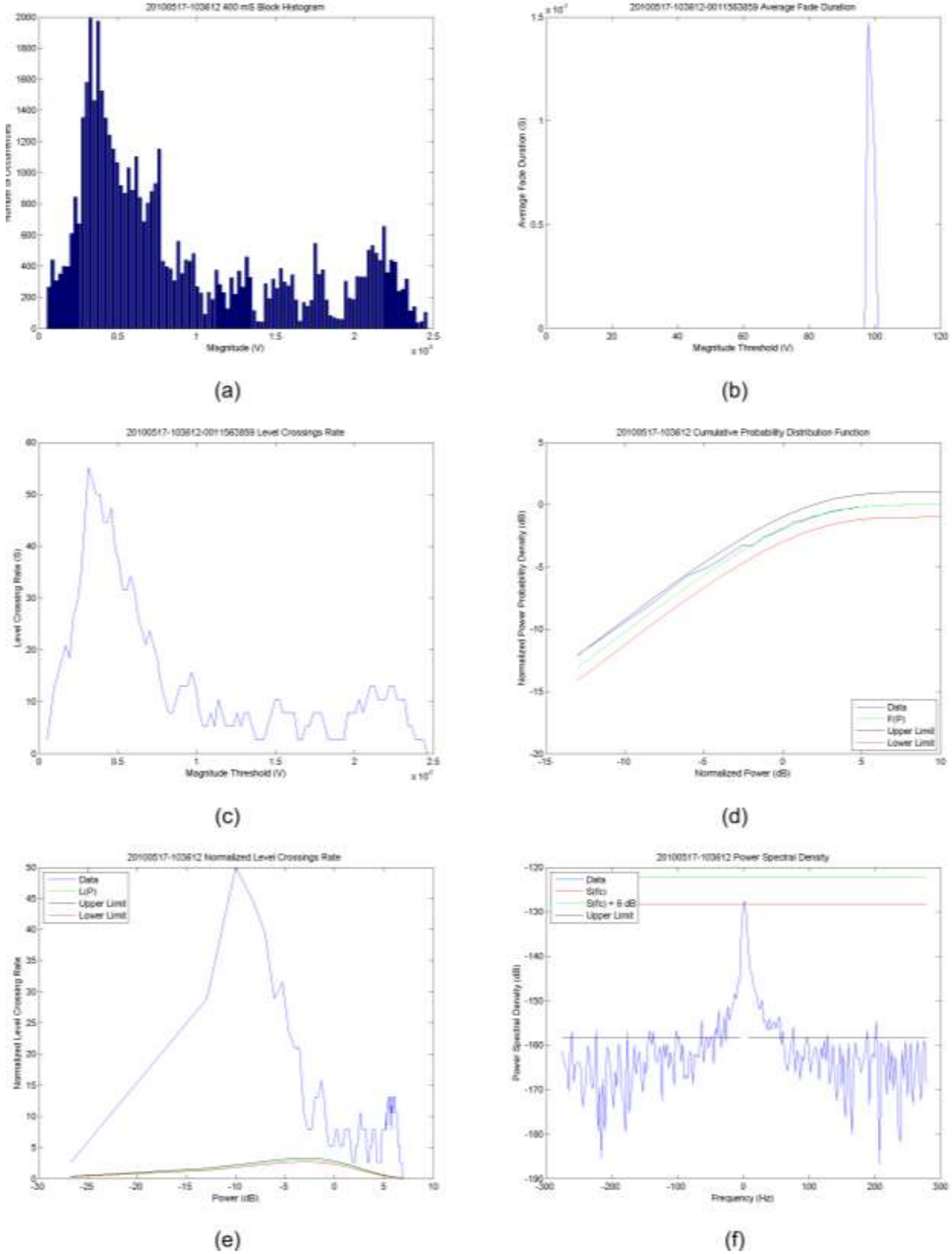

(a) (b)

(c) (d)

(e) (f)

Figure E-25. Plots for data file 2010/05/17 10:36:12 (residential environment, 162 MHz).

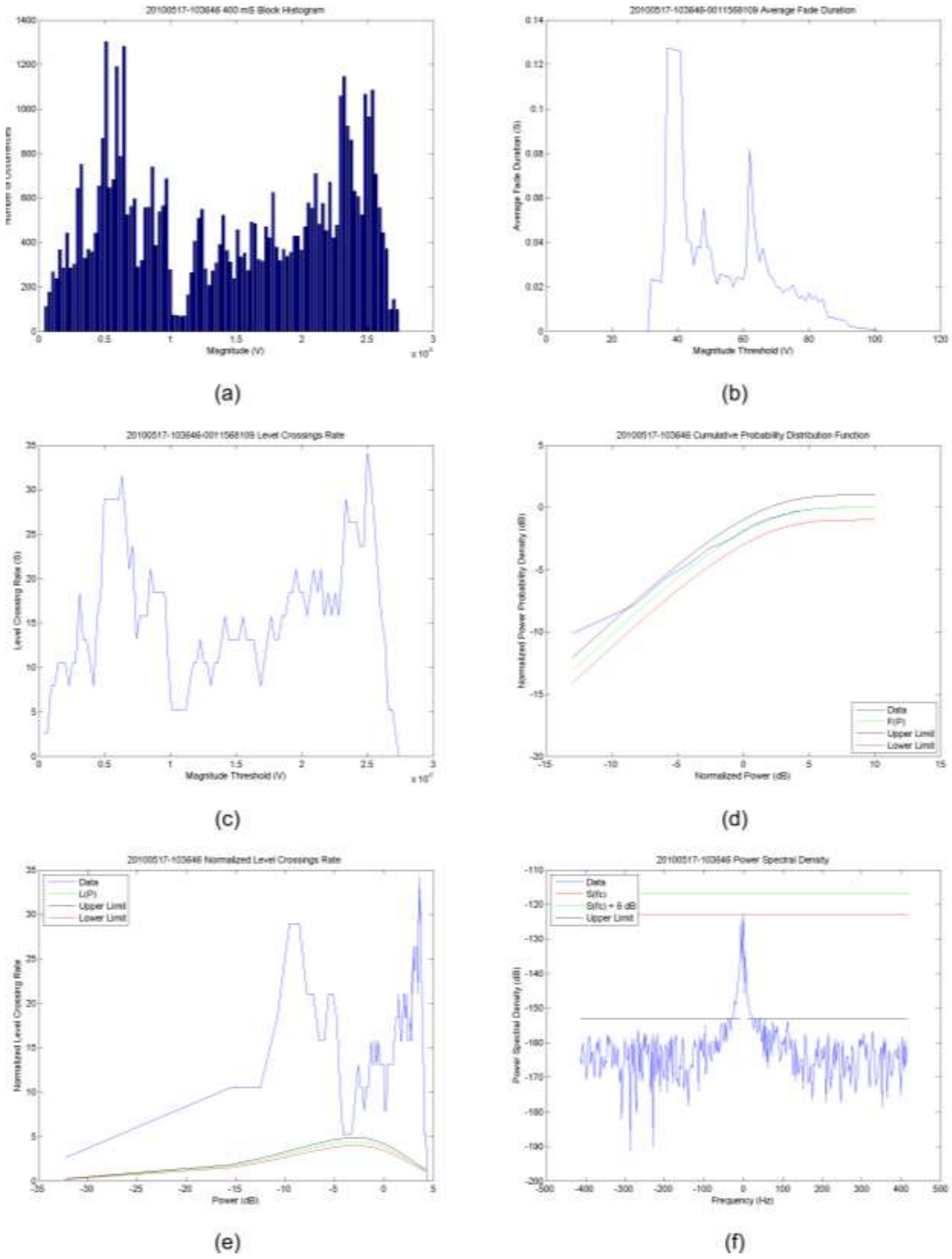

(a) (b)

(c) (d)

(e) (f)

Figure E-26. Plots for data file 2010/05/17 10:36:46 (residential environment, 162 MHz).

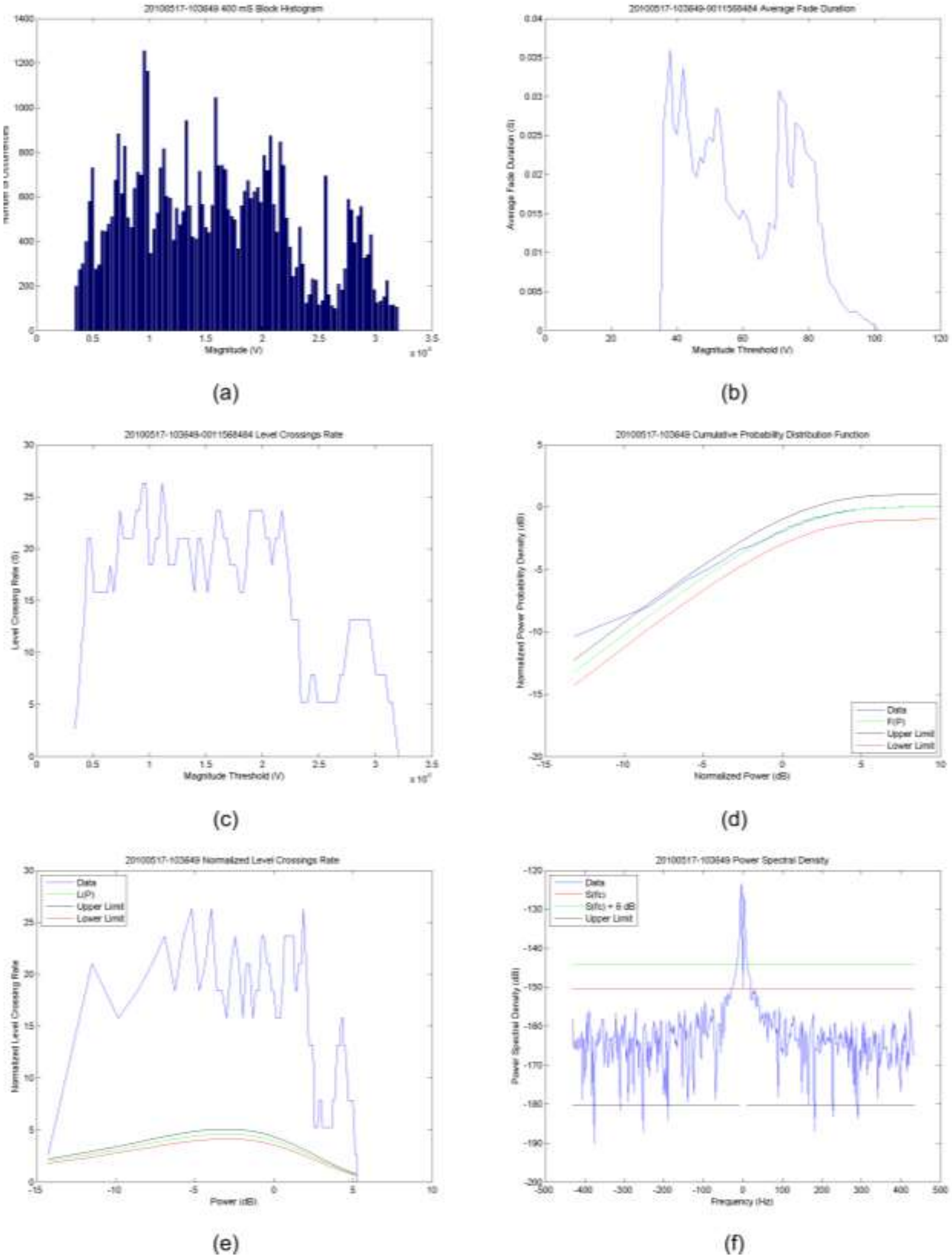

(a) (b) (c) (d) (e) (f)

Figure E-27. Plots for data file 2010/05/17 10:36:49 (residential environment, 162 MHz).

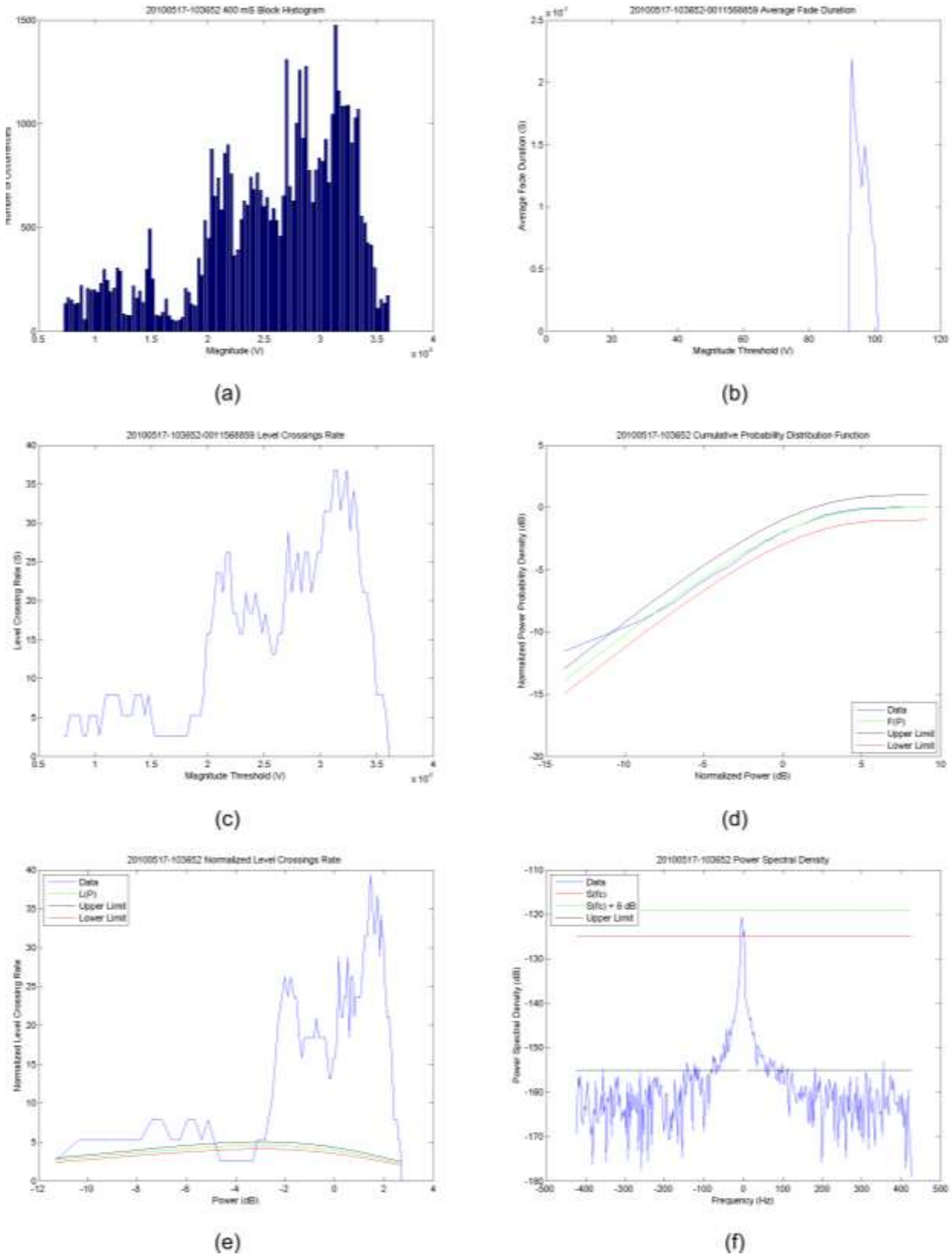

Figure E-28. Plots for data file 2010/05/17 10:36:52 (residential environment, 162 MHz).

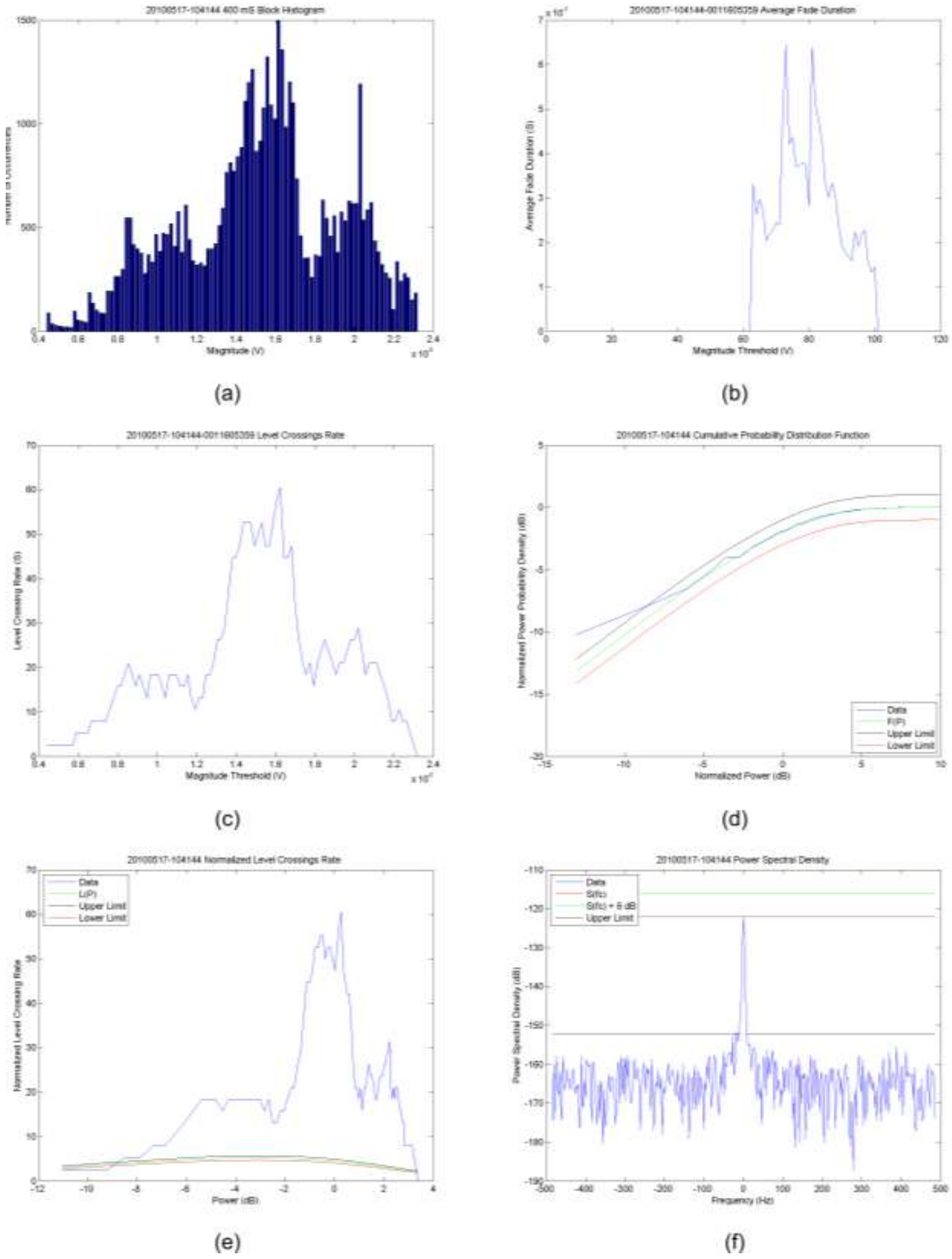

Figure E-29. Plots for data file 2010/05/17 10:41:44 (residential environment, 162 MHz).

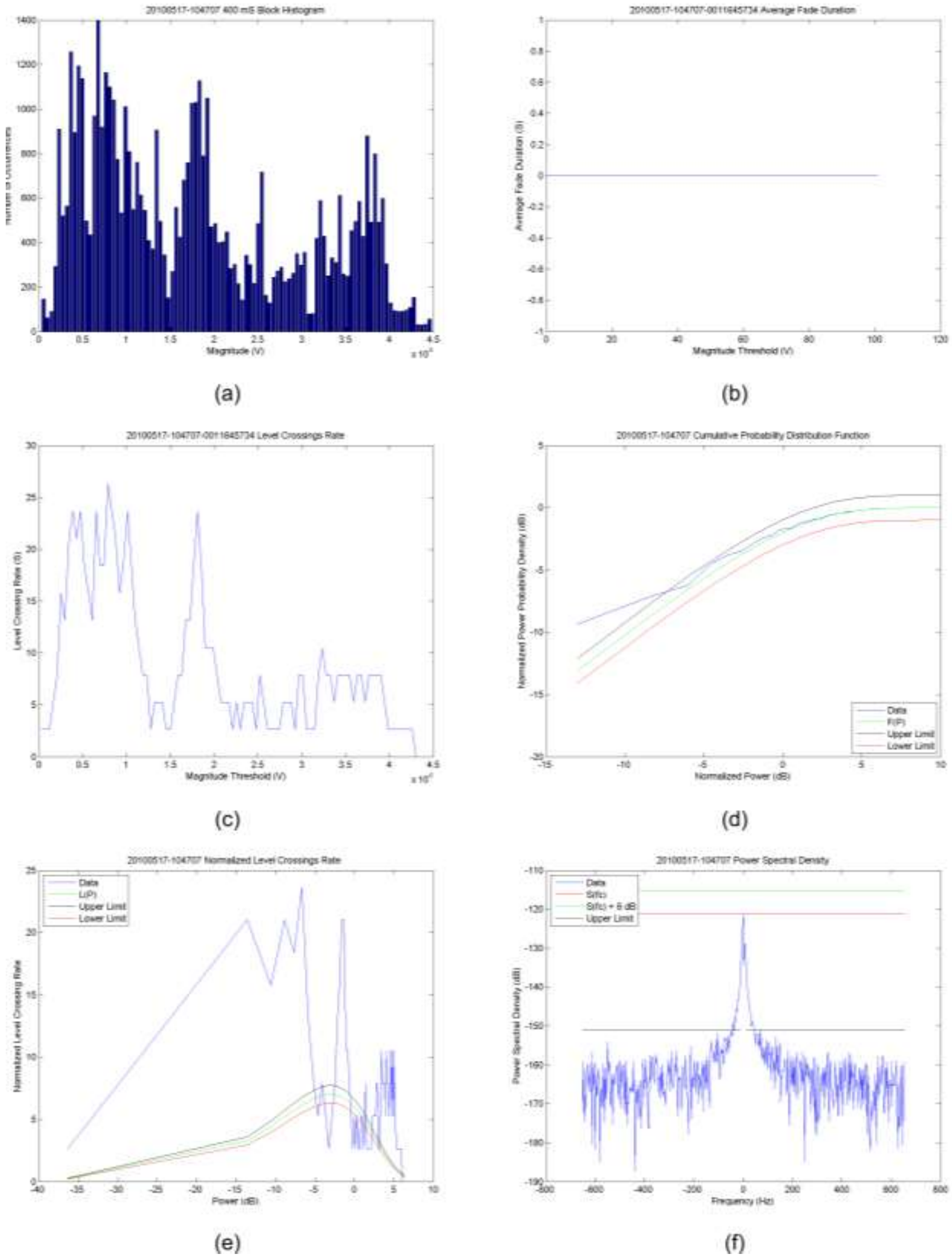

Figure E-30. Plots for data file 2010/05/17 10:47:07 (residential environment, 162 MHz).

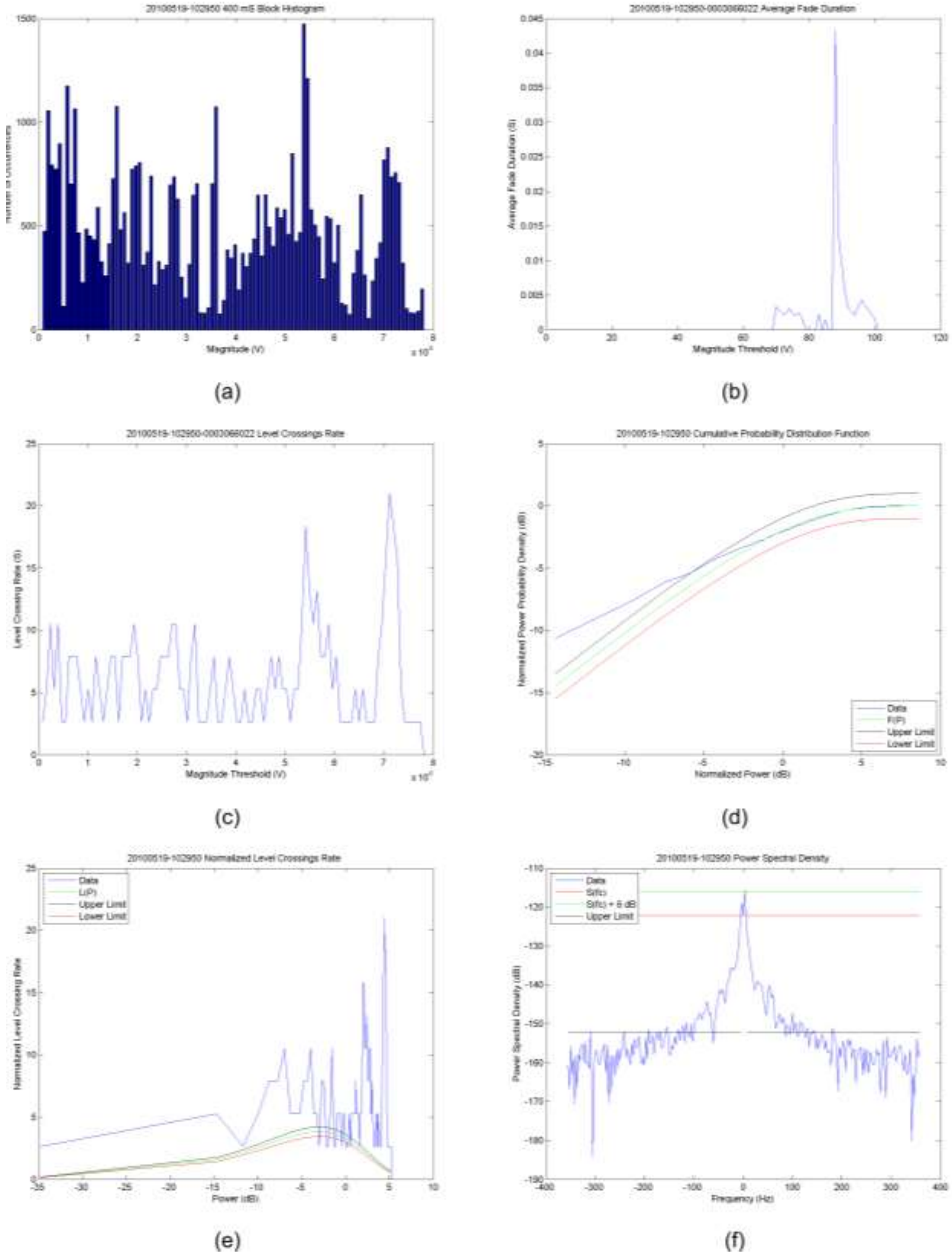

(a) (b)

(c) (d)

(e) (f)

Figure E-31. Plots for data file 2010/05/19 10:29:50 (low-rise urban environment, 162 MHz).

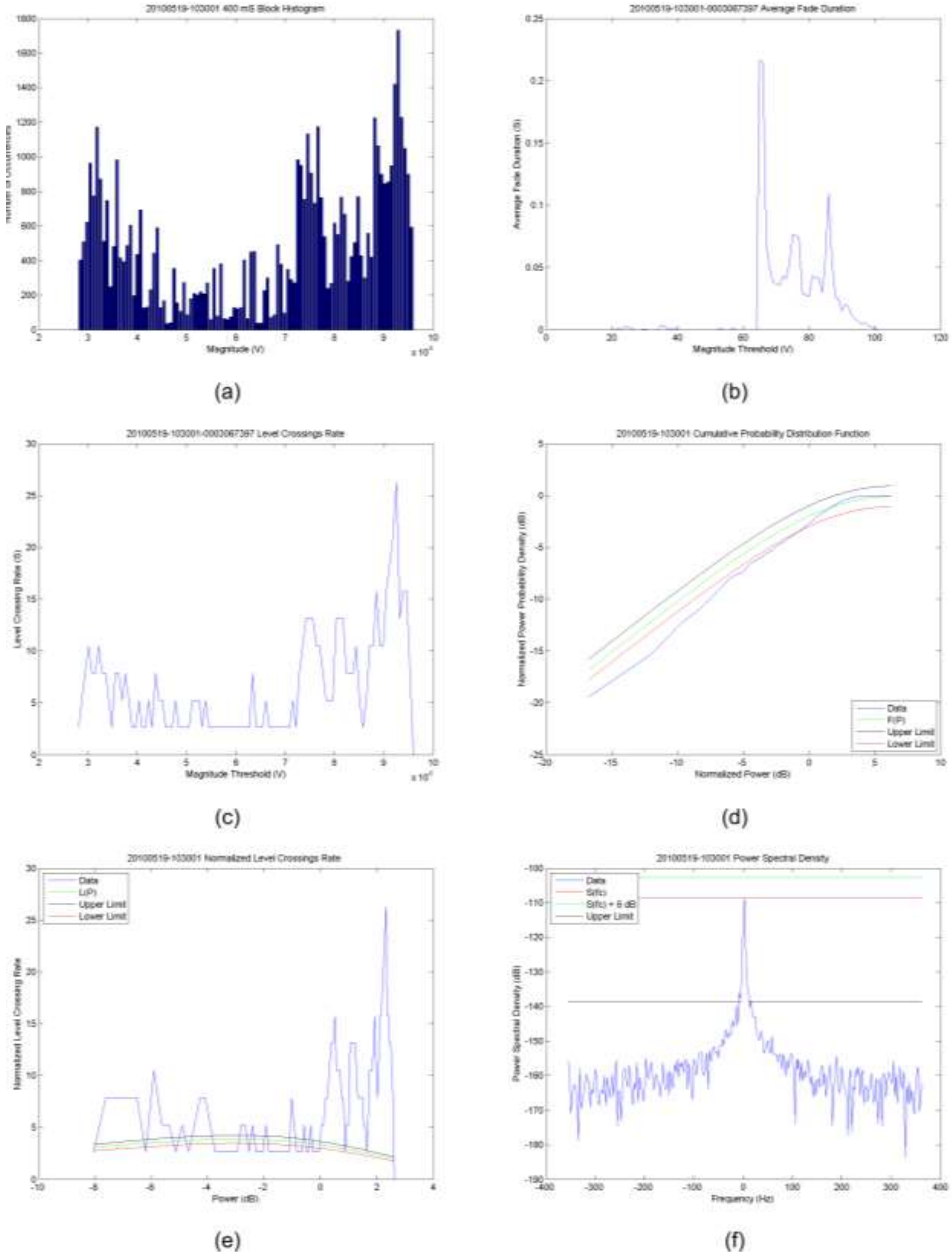

Figure E-32. Plots for data file 2010/05/19 10:30:01 (low-rise urban environment, 162 MHz).

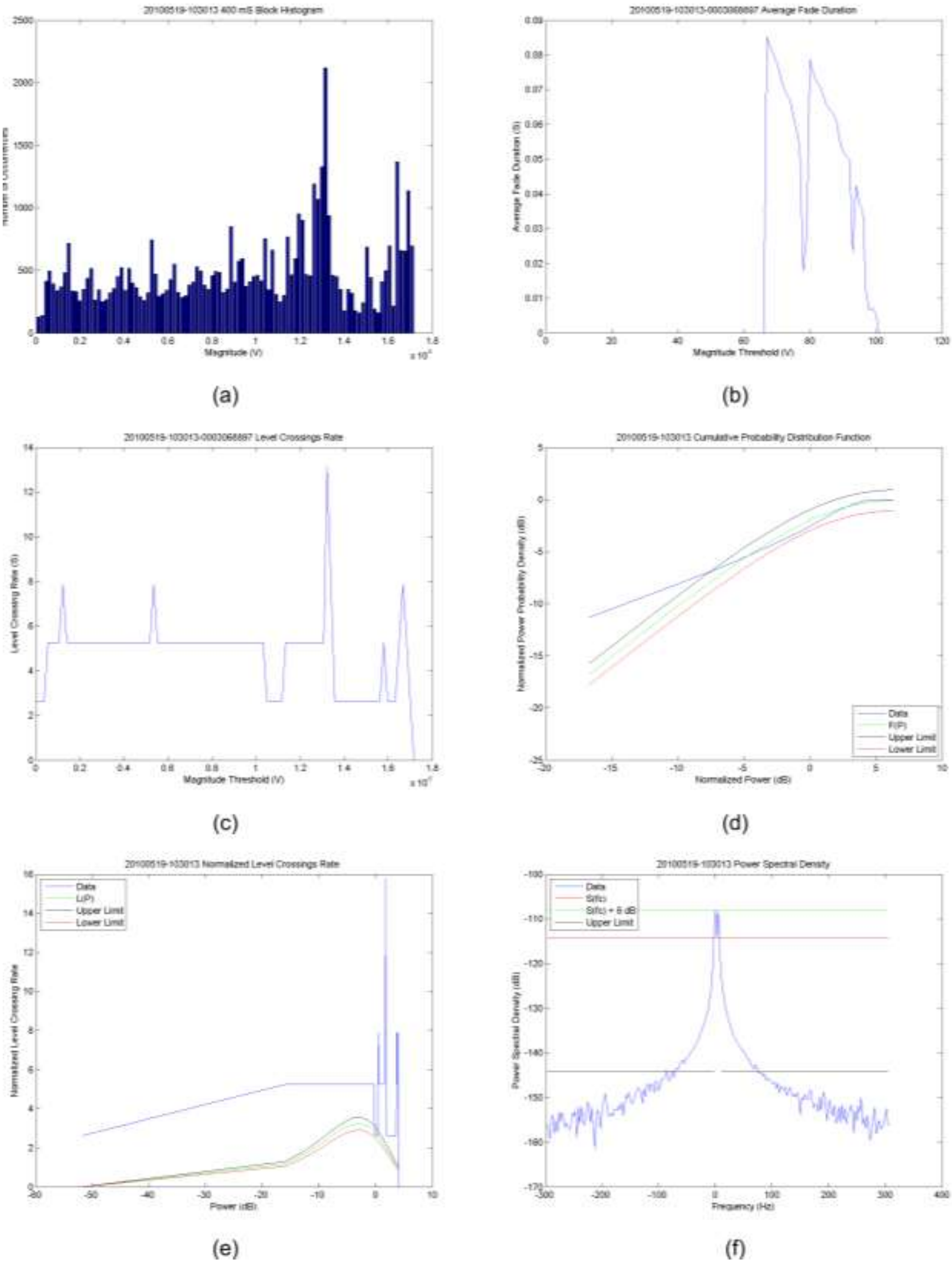

(a) (b)

(c) (d)

(e) (f)

Figure E-33. Plots for data file 2010/05/19 10:30:13 (low-rise urban environment, 162 MHz).

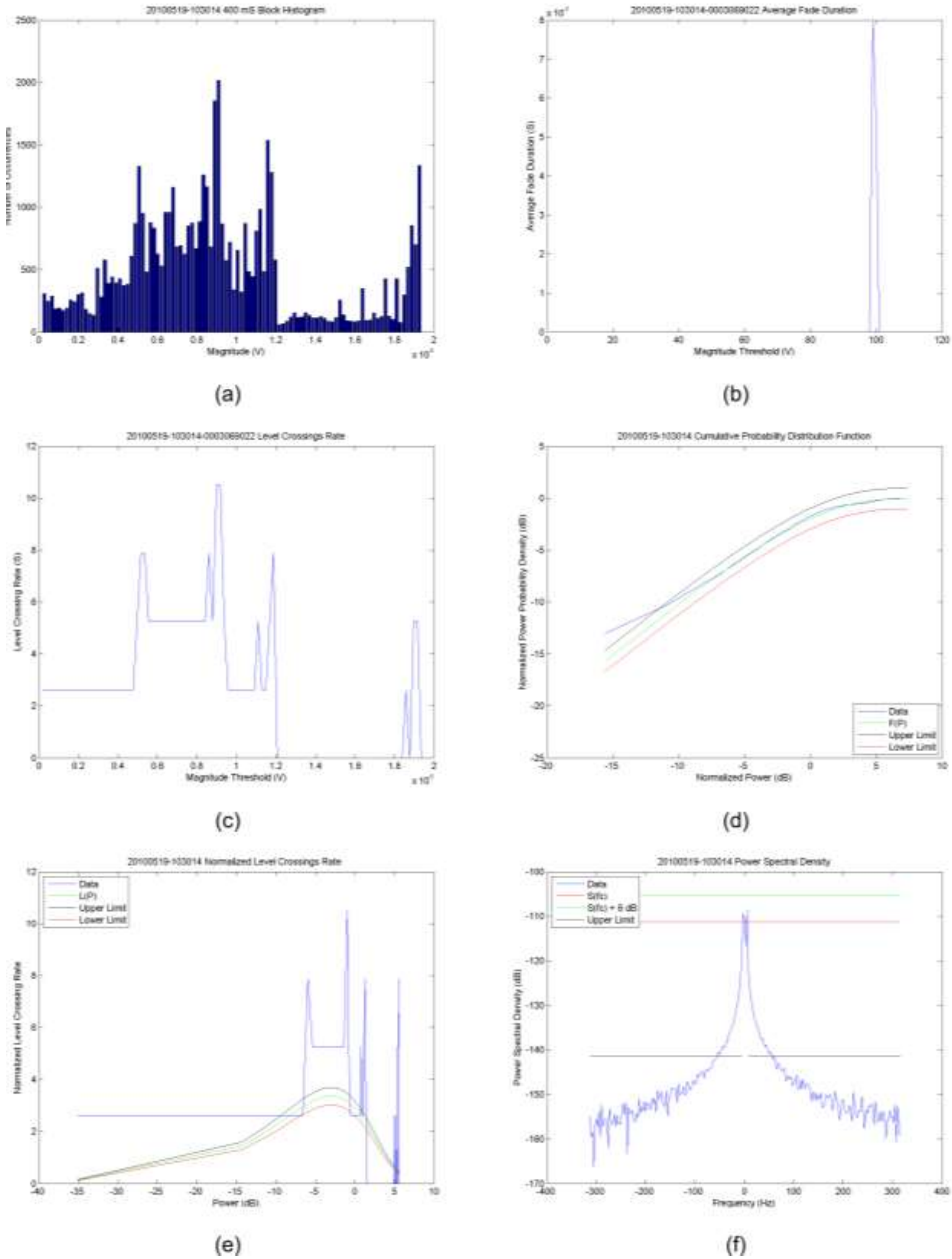

(a) (b)

(c) (d)

(e) (f)

Figure E-34. Plots for data file 2010/05/19 10:30:14 (low-rise urban environment, 162 MHz).

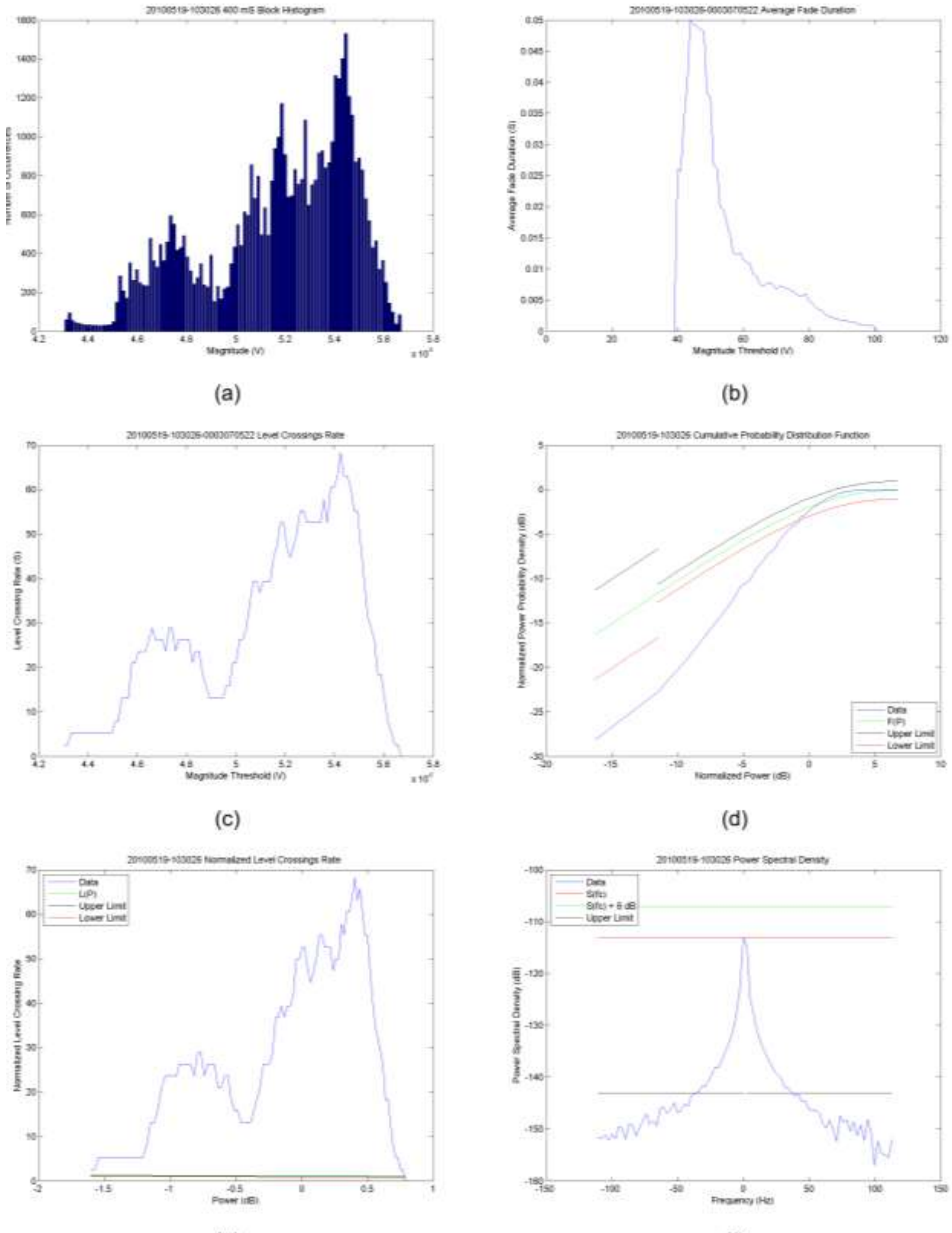

(a) (b) (c) (d) (e) (f)

Figure E-35. Plots for data file 2010/05/19 10:30:26 (low-rise urban environment, 162 MHz).

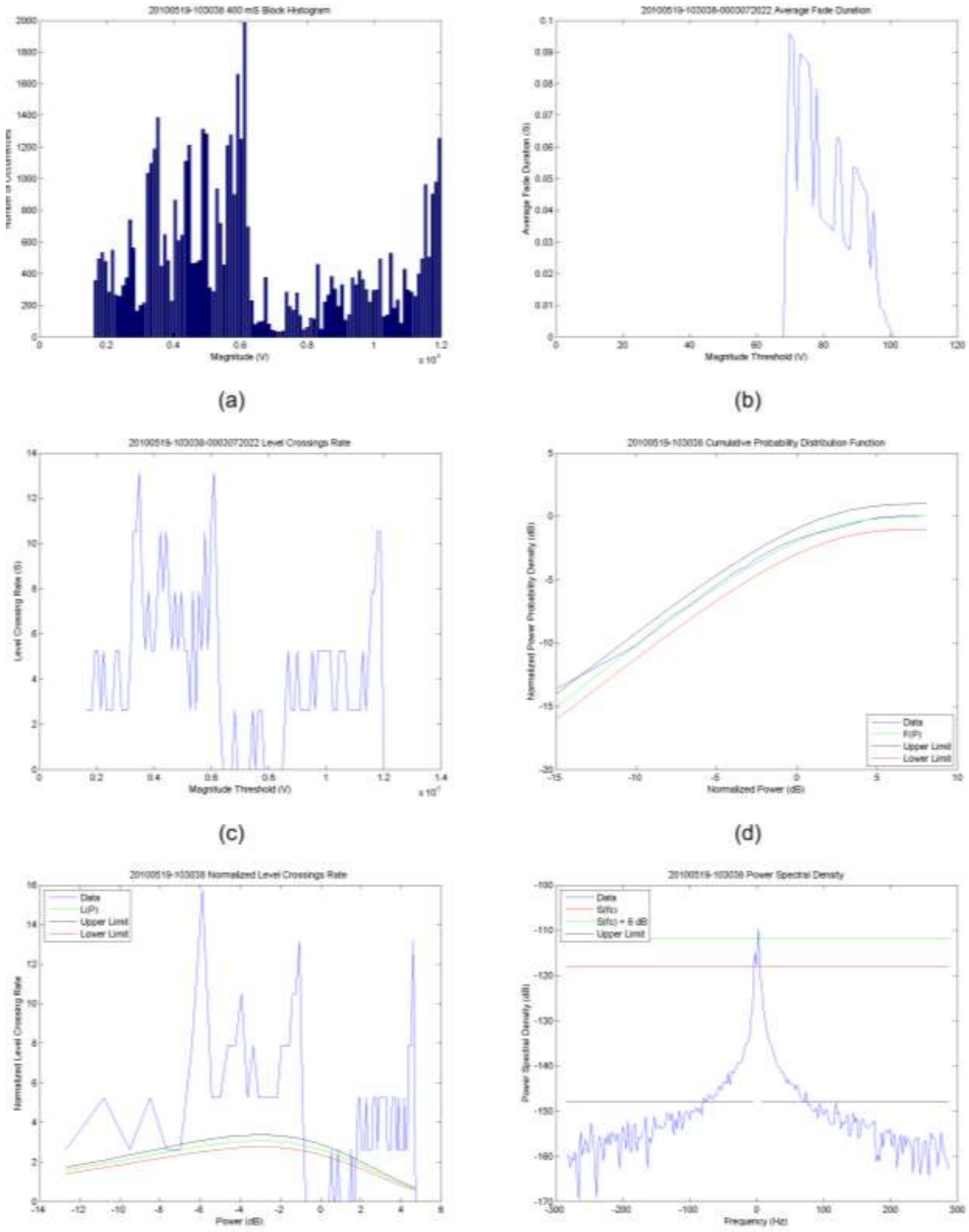

(a)

(b)

(c)

(d)

(e)

(f)

Figure E-36. Plots for data file 2010/05/19 10:30:38 (low-rise urban environment, 162 MHz).

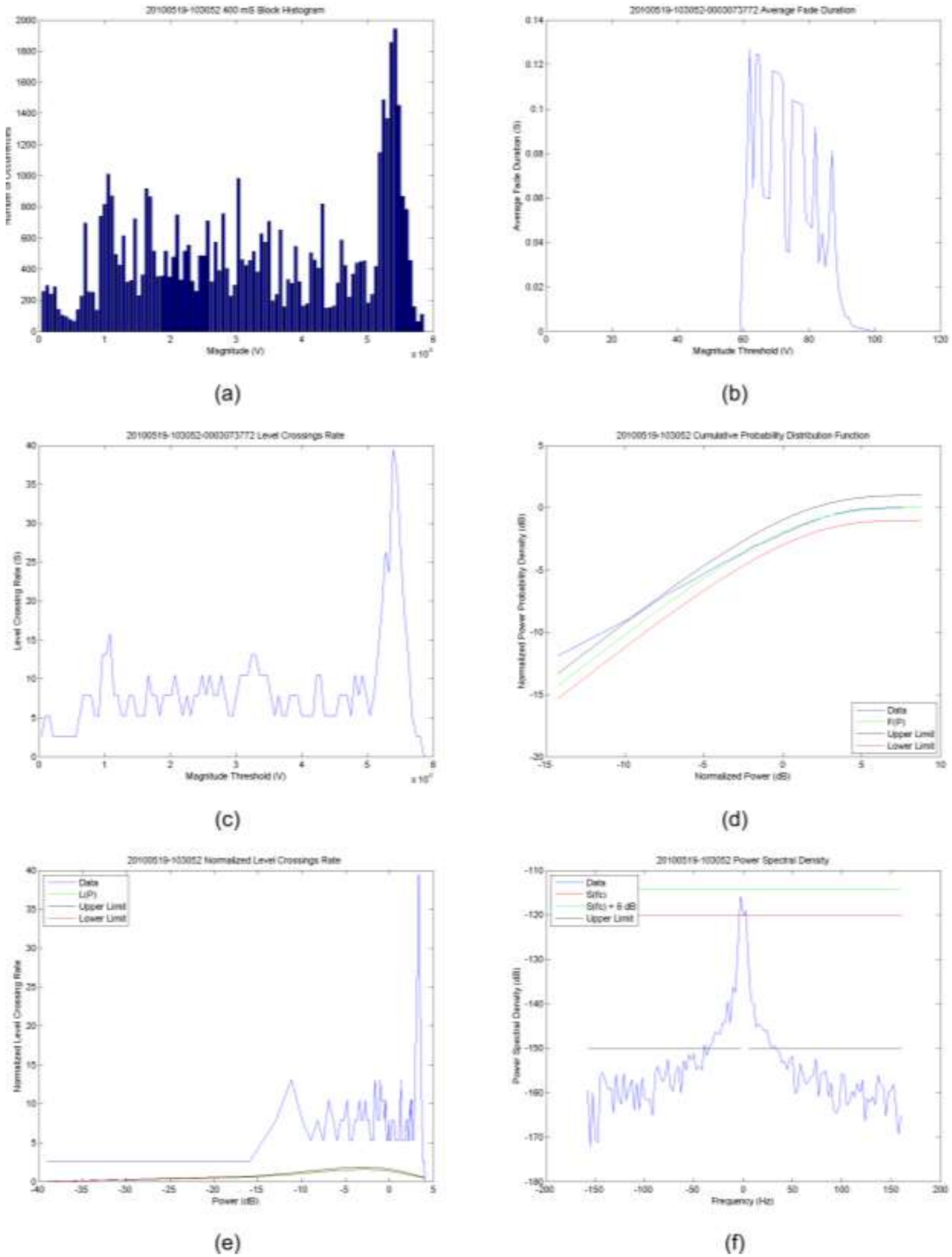

Figure E-37. Plots for data file 2010/05/19 10:30:52 (low-rise urban environment, 162 MHz).

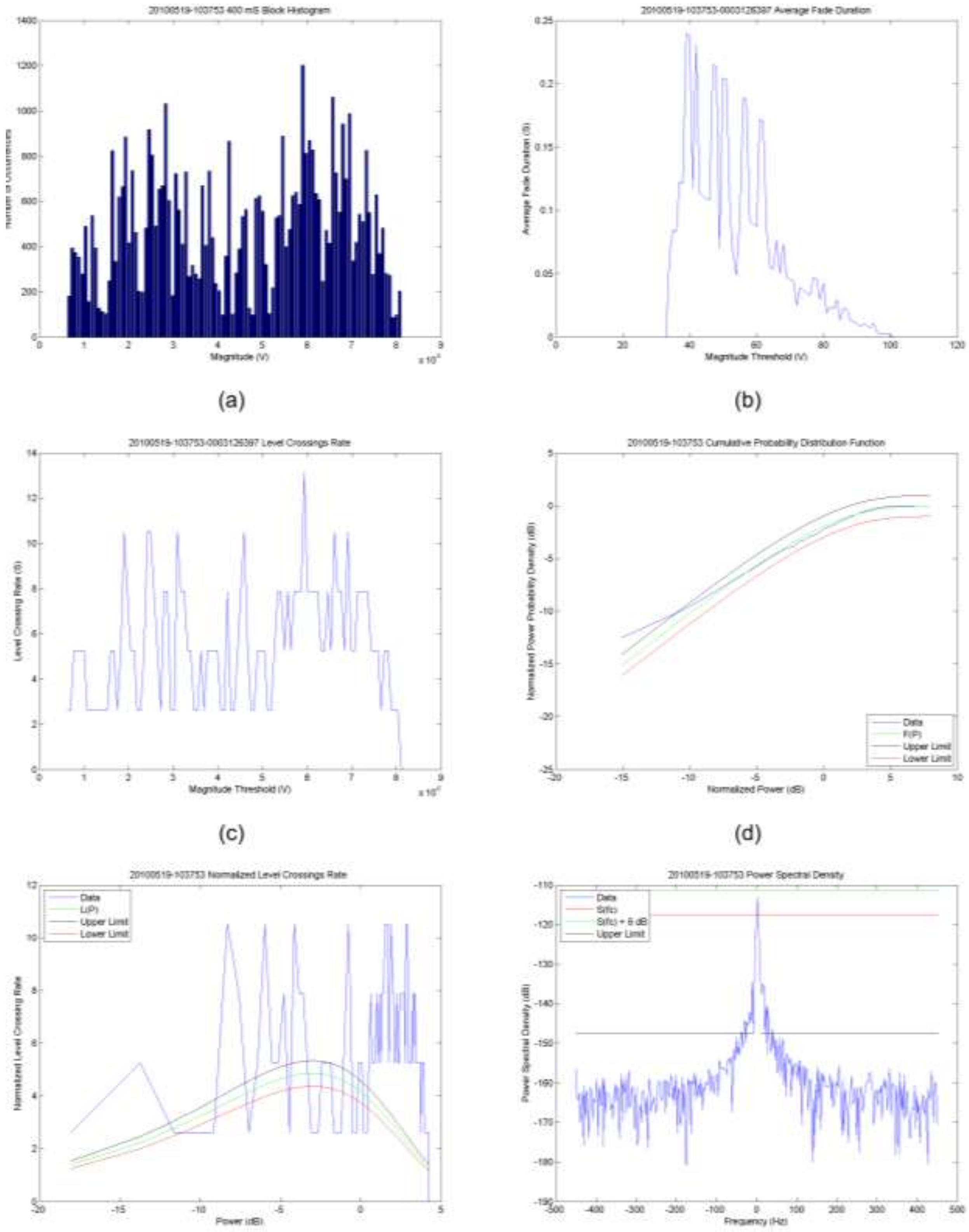

(a) (b)

(c) (d)

(e) (f)

Figure E-38. Plots for data file 2010/05/19 10:37:53 (low-rise urban environment, 162 MHz).

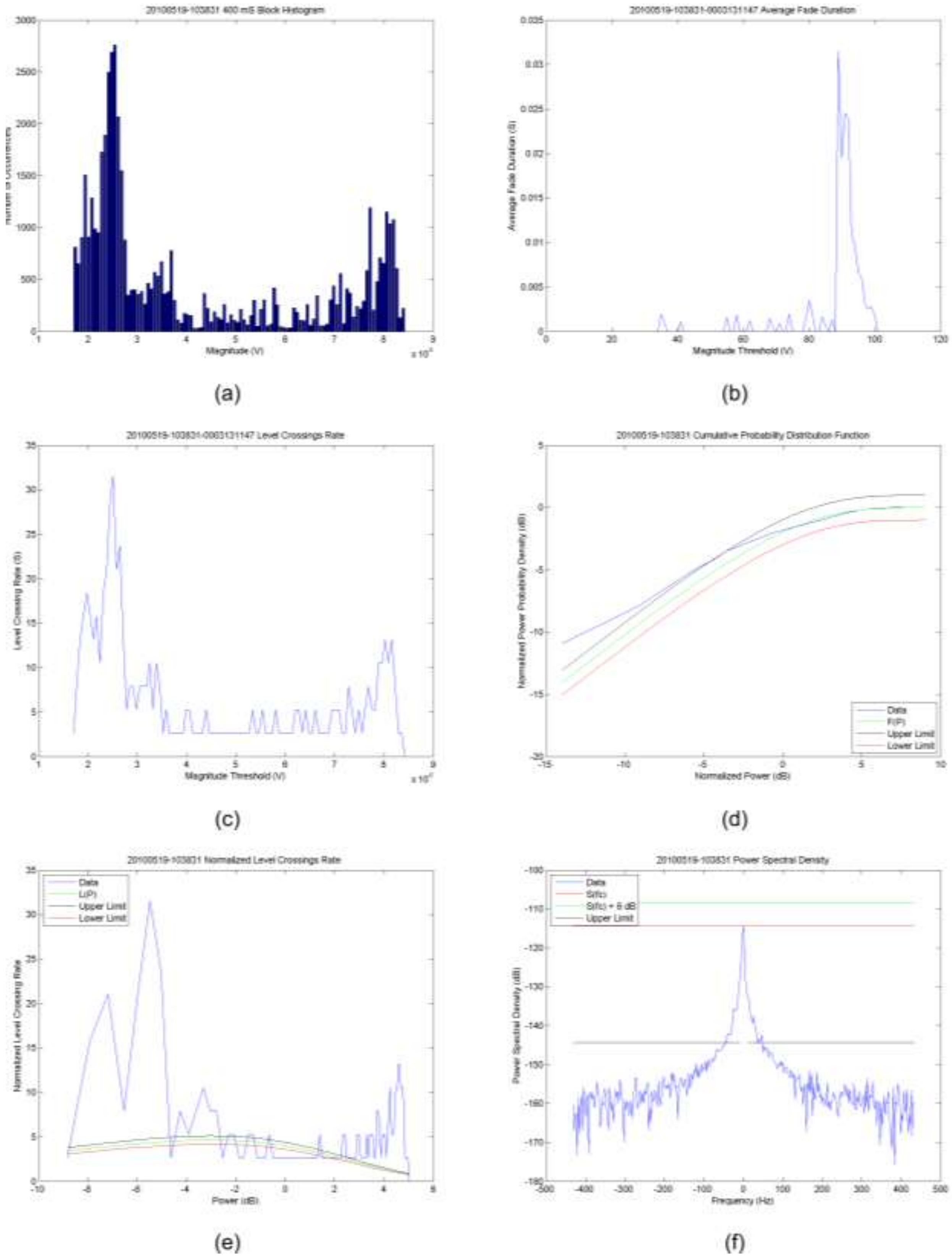

(a) (b)

(c) (d)

(e) (f)

Figure E-39. Plots for data file 2010/05/19 10:38:31 (low-rise urban environment, 162 MHz).

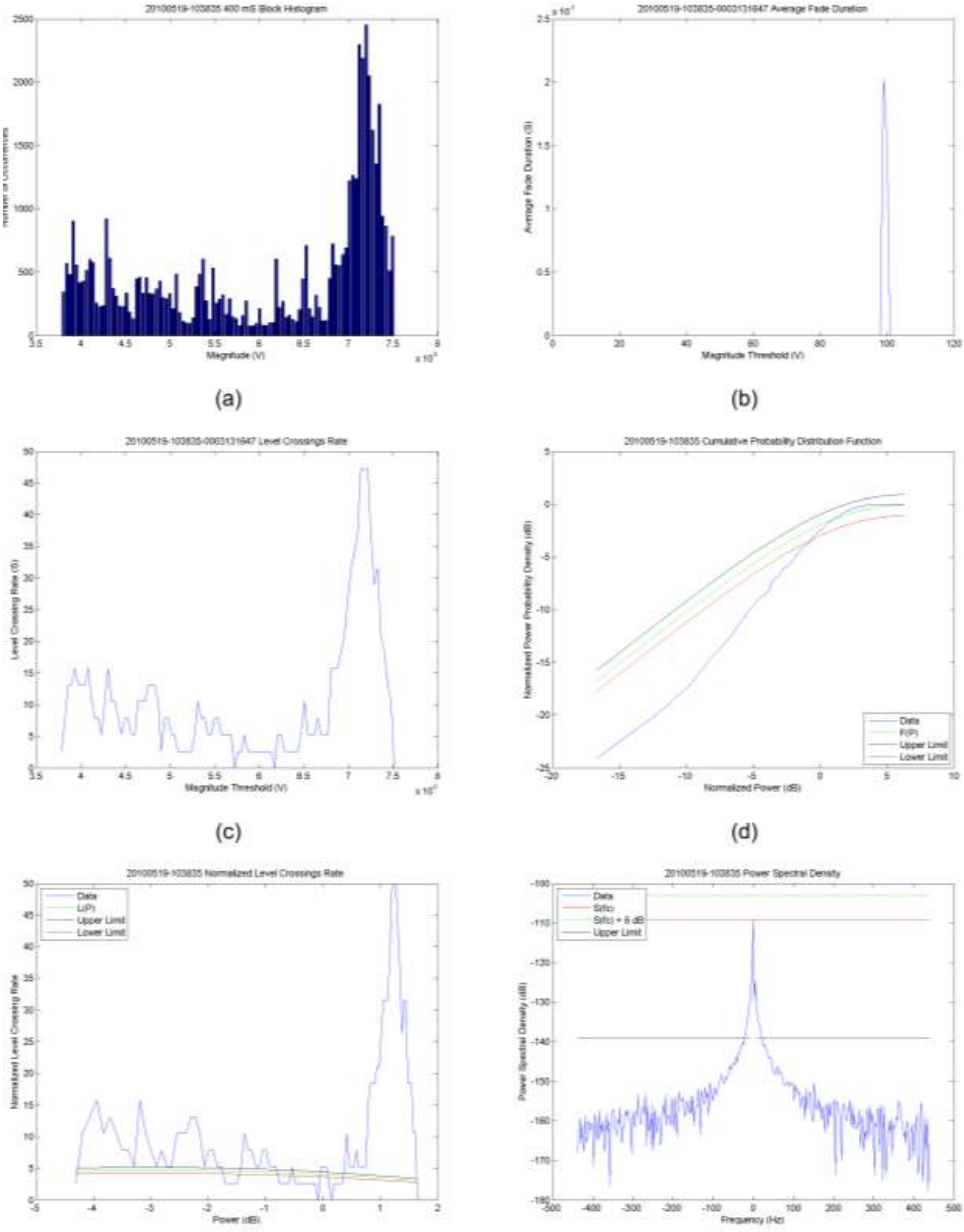

(a) (b)

(c) (d)

(e) (f)

Figure E-40. Plots for data file 2010/05/19 10:38:35 (low-rise urban environment, 162 MHz).

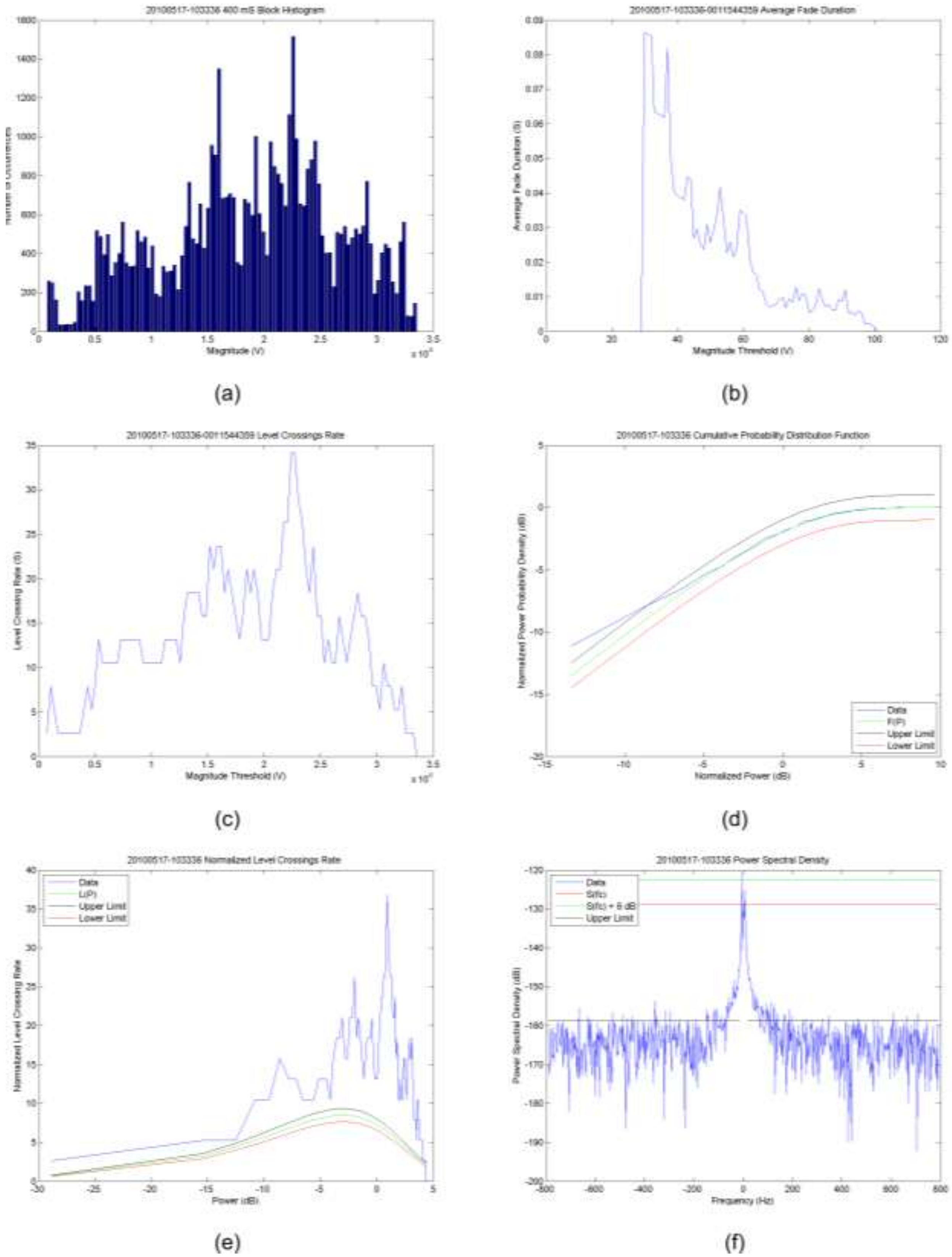
20100517-103336 400 mS Block Histogram

20100517-103336-0011544359 Average Fade Duration

20100517-103336-0011544359 Level Crossings Rate

20100517-103336 Cumulative Probability Distribution Function

20100517-103336 Normalized Level Crossings Rate

20100517-103336 Power Spectral Density

(a) (b)

(c) (d)

(e) (f)

Figure E-41. Plots for data file 2010/05/17 10:33:36 (residential environment, 162 MHz).

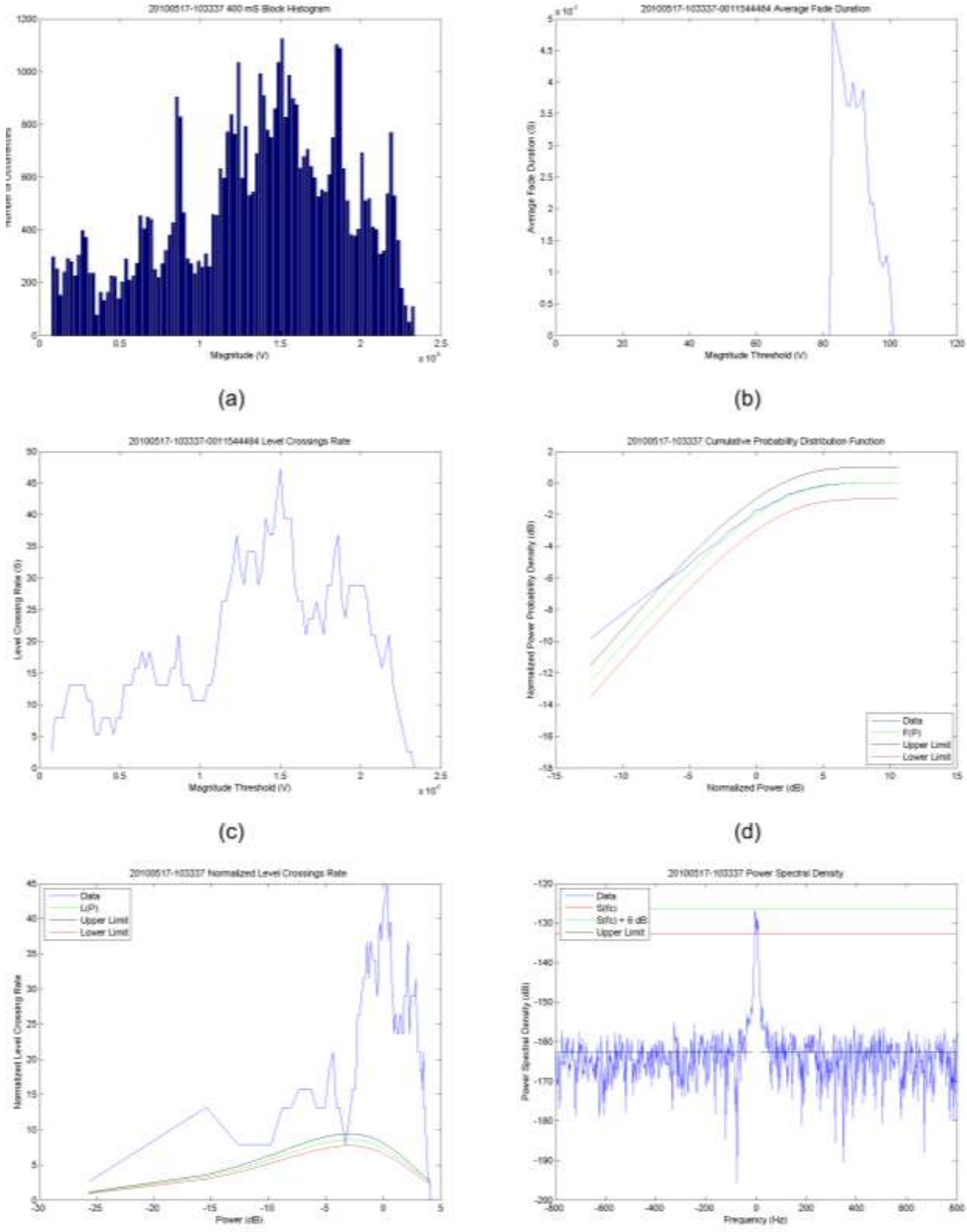

(a) (b)

(c) (d)

(e) (f)

Figure E-42. Plots for data file 2010/05/17 10:33:37 (residential environment, 162 MHz).

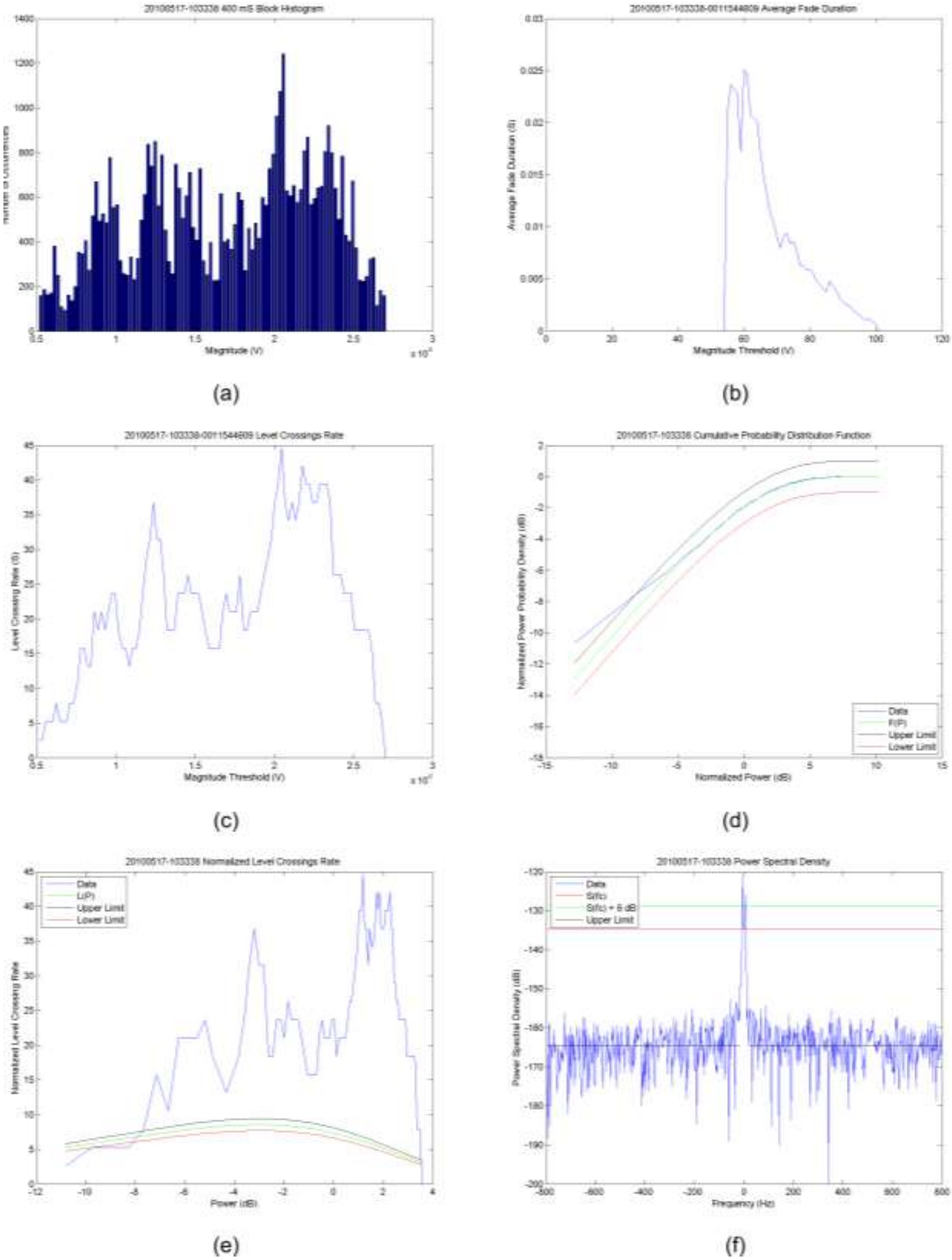

Figure E-43. Plots for data file 2010/05/17 10:33:38 (residential environment, 162 MHz).

APPENDIX F: LIST AND DESCRIPTION OF SOFTWARE ROUTINES.

gps_csv_tbe_0x.py	Python code that converts the output files from the GPS device into **.csv* files. Each line of the file contains the following values for each measurement second: • Longitude • Latitude • Altitude • TOW (time-of-week) • Local time • Velocity along the path (bearing) • Velocity relative to the transmitter (radial) • Velocity measured by the GPS • Doppler frequency based on the path velocity • Doppler frequency based on the radial velocity • Bearing *x* = 0,1 depending on the format of the file the GPS outputs.
gps_kml_tbe.py	Python code that converts the output files from the GPS device into **.kml* files. These can be used to plot the measurement path in Google Earth.
iqt2mat.m	converts the **.iqt* files output by the spectrum analyzer into **.mat* files that can be read by MATLAB®. The **.mat* file contains a single array, *z*; each array element consists of a complex number (I and Q). This routine uses *iqtread.m* which, in turn, uses *getParameterValueFromStr.m*, *convertIQTReadValues.m* and *sampling_frequency_lookup.m*. The **.mat* files are stored in subdirectory *MatFiles*.
mat2filt.m	filters the *z* array in the **.mat* files to a *zf* array and stores it as a **.mat* file in the subdirectory *Filtered*. The filter is a 6-pole Butterworth low-pass filter with a 500 Hz cutoff frequency.
Oneblock.m	generates a histogram of the filtered data and stores a **.png* file for each data file in the subdirectory *OneBlock*.
TwentyBlock.m	concatenates 20 contiguous data files and generates a histogram. The **.png* file is stored in the subdirectory *20Block*. (Note: 20 block statistics were no longer used once the data was sorted by SNR values.)
filt2lvlcr.m	generates level crossing rate plots and average fade duration plots from filtered data files. The **.png* files are stored in subdirectories *LVLCR* and *AFD*.

filt2lvlcr20.m	generates level crossing rate plots and average fade duration plots from 20 contiguous concatenated filtered data files. The **.png* files are stored in subdirectories *20LVLCR* and *20AFD*. (Note: 20 block statistics were no longer used once the data was sorted by SNR values.)
TiaTestsefg.m	calculates the results of TIA tests (e) on unfiltered data and (f) and (g) on filtered data and plots the results. The *.png files (one per test per data file) are stored in subdirectory TIA Plots.
TiaTestsefg_sim.m	calculates the results of TIA tests (e), (f) and (g) on data collected from the Rayleigh simulator and plots the results.
dir_scan.m	scans a directory of unfiltered data and calculates the SNR of each file in both the time domain and frequency domain. Generates a structure *z_result* containing the elements: • file name • transition point location (transmitter off to transmitter on) • SNR in the time domain • SNR in the frequency domain • standard deviation of the signal portion of the file • reject status (for time domain calculations)
snr_freq_cull.m	uses the frequency domain SNR information from the *z_result* structure to extract those elements that pass a defined requirement. The extracted elements are stored in a *z_snr_cull* structure. The requirement used for this report is those SNRs that fall within a range of the mean SNR (over the entire directory, i.e. run) ±0.5 times the standard deviation of the SNR.
SNR_sort.m	uses the elements of the *z_snr_cull* structure to separate the filtered **.mat* files and the analysis image files into separate *Accepted* and *Rejected* subdirectories.
TIA_h.m	calculates the result of TIA test (h) on unfiltered data and stores the result in a structure *z_phase_result*, containing the elements: • file name • calculated Doppler frequency (along the measured path) • Doppler frequency measured by the GPS device • the index point at which the 0.05/f_d occurs (= -999 when out of the correlation coefficient's range) • the index point at which the 0.15/f_d occurs (= -999 when out of the correlation coefficient's range) • the correlation coefficient's value at the 0.05/f_d point (NaN if out-of-range)

	• the correlation coefficient's value at the 0.15/f_d point (NaN if out-of-range)
TIA_h_sim.m	calculates the result of TIA test (h) on data collected from the Rayleigh simulator and stores the result in a structure *z_phase_result*.
Phase_summary.m	scans the structure *z_phase_result* and summarizes: • *bad05*: the elements containing out-of-range locations for the 0.05/f_d point • *bad15*: the elements containing out-of-range locations for the 0.15/f_d point • *good05*: the elements containing passing values for the 0.05/f_d point • *good15*: the elements containing passing values for the 0.15/f_d point • *good_both*: the elements containing passing values for both points
fitdist2.m	used to generate the plots in APPENDIX D:.
CumPDF.m	used to generate Figure 20.
lcrafd_compare3.m	used to generate Figure 21.

FORM **NTIA-29**
(4-80)

U.S. DEPARTMENT OF COMMERCE
NAT'L. TELECOMMUNICATIONS AND INFORMATION ADMINISTRATION

BIBLIOGRAPHIC DATA SHEET

1. PUBLICATION NO. Enter assigned report number.	2. Government Accession No.	3. Recipient's Accession No.

4. TITLE AND SUBTITLE Examining the Validity of Rayleigh Distribution Assumptions in Characterizing the Fading Channel at 162 and 793 MHz	5. Publication Date October 2010
	6. Performing Organization Code ITS.E
7. AUTHOR(S) Chris Redding, Chris Behm, Tim Riley, Rob Stafford	9. Project/Task/Work Unit No. 6513000-341
8. PERFORMING ORGANIZATION NAME AND ADDRESS Institute for Telecommunication Sciences National Telecommunications & Information Administration U.S. Department of Commerce 325 Broadway Boulder, CO 80305	10. Contract/Grant Number.
11. Sponsoring Organization Name and Address National Telecommunications & Information Administration Herbert C. Hoover Building 14th & Constitution Ave., NW Washington, DC 20230	12. Type of Report and Period Covered

14. SUPPLEMENTARY NOTES

15. ABSTRACT (A 200-word or less factual summary of most significant information. If document includes a significant bibliography or literature survey, mention it here.)

This report describes the re-examination of the fading channel. Specifically, it presents an effort to determine if those assumptions implicit in the understanding of fading channels are keeping pace with the persistent desire to increase the bit density in limited spectral bandwidths. This effort involves the measurement, analysis, and assessment of propagation fading and describes the limitations of classical fading theories when applied to ever more sophisticated modulation techniques. Measurements of the mobile radio channel were conducted to analyze the fast fading characteristics of the public safety frequency band. Multiple iterations of a measurement system were employed to improve the system's capability to measure the channel characteristics. Data analysis was conducted without bias toward conventional fading assumptions. It was intended that the data analyzed provide an independent theoretical understanding of RF fading propagation. Finally, an assessment of the efficacy of classical fading theory in the testing of existing public safety VHF transceivers is discussed with conjectures about future transceiver testing and design.

16. Key Words (Alphabetical order, separated by semicolons)

propagation characteristics; fading channel; Rayleigh distribution

17. AVAILABILITY STATEMENT ☒ UNLIMITED. ☐ FOR OFFICIAL DISTRIBUTION.	18. Security Class. (This report) Unclassified	20. Number of pages 116
	19. Security Class. (This page) Unclassified	21. Price:

NTIA FORMAL PUBLICATION SERIES

NTIA MONOGRAPH (MG)

A scholarly, professionally oriented publication dealing with state-of-the-art research or an authoritative treatment of a broad area. Expected to have long-lasting value.

NTIA SPECIAL PUBLICATION (SP)

Conference proceedings, bibliographies, selected speeches, course and instructional materials, directories, and major studies mandated by Congress.

NTIA REPORT (TR)

Important contributions to existing knowledge of less breadth than a monograph, such as results of completed projects and major activities. Subsets of this series include:

NTIA RESTRICTED REPORT (RR)

Contributions that are limited in distribution because of national security classification or Departmental constraints.

NTIA CONTRACTOR REPORT (CR)

Information generated under an NTIA contract or grant, written by the contractor, and considered an important contribution to existing knowledge.

JOINT NTIA/OTHER-AGENCY REPORT (JR)

This report receives both local NTIA and other agency review. Both agencies' logos and report series numbering appear on the cover.

NTIA SOFTWARE & DATA PRODUCTS (SD)

Software such as programs, test data, and sound/video files. This series can be used to transfer technology to U.S. industry.

NTIA HANDBOOK (HB)

Information pertaining to technical procedures, reference and data guides, and formal user's manuals that are expected to be pertinent for a long time.

NTIA TECHNICAL MEMORANDUM (TM)

Technical information typically of less breadth than an NTIA Report. The series includes data, preliminary project results, and information for a specific, limited audience.

For information about NTIA publications, contact the NTIA/ITS Technical Publications Office at 325 Broadway, Boulder, CO, 80305 Tel. (303) 497-3572 or e-mail info@its.bldrdoc.gov.